



Alma Mater Studiorum Università di Bologna

PhD in BIOENGINEERING

XXV Cicle

***“3D nanostructured microcarriers for cell
therapy in regenerative medicine”***

Tutor:

Ch.mo Prof. Angelo Cappello

Co-Tutors :

Prof. Ernesto Reverchon

Prof. Emanuele Giordano

Candidate:

Giovanna Della Porta

.... acknowledgments are for all those joined me this three years wonderful adventure, making it exciting and fun, so to

.... all co-authors of my publications, we shared many hours at work but also our private life and, to the colleagues of the courses and seminars attended, with them I enjoyed also the endless ones.... many of them become friends ...

.... Ernesto, my basic guide for the entire journey; prof. Cavalcanti who imagined it but unfortunately we hadn't the chance to travel together and, to Prof. Cappello, he acquired this adventure and believed in it....

..... a special thank to Emanuele, a friend who showed me the right path when it seemed lost ...

.... and, finally, to Francesca and Federica for their patience, to "Aunt Mary" for the necessary joy when we've been in the "foreign land" and Clemente, without him this trip would not have ever started!

Table of Contents

Table of Contents	3
List of Figures	6
List of Tables.....	10
Abstract	11
Introduction	13
Chapter 1. State of the Art	15
1.1 Tissue engineering: top-down & bottom-up approaches	15
1.2 Materials for scaffolds fabrication	16
1.3 Injectable scaffolds & Pharmacologically Active Microcarriers	17
1.4 Scaffold by conventional technologies: top-down approach	18
1.5 Biopolymer microdevices by conventional technologies: bottom up approach ...	22
1.6 About Supercritical fluids	23
1.7 Supercritical fluids technologies for scaffolds production.....	26
1.8 Supercritical fluids technologies for microcarriers production.....	27
Aims of the thesis	29
Chapter 2. Continuous Supercritical Emulsions Extraction: a new technology for PLGA microcarriers production	30
2.1 Introduction	30
2.2 Experimental Methods	31
2.2.1 Materials, Emulsion Preparation & Methods.....	31
2.2.3 SEE-C apparatus	32
2.2.4 Morphology & Size Distributions	32
2.2.5 Solid state characterization.....	33
2.2.6 Microparticles degradation study	33
2.2.7 Solvent residue analysis	33
2.2.8 Correlations for flooding point calculation	35
2.3 Results & Discussion	36
2.3.1 SEE-C parameters: pressure & temperature.....	36
2.3.2 SEE-C parameter: evaluation of flooding	37
2.3.3 Droplets & microparticles size and morphology.....	40
2.3.4 Comparison between SEE, SEE-C and evaporation	46
2.3.5 Microparticles solid state and degradation.....	47

2.3.6	Proposed process mechanism.....	47
2.4.	Others results on PLGA microcarriers charged with bioactive substances	51
2.5	Conclusions & Perspectives	54
Chapter 3. PLGA microdevices by SEE for Retinoic acid sustained release: evaluation of the kinetics constants.....		55
3.1	Introduction	55
3.2	Experimental Methods	56
3.2.1	Materials.....	56
3.2.2	Emulsions formulation & Liquid Emulsion Extraction (LEE)	56
3.2.3	SEE: apparatuses & microdevices characterization	56
3.2.4	Solid state characterization.....	57
3.2.5	Solvent residue analysis	57
3.2.6	Drug loading & release	57
3.3	Results & Discussion	58
3.3.1	Selection of the operating conditions	58
3.3.2	Comparison with the conventional liquid extraction	58
3.3.3	Batch vs. continuous operation	61
3.3.4	Microspheres size tailoring and solid state characterization.....	62
3.3.5	Drug release study.....	66
3.4	Conclusions & Perspectives	69
Chapter 4. PLGA-PAMs produced by SEE-C: Study on Bioactive Signal Release in Myoblast Culture.....		70
4.1	Introduction	70
4.2	Apparatus, Materials and Methods.....	71
4.2.1	Materials.....	71
4.2.2	Emulsion Formulations	71
4.2.3	Production by SEE-C Technology in GMP sterile conditions.....	72
4.2.4	Droplets & PAMs characterization	72
4.2.5	Protein loading determination	73
4.2.6	In Vitro protein release studies.....	73
4.2.7	PAMs Sterilization & Cell Culture	73
4.3	Results & Discussion	75
4.3.1	PLGA-PAMs loaded with Insulin	75
4.3.2	In Vitro Insulin Release Study from PAMs	78

4.3.3	Cells Viability, Adhesion & Growth on PAMs.....	82
4.4	Conclusions	84
Chapter 5. Synergistic effect of sustained release growth factors from PLGA-PAMs and dynamic bioreactor flow on hMSC osteogenic differentiation in 3D alginate scaffolds		85
5.1	Introduction	85
5.2	Materials & Methods.....	87
5.2.1	PLGA-PAMs production by SEE-C technology.....	87
5.2.2	Morphology & size distributions.....	87
5.2.3	BSA & GFs release and loading	88
5.2.4	h-MSC Culture	88
5.2.5	Alginate bead production loaded with PAMs and h-MSC.....	89
5.2.6	Perfusion Bioreactor for Dynamic Environment	89
5.2.7	Static Environment.....	90
5.2.8	Immunohistochemistry.....	90
5.2.9	Live-dead assay	91
5.2.10	Statistical Analysis	91
5.3	Results & Discussion	92
5.3.1	SEE-C operative conditions	92
5.3.2	PLGA-PAMs: size, loading & in vitro GFs release study	92
5.2.3	Scaffold characterization and bioreactor conditions	94
5.3.4	Immunoassay for cell differentiation monitoring.....	98
5.4	Conclusion & Perspectives.....	104
Conclusions & Perspectives.....		105
References		106
List of publications		122

List of Figures

Figure I.1. Basic principles of Tissue Engineering.	14
Figure 1.1a-b. (a) Carbon dioxide pressure-temperature phase diagram; (b) Images of supercritical carbon dioxide in the biphasic region (1) in the supercritical passage near the critical point (2-4).....	25
Figure 2.1a-b. Schematic representation of SEE and SEE-C processes layouts. SEE is an intrinsically batch process (a); SEE-C allows a continuous emulsion processing by using a countercurrent packed tower (b).....	34
Figure 2.1c. SEE-C apparatus P&I description. C, CO ₂ supply; E, emulsion supply; PG_1 and PG_2, pressure gauges; SC_P, diaphragm pump used for high pressure SC-CO ₂ ; L_P, piston pump used for the emulsion; TC1-TC8, thermocouples/controllers; S, separator; R, rotameter; E_1 and E_2, heat exchangers; V1-V8, valves.....	35
Figure 2.2. Effect of the gas density upon flooding for different L/G ratios (dashed line: boundary line between proper process conditions and flooding).....	39
Figure 2.3. Flooding velocities as a function of the liquid/gas ratio (L/G) for different CO ₂ densities: (■) P = 80 bar, T = 38°C, ρ = 0.31 g/cm ³ and (●) P = 100 bar, T = 44°C, ρ = 0.52 g/cm ³	39
Figure 2.4a-b. Optical Microscope images of two emulsions: (a) single <i>o-w</i> (20:80; composition: EA plus PLGA 10% w/w; external water with PVA 0.8% w/w) and (b) double <i>w-o-w</i> (1:19:80; composition: internal water plus PVA solution 0.04% w/w; oil EA plus PLGA 10% w/w; external water with PVA 0.8% w/w.	42
Figure 2.5a-b. SEM images of PLGA microparticles obtained by SEE-C by processing both single and double emulsions containing PLGA in concentration of (a) 5% w/w and (b) 10% w/w; Operating conditions: 80 bar and 38°C, L/G ratio 0.1.	44
Figure 2.6. PSDs of PLGA particles produced from single (<i>o-w</i>) emulsions containing 5% and 7.5% w/w of PLGA in the oily phase. The DSDs of the two emulsions processed by SEE-C are also reported (dashed curves), for comparison.	45
Figure 2.7. PSDs of PLGA particles produced from single and double emulsions containing 10% w/w of PLGA in the oily phase. The DSDs of the two emulsions processed by SEE-C are also reported (dashed curves), for comparison. The gap between PSD/DSD at D50 values for single emulsion is 0.74 μm); the gap between PSD/DSD at D50 values for double emulsion is 0.49 μm).	45
Figure 2.8. DSC traces of unprocessed and PLGA microparticles produced by SEE-C. The polymer glass transition did not change after SEE-C processing.	48
Figure 2.9. X-ray profiles of unprocessed and PLGA microparticles produced by SEE-C. The polymer is clearly amorphous in both case.	48
Figure 2.10. Schematic representation of the possible mass transfer pathways of the oily phase during the SEE-C process. Two parallel pathways: (A) diffusion of the organic solvent into water followed by subsequent supercritical extraction of the solvent from the aqueous	

phase; (B) direct supercritical extraction upon contact between SC-CO ₂ and the organic phase into the droplet.	49
Figure 2.11a-b. SEM images (Mag = 50.00 K X) related to a morphological study of PLGA microparticles degradation in water after 14 (a) and 34 days (b), respectively. The particles have a diameter of almost 3 μm and were produced by SEE-CM using a single (left side) and double <i>w-o-w</i> emulsions (right side).	51
Figure 2.12a-b. SEM image of the PLGA/VH microspheres obtained by SEE from <i>w-o-w</i> emulsion. Mean Size: 1.5 μm (SD ± 0.3 μm), Variation Coefficient: 40% (a). Particle Size Distribution (PSD) curve of PLGA/VH microspheres obtained by SC-CO ₂ extraction (continuous line) and Droplets Size Distribution (DSD) curve of the droplets in the emulsion before SC extraction (dashed line) (b).....	52
Figure 2.13a-b. Optical Microscope image of a double <i>w-o-w</i> emulsion (1:19:80 composition) containing PLGA in concentration of 10% w/w in the oily phase (HA is 9% w/w of PLGA) (a). SEM image of PLGA microspheres charged with HA (loading 6 % w/w) produced by SEE-C operating at 80 bar and 38°C, L/G ratio 0.1 (b).	53
Figure 2.14a-b. (a): Emulsion o-w ratio 20/80, Oil: 45% PLGA with 3% RA; Water 80% glycerol, 20% water and 0.6% PVA. (b): Emulsion o-w ratio 20/80, Oil:45% PLGA and 6% β-carotene; Water 80% glycerol, 20% water and 0.6% PVA.....	53
Figure 2.15a-b. SEM images of the PAMs produced (a): PLGA with 3% w/w of RA; PLGA with 6% β-carotene (b).	53
Figure 3.1. Phase diagram of water-glycerol-acetone ternary system with the representation of operating points I: <i>o-w</i> 20/80 and operating point II: <i>o-w</i> 10/90. Experimental data adapted from Matsumoto <i>et al.</i> , 2008.	59
Figure 3.2 a-b. SEM images of the microparticles obtained by SEE using emulsions with different <i>o-w</i> ratios; (a) well shaped microspheres using an <i>o-w</i> ratio of 20/80; (b) collapsed and connected microspheres using an <i>o-w</i> ratio of 10/90. <i>Oily phase</i> : acetone with 45% PLGA and 3% RA w/w (theoretical loading); <i>water phase</i> : glycerol-water 80:20 with 0.6% w/w of PVA.....	59
Figure 3.3a-b. SEM images of PLGA/RA microspheres produced by: (a) SEE-B; (b) conventional Liquid Extraction (LEE). Emulsion (<i>o-w</i> ratio 20/80) composition: <i>oily phase</i> , acetone with PLGA 45% w/w; <i>water phase</i> , glycerol-water 80:20 and 0.6% w/w of PVA.	60
Figure 3.4a-d. Optical microscope images of the emulsions and SEM images of the related microspheres produced by SEE-C using emulsions (<i>o-w</i> ratio 20/80) with different PLGA content in the oily phase of 45 (a-b) and 55% (c-d) w/w, respectively. The theoretical drug loading was of 3% RA w/w (effective loading 2.7 and 2.5 % respectively); <i>water phase</i> , glycerol-water 80:20 and 0.6% w/w of PVA.	64
Figure 3.5. DSC traces of PLGA/RA microspheres produced by SEE with a MS of 4.3 μm (SD ± 2.3 μm) and effective RA loading of 8.8% w/w. Traces of untreated PLGA and RA are also reported, for comparison.	65
Figure 3.6. XRD patterns of PLGA/RA microspheres produced by SEE with a MS of 4.3 μm (SD ± 2.3 μm) and effective RA loading of 8.8% w/w. Patterns of untreated PLGA and RA are also reported, for comparison.	65

Figure 3.7. Release profiles from PLGA microspheres with effective RA loadings of 2.7% (□), 5.2 % (Δ), 8.8 % (○). The release profile of pure RA is also proposed, for comparison (*). Curve fittings obtained using equation (4) are reported, as continuous line.	68
Figure 4.1a-b. OM image of 80% confluent embryonic ventricular myoblasts (cell line H9c2) obtained from rat cultivated in a standard medium(a); PLGA microspheres were suspended in the cell medium with cells stuck at the bottom of the culture flask (b).	74
Figure 4.2a-c. FE-SEM images of PLGA-PAMs obtained after the emulsion processing by SEE-C at 80 bar and 37°C. (a) PAMs with MD of 2 μm and loading of 3 mg/g; (b) PAMs with MD of 3 μm and loading of 3 mg/g; (c) PAMs with MD of 3 μm and loading of 6 mg/g.....	77
Figure 4.3. PSDs of the insulin-loaded PLGA-PAMs batches tested.	78
Figure 4.4a-b. Comparison between the release profiles (days) of insulin from PLGA-PAMs suspended in PBS with: (a) different MDs of 2 and 3 μm and charged with the same loading of 3 mg/g; (b) different loadings of 3 and 6 mg/g and with the same MD of 3 μm. Dashed lines are model fittings.	81
Figure 4.5a-b. Comparison between the release profiles (days) of insulin from PLGA-PAMs suspended in DMEM with: (a) different MDs of 2 and 3 μm and charged with the same loading of 3 mg/g; (b) different loadings of 3 and 6 mg/g and with the same MD of 3 μm. Dashed lines are model fittings.	81
Figure 4.6. Number of cells growth after 72 h of incubation with different PLGA-PAMs amounts (MD of 3 μm, insulin loading of 3 mg/g) against the insulin concentrations delivered in the serum free medium. The number of cell growth after 72 h in serum free media without PAMs is reported in red, for comparison.	83
Figure 4.7. Cell growth on PLGA-PAMs of different size 2 and 3 μm (insulin loading of 3 mg/g) into serum free media with a fixed insulin concentration ranging from 15-17 ug/mL released after 72 h.....	84
Figure 5.1a-b. Schematic representation of the bioactive scaffold charged in a tubular bioreactor (a). Image of the bioreactor with the four chambers (b).	90
Figure 5.2a-d. Optical microscope (OM) images of emulsion and FE-SEM image of the microspheres obtained by SEE-C. B1, only BSA charged PAMs; B2, BSA and h-Bone Morphogenic Protein 2 (h-BMP-2) charged PAMs; B3, BSA and h-Vascular Endothelial Growth Factor (h-VEGF) PAMs; B4, BSA and GFs mix (ratio 1:1) charged PAMs....	93
Figure 5.3. Particle Size Distribution curves of the PAMs produced by SEE-C; the size distribution curve of the droplets in emulsion is also reported in grey, for comparison purpose.	95
Figure 5.4. Release profiles (days) of GFs from PLGA-PAMs suspended in DMEM medium.	95
Figure 5.5a-b. A schematic representation of the bioactive scaffold with the PAMs (green), the cells (yellows and red) and the alginate gel (pink) (a); live & dead image of part of a bead taken from 28 days of cultivation with an enlargement of 10 X; the PAMs were stained in red (b).	96

Figure 5.6a-b. OM images of alginate beads sections reported with two different enlargements; sections of the alginate beads after Hematoxylin and Eosin staining observed at optical microscope with a phase contrast condenser; in the two images are evident the h-MSC in pink and the PAMs (as a white spots) uniformly distributed in the alginate matrix. 96

Figure 5.7a-c. FE-SEM images at different enlargements of the alginate beads fractured after its freezing in liquid nitrogen. PAMs are uniformly distributed in the gel matrix. The h-MSC is highlighted by a red circle. 97

Figure 5.8a-d. Alkaline phosphatase staining of alginate beads after 7 days of culture in a TPS. All the images are made with the 40 X objective. B1, empty; B2, h-BMP-2; B3, h-VEGF; B4, GFs mix (ratio 1:1). ALP activity is marked in brown and appeared well stained in the group B2 and B4, revealing a great influence of h-BMP-2 released into the scaffold on the earlier cell differentiation. 100

Figure 5.9a-d. Osteopontin (OPN) staining of alginate beads after 21 days of culture in a TPS. All the images are taken using a 40 X objective. B1, empty; B2, h-BMP-2; B3, h-VEGF; B4, GFs mix (ratio 1:1). OPN activity is marked in brown and appeared well stained in the group B2 and B4..... 101

Figure 5.10a-d. Osteocalcin (OCN) staining of alginate beads after 21 days of culture in a TPS. All the images are taken using a 40 X objective. B1, empty; B2, h-BMP-2; B3, h-VEGF; B4, GFs mix (ratio 1:1). OCN activity is marked in brown and appeared well stained in the group B2 and B4, confirming the great influence of h-BMP-2 released into the scaffold on the earlier cell differentiation. 102

Figure 5.11a-d. Von Kossa staining of alginate beads after 21 of culture in a TPS. All the images are taken using a 40 X objective. B1, empty; B2, h-BMP-2; B3, h-VEGF; B4, GFs mix (ratio 1:1). The calcium deposition started into the scaffolds belonging to all groups; however, a more homogeneous calcium deposition was always observed in the beads charged with PAMs able to release h-BMP-2 growth factors..... 103

List of Tables

Table 2.1. Evaluation of the Gf conditions varying the L/G ratio between 0.1 and 0.4 at fixed T = 38°C and P = 80 bar ($\rho = 0.31 \text{ g/cm}^3$) using the correlations previously discussed.	40
Table 2.2. Evaluation of the flooding conditions varying the density at fixed L/G = 0.1, using the correlations previously discussed. CO ₂ density of 0.31 g/cm ³ correspond to 80 bar and 38°C; 0.52 g/cm ³ to 100 bar and 44°C.	40
Table 2.3. Liquid and SC-CO ₂ flow rates used at different values of L/G.	40
Table 2.4. Dynamic laser scattering size distribution data of droplets (DSD) and of microparticles (PSD) produced at different PLGA concentrations in the oily phase using SEE-C of single (<i>o-w</i>) and double (<i>w-o-w</i>) emulsions. Legend: MS = mean size; SD = standard deviation; CV = coefficient of variation; SF = shrinking factor.	43
Table 2.5. Dynamic laser scattering size distribution data of droplets contained in double <i>w-o-w</i> emulsions and related PLGA microparticles size distribution produced using standard SEE layout, SEE-C and solvent evaporation process (SE). Legend: MS = mean size; SD = standard deviation; CV = coefficient of variation.	46
Table 3.1. Results of liquid emulsion extraction (LEE) and supercritical extraction (SEE-B) proposed in term of PSDs produced using an <i>o-w</i> emulsion (ratio: 20:80).	61
Table 3.2. Results of different SEE process layouts batch (B) and continuous (C) proposed in term of PSDs of the microspheres produced using an <i>o-w</i> emulsion (ratio 20:80).	62
Table 3.3. DSDs and PSDs of microspheres produced by SEE-C using an <i>o-w</i> emulsion (ratio 20:80; PLGA concentration: 45% and 55% w/w; drug loading: 3% w/w).	63
Table 3.4. Best fit model parameters estimated from RA release profiles obtained from PLGA microspheres.	68
Table 4.1. Characteristics of the PLGA-PAMs produced by SEE-C technology: Mean Diameter (MD) and Standard Deviation (\pm), theoretical (TL) and effective (EL) insulin loading and encapsulation efficiency (EE); percentage amount of insulin released in DMEM media after 72 h (that corresponds to the period selected to monitor the cell growth on PAMs).	76
Table 4.2. Best fit model parameters estimated from insulin release profiles obtained from PLGA-PAMs of different sizes and protein loadings and in different media: phosphate buffer solution (PBS) and Dulbecco's Modified Eagle Medium (DMEM).	82

Abstract

Biopolymer microcarriers with an adapted size and/or a special coating can serve as a support for cell culture and/or differentiation when embedded in more complex 3D scaffold for local sustained delivery of biological signal. The programmed delivery of an appropriate active principle and/or growth factor can stimulate the grafted cells survival and differentiation and also modify the host microenvironment. *Poly-lactic-co-glycolic acid* (PLGA) is a well-know biocompatible and bioresorbable polymer which has received a great interest for the development of nanostructured microdevices to be used in tissue engineering; as a consequence, considerable scientific efforts have been made in the technology for the manufacturing these microdevices. Supercritical Emulsion Extraction (SEE) was recently proposed for the production of biopolymer microparticles starting from *oil-in-water* emulsions. This technology can improve the product quality because of the fast and selective extraction of the dispersed oily phase by using supercritical carbon dioxide (SC-CO₂). However, until now, SEE was proposed in batch configuration, sharing with the traditional processes an intrinsically discontinuous operation, problems of batches reproducibility and process yield.

In this study, by using a counter-current packed column, the SEE process was proposed in a Continuous operating mode (SEE-C) for the production of PLGA microcarrier loaded with bioactive signals. The new process design takes advantage of the large contact area between the SC-CO₂ and emulsion allowing the production of microspheres with controlled and narrow size distributions in only few minutes. SEE-C operating parameters such as pressure, temperature and flow rate ratios were analyzed and the process efficiency was optimized in terms of size distribution of the recovered material and encapsulation efficiency, and it was compared with the one of SEE (in batch operation mode) and conventional evaporation/extraction technology. PLGA microparticles showed a mean particle size between 1-3 μm (depending on the droplet sizes) with a standard deviation that was always smaller than that associated with particles produced by discontinuous processes. Single and double emulsions were successfully treated and the microdevices physico-chemical properties were investigated. Several bioactive compounds were selected to be encapsulated. In the case of retinyl acetate (RA), for example, several emulsions were tested and processed by SEE-C. Operating at 80 bar and 36°C, SEE-C produced PLGA/RA microspheres with mean sizes between 3.3 and 4.5 μm with an excellent encapsulation efficiency (90%). The investigation

of the release profiles showed that all the RA was released in about 6 days when charged at 2.7% w/w; whereas, only 40% and 10% of RA was released in the same period of time when the charge was 5.2% and 8.8% w/w, respectively. Release kinetics constants calculated from the experimental data by using a mathematical model were also proposed. PLGA microdevices loaded with bovine serum insulin, selected as a model of bioactive signal, were also produced. Different sizes (2 and 3 μm) or insulin charges (3 and 6 mg/g) and with a good encapsulation efficiency (60%) were obtained by SEE-C after processing of several *water-oil-water* emulsions. These microcarriers were characterized in terms of insulin release profile in two different media (PBS and DMEM) and the diffusion and degradation constants were also estimated by using a mathematical model; a faster insulin release in the first two days was observed, followed by its sustained release for the subsequent 28 days. These microdevices were also used in a cultivation of embryonic ventricular myoblasts (cell line H9c2 obtained from rat) in a FBS serum free medium to monitor cell viability and growth in dependence of insulin released. Good cell viability and growth were observed on 3 μm microdevices loaded with 3 mg/g of insulin. PLGA microspheres loaded with growth factors (GFs) were also charged inside an alginate scaffold together with *human* Mesenchymal Stem Cells (hMSC), that are promising cell source for bone tissue engineering. The aim was to monitor the effect of the local release of these signals on cells differentiation. These “living” 3D scaffolds were incubated in a direct perfusion tubular bioreactor to enhance nutrient transport and exposing the cells to a given shear stress. Different GFs such as, h-VEGF, h-BMP2 and a mix of two (ratio 1:1) were loaded by processing several *water-oil-water* emulsions at 80 bar and 36°C, with an L/G ratio of 0.1 by SEE-C. Alginate beads were recovered from dynamic (tubular perfusion system bioreactor) and static culture at different time points (1st, 7th, 21st days) for the analytical assays such as, live/dead; hematoxylin and eosin (H&E) staining; alkaline phosphatase; osteocalcin; osteopontin and Van Kossa Immunoassay. The immunoassay confirmed always a better cells differentiation in the bioreactor with respect to the static culture and revealed a great influence of the BMP-2 released in the scaffold on cell differentiation. Indeed, a more homogeneous calcium deposition and a larger cell cluster were observed in the beads charged with BMP-2.

Introduction

Tissue engineering is an emerging multidisciplinary field involving biology, medicine, and engineering that is likely to revolutionize the ways we improve the health and quality of life for millions of people worldwide by restoring, maintaining, or enhancing tissue and organ function. In addition to having a therapeutic application, where the tissue is either grown in a patient or outside the patient and transplanted, tissue engineering can have diagnostic applications where the tissue is made *in vitro* and used for testing drug metabolism and uptake, toxicity, and pathogenicity. The foundation of tissue engineering for either therapeutic or diagnostic applications is the ability to exploit living cells in a variety of ways.

Tissue engineering research includes the several areas such as, *novel biomaterials* that are designed to direct the organization, growth, and differentiation of cells in the process of forming functional tissue by providing both physical and chemical cues; methodologies for cells proliferation and differentiation to acquire the appropriate source of cells such as autologous (from the same individual to which they will be reimplanted), allogeneic (from donor of the same species), xenogeneic (from individuals of another species), stem cells (undifferentiated cells with the ability to give rise to different forms of specialized cells) and genetically engineered cells; *engineering design and biomechanical aspects* including 2D cell expansion, 3D tissue growth in bioreactors, vascularisation, mechanical signals regulating engineered tissues and efficacy and safety of engineered tissues. Informatics may also support tissue engineering helping the quantitative cellular image analysis, quantitative tissue analysis, *in-silico* tissue and cell modelling and digital tissue manufacturing, as well as, research that involves stem cells (human and non-human) in which they are isolated, derived or cultured for studying cellular differentiation or specialization in presence of specific growth factors, 3D biomaterials or mechanical solicitations. The term *regenerative medicine* is often used synonymously with tissue engineering, although those involved in regenerative medicine place more emphasis on the use of stem cells to produce tissues [1].

Tissue engineering utilizes living cells as engineering materials; they are often implanted or “seeded” into an artificial structure capable of supporting three-dimensional tissue formation. These structures, typically called *scaffolds*, are often critical, both *ex vivo* as well as *in vivo*, to influence their own microenvironments. Scaffolds usually serve the

following purposes: allow cell attachment and migration, deliver and retain cells and biochemical factors, enable diffusion of vital cell nutrients and expressed products and exert certain mechanical and biological influences to modify the behavior of the cell phase. To achieve the goal of tissue reconstruction, scaffolds must meet some specific requirements. A high porosity and an adequate pore size are necessary to facilitate cell seeding and diffusion throughout the whole structure of both cells and nutrients. Biodegradability is often an essential factor since scaffolds should preferably be absorbed by the surrounding tissues without the necessity of a surgical removal. The rate at which degradation occurs has to coincide as much as possible with the rate of tissue formation. Injectability is also important for clinical uses. Recent research on organ printing is showing how crucial a good control of the 3D environment is to insure reproducibility of experiments and offer better results.

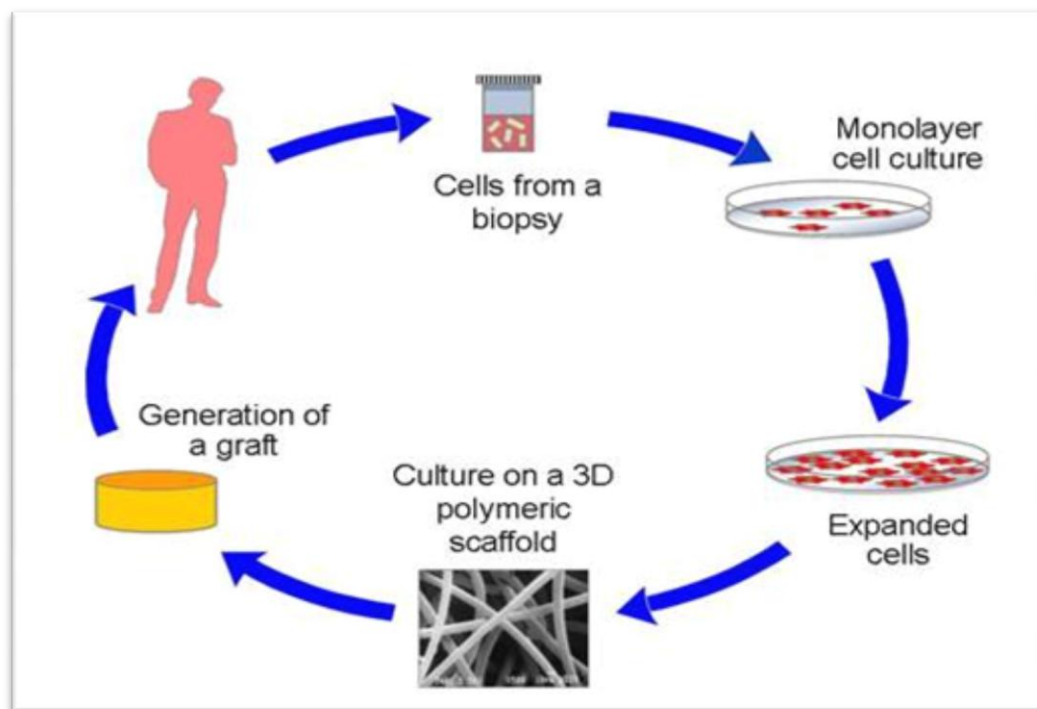


Figure I.1. Basic principles of Tissue Engineering.

Chapter 1. State of the Art

1.1 *Tissue engineering: top-down & bottom-up approaches*

The field of tissue engineering has emerged to fill the void where neither native physiology nor purely artificial implantable materials can sufficiently replace or repair these damaged tissues [2]. While tissues such as bone [3] or skin [4-5] can effectively repair a small injury given sufficient time, many tissues such as myocardium [6] and cartilage [7] do not regenerate properly without intervention. Traditional tissue engineering strategies typically employ a “*top-down*” *approach*, in which cells are seeded on a biodegradable polymeric scaffold [8-10]. In top-down approaches, the cells are expected to populate the scaffold and create the appropriate extracellular matrix (ECM) and micro-architecture often with the aid of perfusion, growth factors and/or mechanical stimulation [11].

The *bottom-up approach*, also known as modular tissue engineering, aims to address the challenge of recreating bio-mimetic structures by designing structural micro-features to build modular tissues that can be used as building blocks to create larger tissues. These modules can be created in different ways, such as through self-assembled aggregation [12], microfabrication of cell-laden hydrogels [13], creation of cell sheets [14] or direct tissue printing [15]. Once created, these modules can be assembled into larger tissues through a number of methods such as random packing [16-17], stacking of layers [18] or directed assembly [19]. By mimicking native micro-structural functional units, bottom-up approaches aim to create more bio-mimetic engineered tissues. The historical roots of this modular approach trace back to microencapsulation techniques, such as encapsulating pancreatic islet cells in alginate gels for transplantation in diabetic rats [20]. Although these studies were not conceived as modular tissue engineering, each cell-containing microcapsule behaves as a tissue module performing a particular function. Current techniques for creating modular tissues draw from research in microencapsulation and micro-fabrication, as well as, traditional cell and tissue culture procedures. By creating modular tissues with more physiological micro-architectural features, bottom-up tissue engineering aims to provide more guidance on the cellular level to direct tissue morphogenesis.

The major challenges to overcome in the future will be the potential integration of bottom-up techniques with more traditional top-down approaches to create more complex

tissues than are currently achievable using either technique alone by optimizing the advantages of each technique. Modular tissue engineering possesses immense potential for advancing the fields of tissue engineering while bringing us closer to the ultimate goal of creating clinically relevant engineered tissues for human implantation and the treatment of disease [21].

1.2 Materials for scaffolds fabrication

Biopolymers are the materials mainly used for scaffolds in various tissue engineering applications. *Poly-(glycolic acid)* (PGA), *poly-(lactic acid)* (PLA), and their copolymers are a family of linear aliphatic polyesters, which are the most frequently used in tissue engineering. These polymers degrade through hydrolysis of the ester bonds. PGA is one of the most widely used scaffolding polymers. Because of its relatively hydrophilic nature, PGA degrades rapidly in aqueous solutions or in vivo, and loses mechanical integrity between two and four weeks. PLA is also widely used for scaffold fabrication. The extra methyl group in the PLA repeating unit (compared with PGA) makes it more hydrophobic, reduces the molecular affinity to water, and leads to a slower hydrolysis rate. It takes many months or even years for a PLA scaffold or implant to lose mechanical integrity in vitro or in vivo. To achieve intermediate degradation rates between PGA and PLA, various lactic and glycolic acid ratios are used to synthesize PLGA.

Particularly, *Poly-lactic-co-glycolic acid* (PLGA, with a copolymer ratio of 75:25 or 50:50) has received a great interest for the development of injectable micro-particulate devices [22]. For example, PLGA micro particles can be administered by in-situ injection to achieve a precise and localized drug delivery which is more effective in chemotherapy, hormone therapy, DNA/protein or vaccine delivery [23-26]. Moreover, PLGA micro particles with a specific size and distribution have also been proposed for the use in tissue engineering as building blocks of implantable 3D scaffolds offering benefits such as good morphology control and better versatility in the release kinetics of specific growth factors for cellular function orienting and directing or biodegradable support for cell culture and/or cell administration [27].

There are other linear aliphatic polyesters, such as *poly-(ϵ -caprolactone)* (PCL) and *poly-(hydroxy butyrate)* (PHB), which are also used in tissue engineering research. PCL

degrades at a significantly slower rate than PLA, PGA, and PLGA. The slow degradation makes PCL less attractive for general tissue engineering applications, but more attractive for long-term implants and controlled release applications. Natural polymers are also used such as proteins and polysaccharides. Collagen is a fibrous protein and a major natural extracellular matrix component. It has been used for various tissue regeneration applications [28].

1.3 Injectable scaffolds & Pharmacologically Active Microcarriers

For some specific tissue regeneration, the cell therapy and the in-vivo approach will probably become a major therapeutic strategy in the coming years. Nevertheless, to overcome certain problems such as cell survival, lack of cell differentiation and integration in the host tissue a new tool described as *pharmacologically active microcarriers* (PAMs) have been described. PAMs are bioresorbable microparticles coated with cell adhesion molecules and presenting a controlled delivery of growth factor. In this configuration they may serve as a support for cell culture, survival and differentiation, as well as to influence their microenvironment. Indeed, the combined effect of growth factor and coating can influence the transported cells by promoting their survival and differentiation and favoring their integration in the host tissue after PAMs complete degradation. Furthermore, the released factor may also influence the microenvironment. Several studies indicated that PAMs could be a promising strategy for cell therapy of neurological diseases and could be employed in other situations with fetal cell transplants or with stem cells [29-30]. For example, PLGA-PAMs coated with adhesion molecules and loaded with nerve growth factor (NGF) and conveying PC12 cells, were produced and characterized. These cells showed the ability to differentiate into sympathetic-like neurons after adhering to PAM substrates in the presence of NGF and, can then, release large amounts of dopamine. Certain parameters such as, the size of the microcarriers, the conditions enabling the coating of the microparticles and the subsequent adhesion of cells have to be optimized to produce engineered microdevices.

PLGA microspheres have been also reported as a moldable scaffold for cartilage tissue engineering [31-33]. For example, PLGA based cell carrier has been obtained with RGDS peptides immobilized by bonding with the gelatin molecules under the catalyzation of water soluble carbodiimide (EDAC). Chondrocytes were thus cultured to detect the applicability of the microspheres, as the injectable cell carriers. It is known that the RGD peptide family can bind with the integrins on cell membrane, thus facilitating cell adhesion. Cell adhesion is the

first event in which the anchorage-dependent cells come into contact with a substrate. Only after that event the cells can spread and proliferate. Since the gelatin contains also lots of bioactive domains including RGD peptides, the adopted strategy then results in more cytocompatible microcarriers which are suitable to attract and deliver live cells such as chondrocytes. PLGA/gelatin-RGDS microspheres revealed their applicability as chondrocyte microcarriers and as injectable scaffold for *in vivo* chondrogenesis [34].

Microspheres seeded with specific cells can be also considered as smaller building blocks in a recent approach [35]. For example, micrometric Tissue Precursors (microTPs) were obtained by dynamic cell seeding of bovine fibroblasts on porous gelatine microcarriers using a spinner flask bioreactor. During the dynamic seeding, cells adhered, proliferated and synthesized a thin layer of extracellular matrix (ECM) in and around the macroporous beads, generating the microTPs. The cells and ECM layer around the microTPs allowed their biological sintering via cell-cell and cell-matrix interaction after only a few days of dynamic seeding. The assembling ability of microTPs was exploited and the results obtained in this survey pave the way to realizing a 3-D dermal tissue equivalent by means of a bottom-up tissue engineering approach.

1.4 Scaffold by conventional technologies: top-down approach

In the *top-down approach* the *scaffold* is an artificial extracellular matrix which supports three-dimensional cellular tissue formation. It has to be characterized by an high porosity ($\geq 90\%$), by a proper cell size and high interconnectivity (for uniform cell seeding and easy nutrients/metabolites diffusion); by biodegradability associated with mechanical integrity (to maintain the predesigned tissue structure) and it is also expected a positive interaction with cells, including enhanced cell adhesion, growth, migration, and differentiated function [36]. The most commonly used method for fabricating scaffolds for tissue engineering is the *solvent casting and particulate leaching*. This method involves mixing water-soluble salt (sodium chloride, sodium citrate) particles into a biodegradable polymer solution. The mixture is then cast into the mold of the desired shape. After the solvent is removed by evaporation or lyophilization, the salt particles are leached out to obtain a porous structure. The advantages of the method are the possibility of obtaining controlled porosity and interconnection degree. On the other hand, several post-treatments on the scaffolds are

required to eliminate the residual solvents and the smooth wall usually obtained that are not suitable for the cellular growth [37].

Emulsion freeze-drying technique was also used for the fabrication of highly porous PLGA scaffolds. The processing method consists of creating an emulsion by homogenization of a polymer solution (in an organic solvent) and water mixture, rapidly cooling the emulsion to lock in the liquid state structure, and removing the solvent and water by freeze-drying. Scaffolds with porosity greater than 90% and a cell size ranging from 20 to 200 μm can be fabricated with this method [38]. One important disadvantage of this technique is the closed cell structure obtained in the resulting matrix; moreover, it is not simple to control the cell size.

Electrospinning is a fabrication process that uses an electric field to control the formation and deposition of polymer fibers onto a target substrate. In electrospinning, a polymer solution or melt is injected with an electrical potential to create a charge imbalance. At a critical voltage, the charge imbalance begins to overcome the surface tension of the polymer solution to form an electrically charged jet. The jet within the electric field is directed toward the ground target, during which time the solvent evaporates and fibers are formed. This electrospinning technique can fabricate fibrous polymer scaffolds with fiber diameters ranging from several microns down to several hundred nanometers [39]. Limitations to produce scaffold with this technique are: low mechanical strength and difficult in controlling cells shape and cells size.

Rapid prototyping is a technology based on the advanced development of computer science and manufacturing industry. The main advantage of these techniques is their ability to produce complex products rapidly from a computer-aided design (CAD) model. One of these rapid prototyping techniques, called 3D printing, has been used to process biodegradable polymer scaffolds for tissue engineering applications [40]. This process generates components by ink-jet printing a binder on to sequential powder layers. The operation parameters such as the speed, flow rate, and drop position can be computer controlled to produce complex 3D polymer scaffolds. Biological agents, such as growth factors, can also be incorporated into the scaffolds in the printing process. However, the limitation of this method is that the resolution is determined by the jet size, which makes it difficult to design and fabricate scaffolds with fine microstructures.

Phase-separation techniques have been used to fabricate porous membranes for filtration and separation. Controlled phase separation processes, primarily thermally induced phase separation (TIPS), have been also explored for scaffolds fabrication [41]. This technique was recently utilized to fabricate biodegradable 3D polymer scaffolds. With this technique it is possible to obtain a fibrous structure with small pore size. On the other hand, the phase separation presents various problems such as, mean pore size obtained is often too small, long time of processing and post-treatments to eliminate the residual solvent are also necessary.

Gas foaming process can be used to fabricate highly porous polymer foams without the use of organic solvents. Recently, also supercritical carbon dioxide (CO₂) has been used as an agent for the formation of polymer foams. Solid polymer disks are exposed to high pressure CO₂ to allow saturation of CO₂ in the polymer. Thermodynamic instability is then created by rapidly releasing CO₂ gas from the polymer system, followed by the nucleation and growth of gas bubbles in the material. Polymer sponges with a cell size of 100 µm and porosity up to 93% can be fabricated using this technique. The disadvantage of this method is that it yields mostly a nonporous surface and closed-cell structure, with only 10–30% of interconnected cells. The porosity and inter-cell connectivity can be significantly improved by combining particulate leaching technique with the gas-foaming process although completely eliminating closed cells remains challenging [42].

One of the major challenges of *bottom-up tissue engineering approach* is to assemble modular tissues with specific micro-architectures into macroscale bio-mimetic engineered tissues. The challenge is to retain the micro-architecture and cellular behavior of modular tissues, while creating engineered tissues with robust mechanical properties to withstand clinical implantation and interact appropriately with the native tissues. *Micro & nano particles sintering* technology can be also considered a bottom-up approach rely upon the employment of biomaterials that integrate biodegradable scaffolds with growth factor delivery devices to better guide cellular activities and enhance tissue neogenesis. These bioactive scaffolds are recently obtained through the thermal assembly of protein activated PLGA or PCL microspheres and larger protein free microspheres obtained by emulsion evaporation technology. It is shown that the pore dimension, interconnectivity and mechanical properties in compression of the scaffold could be predefined by an appropriate choice of the size of the protein-free microparticles and sintering process conditions. These matrices offer the

possibility to concurrently modulate and control the size and extension of the porosity, mechanical properties and the spatial-temporal distribution of multiple bioactive signals [43]. The methods to produce microsphere-based scaffolds are: heat-sintering and solvent vapour treatment (dichloromethane) or solvent/non-solvent sintering method (acetone and ethanol treatment) or a non-solvent sintering technique (ethanol treatment); all of which involve exposure to elevated temperatures or organic solvents that may be a potential limitation to their pharmaceutical or medical applications.

Additive photo-crosslink of cell-laden hydrogels technique uses 2D arrays of cells and ExtraCellular Matrix (ECM)/polymers as the building blocks to create tissues layer-by-layer [44-45]. Using additive photopolymerization, dual layer modular tissues were created to fabricate living tissues of cellular hydrogels for hepatic tissue engineering. While this technique successfully creates modular tissues with geometries similar to the native hepatocyte environment, one potential drawback of this technique is the inability to restrict the thickness of subsequent layers. Despite progress in using micro-fabrication techniques to improve the vascularization of engineered tissues this limitation is still present in many engineered tissues. In an alternative approach to creating capillary networks, a *random packing of encapsulated modules technology* was developed to create tortuous channels of perfusable modular tissues. Cylindrical, perfused tissues were created by assembling cell-laden collagen units together within perfused tubing [46-47].

Tissue printing deposits cells in small groups using similar technology to traditional printing systems. The advantage of this technique is the high potential level of control in cell and ECM placement and alignment to create engineered tissues with a wide array of properties and geometries. Replacing ink with cells suspended in liquid ECM or self assembled ECM mimics, a specific pattern is designed and printed onto a substrate, then the resultant cell aggregate is cultured to allow the cells and ECM to integrate into tissue structures [48-49]. While this technique could be effective in creating modular 2D tissues, one disadvantage of this technique is the impact on cell viability in the time elapsed between creation of subsequent tissue layers. Finally, one technique that has successfully addressed the insufficient mechanical properties and cell alignment in engineered modular tissues is *cell sheet engineering*, by creating sheets of cells under conditions that encourage ECM production. Engineered modular tissues, made using these techniques, have shown mechanical properties on the order of native tissues. Some potential limitations, however, are

the limited possible geometries that can be fabricated using sheets as well as reported leaking between layers indicating insufficient joining between them [50].

1.5 Biopolymer microdevices by conventional technologies: bottom up approach

Several techniques can be used to prepare biopolymer microcarriers, but the *solvent evaporation/extraction of emulsion* (single, double or multiple) is the most widely used. In the most simplified case (*i.e., the single emulsion processing*) the process involves *oil-in-water (o/w)* emulsification. The polymer is first dissolved in a water immiscible, volatile organic solvent. The drug is then added to the polymer solution to produce a solution or dispersion of the active substance. This polymer-solvent-drug solution/dispersion is, then, emulsified (with appropriate stirring and temperature conditions) in a larger volume of water in presence of an emulsifier (as poly-vinyl alcohol, PVA) to yield an *o/w* emulsion. The emulsion is subjected to solvent removal by either evaporation or extraction process to harden the oil droplets [51]. In the former case, the emulsion is maintained at reduced pressure or at atmospheric pressure, with a low stir rate to enable the volatile solvent to evaporate. In the latter case, the emulsion is transferred into a large quantity of water (with or without surfactant) or other quench medium, into which the solvent associated with the oil droplets is diffused out. The solid microspheres obtained are, then, washed and collected by filtration, sieving, or centrifugation. They are dried under appropriate conditions or lyophilized.

One of the disadvantages of the *o/w* emulsification method is the poor encapsulation efficiencies of moderately water-soluble and water-soluble drugs. The drug could diffuse out or partition from the dispersed oil phase into the aqueous continuous phase and microcrystalline fragments of the hydrophilic drugs can be deposited on the microsphere surface and dispersed in the polymer matrix [52].

The *double (or multiple) emulsion processing* is a water-in-oil-in-water (*w/o/w*) method and is best suited to encapsulate water-soluble drugs like peptides, proteins, and vaccines, unlike the *o/w* method which is ideal for water-insoluble drugs. A buffered or plain aqueous solution of the drug (sometimes containing a viscosity enhancer and/or stabilizing protein like gelatin) is added to an organic phase consisting of the polymer and an organic solvent with vigorous stirring to form the first microfine *w/o* emulsion. This emulsion is gently added with

stirring into large-volume water containing an emulsifier to form the *w/o/w* emulsion. The emulsion is, then, subjected to solvent removal by either evaporation or extraction process. The solid microspheres so obtained are then washed and collected by filtration, sieving, or centrifugation. These are then dried under appropriate conditions or are lyophilized to give the final free flowing microsphere product. It should be noted that the solvent evaporation process is similar to the extraction ones; i.e., the solvent must first diffuse out into the external aqueous dispersion medium before its evaporation. The rate of solvent removal by the extraction method depends on the temperature of quench water or other medium, ratio of emulsion volume to quench water/medium volume and the solubility characteristics of the polymer, the solvent and the dispersion medium. The rate of solvent removal by evaporation method strongly influences the characteristics of the final microspheres and it depends on the temperature, pressure, and the solubility parameters of the polymer, the solvent, and the dispersion medium [53]. Solvent evaporation has several drawbacks because it requires relatively high temperatures or reduced pressures and shows batch to batch reproducibility disturbances. Solvent extraction uses relatively large amounts of a second solvent with the subsequent problem of solvent mixtures recovery. Both processes, also, require quite long processing times (several hours) and, as a consequence, aggregation phenomena may occur between the droplets, producing microspheres with a larger poly-dispersity with respect to the droplets in the starting emulsion [54].

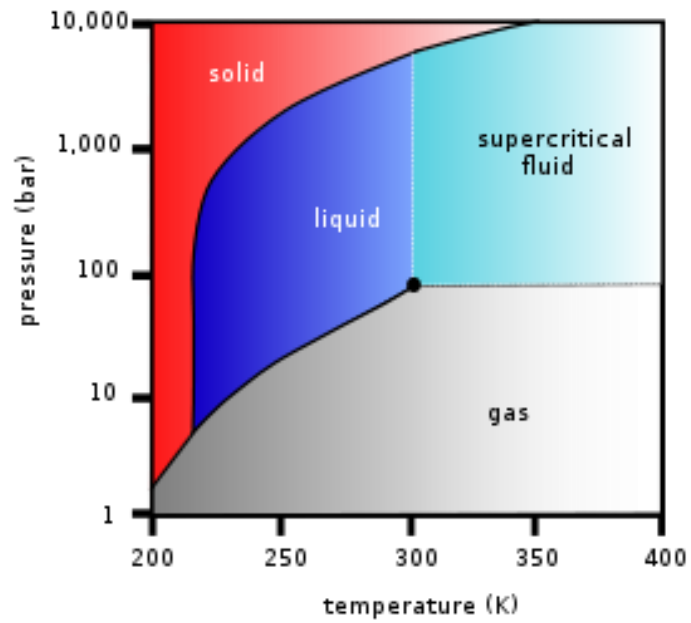
Spray-drying is also used for biopolymer microsphere production because it is a relatively simple and of high throughput technology, but, cannot be used for almost all the PLGA co-polymer ratios because many of them are highly temperature sensitive biopolymers. As a consequence the production of PLGA submicro and microparticles with a controlled and narrow particle size in a robust and reproducible manner is still a challenge [55].

1.6 About Supercritical fluids

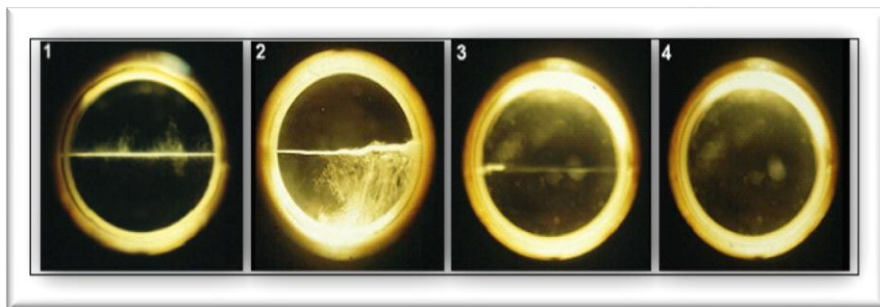
A supercritical fluid (SCF) is any substance at a temperature and pressure above its critical point. It can effuse through solids like a gas, and dissolve materials like a liquid. In addition, close to the critical point, small changes in pressure or temperature result in large changes in density, allowing many properties of a supercritical fluid to be "fine-tuned". Supercritical fluids are suitable as a substitute for organic solvents in a range of industrial and laboratory processes.

There is also reduced surface tension in a supercritical fluid, as well as, no liquid/gas phase boundary and by changing the pressure and temperature of the fluid, the properties can be *tuned* to be more *liquid-* or *gas-like*. One of the most important properties is the solubility of material in the fluid; it increases with density of the fluid (at constant temperature); whereas, at constant density, it increases with temperature. However, close to the critical point, the density can drop sharply with a slight increase in temperature. Therefore, close to the critical temperature, solubility often drops with increasing temperature, then rises again [56]. The continuous adjustable solvent power/selectivity obtainable by varying pressure and temperature of a supercritical fluid can be used in different sections of the plant to obtain different extraction/separation performances. The diffusivity of supercritical fluids is similar to that of gases; it is about two orders of magnitude larger than that of liquid solvents.

Carbon dioxide and water are the most commonly used supercritical fluids, nowadays used in several industrial processes, such as, coffee decaffeination and power generation, respectively. Particularly, carbon dioxide (SC-CO₂) behaves like a lipophilic solvent, it is not toxic, non flammable, it does not produce pollution (it is not produced during the process and is used many times before discharge), it is very cheap and its critical parameters of pressure and temperature are readily accessible on the industrial scale. **Figures 1.1** show projections of a carbon dioxide phase diagram. In the pressure-temperature phase diagram the boiling separates the gas and liquid region and ends in the critical point, where the liquid and gas phases disappear to become a single supercritical phase. At well below the critical temperature (280K for CO₂), as the pressure increases, the gas compresses and eventually (at just over 40 bar) condenses into a much denser liquid, resulting in the discontinuity in the line (vertical dotted line). The system consists of 2 phases in equilibrium, a dense liquid and a low density gas. As the critical temperature is approached (300K for CO₂), the density of the gas at equilibrium becomes denser and that of the liquid lower. At the critical point, (304.1 K and 73.8 bar for CO₂), there is no difference in density and the two phases become one fluid phase. Thus, above the critical temperature a gas cannot be liquefied by pressure. At slightly above the critical temperature (310K for CO₂), narrow to the critical pressure, the line is almost vertical; it means that a small increase in pressure causes a large increase in the density of the supercritical phase. Many other physical properties also show large gradients with pressure near the critical point, e.g. viscosity, the relative permittivity and the solvent strength, which are all closely related to the density.



(a)



(b)

Figure 1.1a-b. (a) Carbon dioxide pressure-temperature phase diagram; (b) Images of supercritical carbon dioxide in the biphasic region (1) in the supercritical passage near the critical point (2-4).

1.7 *Supercritical fluids technologies for scaffolds production*

The first use of SCF for temporary scaffolds production has been tested into the *SC gas-foaming technique* (also described previously). The process is solventless and very efficient in producing the porous biopolymeric structure, but generally closed-cells structures are generated; therefore, a CO₂ foaming plus solid porogen technique (i.e., foaming/particulate leaching technique) to overcome the limited cell connectivity of the scaffolds was adopted [57]. For example, *Mathieu et al.* [58]. have shown that the morphology of the foams can be controlled to mimic the bone structure. Bone from different sites around the body is anisotropic, both morphologically and mechanically. They found that similar anisotropic structures can be formed by controlling the depressurization rate of the foamed PLLA and the density of the gas: rapid depressurization locked in large numbers of spherical cells, whereas a slower depressurization enabled cell elongation. However, in the foaming process, the rough nano-porous internal structure that should mime the natural extra-cellular matrix necessary to obtain a good cell adhesion and growth is completely missing.

Another technology proposed for scaffold production is the *supercritical assisted phase inversion*. Compared with the traditional phase inversion method the main advantage is that SC-CO₂ can dry the polymer membrane rapidly and totally avoiding structure due to the absence of a liquid-vapour interface. Moreover, the dry polymeric structures can be obtained without additional post-treatment because there are no traces of organic solvents. The substitution of SCF to the traditional liquid non-solvent phase allows for the tuning of antisolvent strength (density) by means of pressure introducing an additional variable to influence the demixing process and the membrane morphology. For example, *Tsivintzelis et al.*, [59] reported that it is possible to control the scaffolds morphology changing the operative conditions; indeed, the average pore size decreased with the increase of CO₂ density either by increasing the pressure or by decreasing the temperature, whereas the average pore diameter decreased with the increase of the initial polymer concentration. All the nano-composite materials exhibited more uniform cellular structures with large pores than the pure polymer. However, the structures obtained using this approach suffers various limitations. Indeed, it is very difficult to obtain complex 3D structures and rough nanofibrous internal structure that should mime the natural extra-cellular matrix necessary to obtain a good cell adhesion and growth (smooth cell walls are usually obtained).

To fulfil the necessity of producing interconnected microcells and a nanometric substructure, a new supercritical fluid assisted technique for the formation of 3D PLLA scaffolds has been proposed [60]. It consists of three sub-processes: the formation of a polymeric gel loaded with a solid porogen, the drying of the gel using SC-CO₂, the washing with water to eliminate the porogen. When PLLA gel drying is performed by supercritical CO₂, the supercritical mixture formed during the process (solvent plus CO₂) has no surface tension and can be easily eliminated in a single step by the continuous flow of SC-CO₂ in the drying vessel. The major problem in gel drying is the possibility of gel collapse. In this case, the absence of surface tension avoids this problem preserving the nanoporous structure. On the other side, large interconnected cavities necessary to mime the tissue to be replaced are completely missing. To overcome this limitation, the authors proposed a hybridization of the supercritical drying process with the particulate leaching. These scaffolds were successfully tested for human mesenchymal cells cultivation [61].

1.8 Supercritical fluids technologies for microcarriers production

In the last ten years, different supercritical fluid technologies were tested to produce PLGA nano and microdevices such as, the *Rapid Expansion of Supercritical Solutions* (RESS) and the *Supercritical AntiSolvent* (SAS) [62]. In RESS technology, SC-CO₂ solubilizes the compound to be treated and produces microparticles by a rapid decompression of the supercritical solution and the subsequent oversaturation of the solubilized biopolymer. SAS technique uses SC-CO₂ as anti-solvent agent to induce the biopolymer precipitation from its liquid solution. The main problem reported for RESS technology is the very low solubility of almost all PLGA co-polymers in SC-CO₂ that will prevent affordable process yields or will require the use of co-solvent [63]. On the other hand, the solubility of SC-CO₂ in the PLGA (even if very low) is again the main problem for SAS technology. Indeed, the SC-CO₂ solubility in PLGA microparticles caused their agglomeration in products with irregular shapes [64] or recovered with a low yield due to the strong tendency to form a film [65]. It is also worth of mention that PLGA is able to uptake CO₂ by sorption, leading to a significant decrease in its glass transition temperature [66] that will advantage the formation of glued particles.

The use of SC-CO₂, for PLGA microparticles manufacturing, has also been proposed starting from emulsions containing PLGA in the dispersed oily phase. Particularly, SC-CO₂

was proposed as extracting agent of the oily phase of *oil-in water (o-w)* emulsions to lead to solvent-free microparticles [67-68]. In details, the Supercritical Emulsion Extraction process (SEE) produces an aqueous suspension of PLGA microparticles using CO₂ to extract the solvent of the oily phase of an *oil-in-water* emulsion. In the SEE process, the above mentioned PLGA microparticles aggregation phenomena, were not observed, due to the presence of the external water phase, immiscible with SC-CO₂, which prevents their aggregation [69]. One of the major limitations of the SEE technology, also shared with traditional evaporation/extraction processes, is the fact that this process is intrinsically discontinuous. Indeed, a batch of emulsion can be treated for each run; therefore, from a biotechnological and regulatory point of view, there will be problems of batches reproducibility and low process yield, due to material lost on the walls of the precipitation vessel.

As discussed above, PLGA microcarriers also attracted significant attention in recent years, as building blocks for sintered scaffold formation offering several benefits including control over morphology and physicochemical characteristics and versatility of encapsulated factors release kinetics. The properties of a scaffold, in turn, can be tailored by altering the microsphere design and fabrication method, e.g., to create gradient-based scaffolds. In lieu of conventional temperature-regulated or organic solvent-assisted scaffold fabrication, supercritical fluid (SCF) technology has offered an alternative method of melt processing of the polymers. *Singh et al.* [70] capitalizing on the plasticizing ability of CO₂, described a novel microsphere-based scaffold fabrication technique which also allows the production of PLGA shape-specific scaffolds. The authors also demonstrated that the *CO₂ sintering technique* is suitable for producing cell-containing, shape-specific matrices (patches and scaffolds) under relatively mild conditions via a single-step sintering of PLGA microspheres in the presence of cells, with high cell viability.

Aims of the thesis

Regenerative medicine requires engineered temporary scaffold able to support and influence cell microenvironment during their growth and/or differentiation. Supercritical Fluid processes are promising technologies for bioactive microdevices production able to overcome many drawbacks presented by conventional methods. As a consequence the aims of this work are:

- ✓ to develop and optimize an innovative *Supercritical Emulsion Extraction* (SEE) technique, operating in Continuous mode to produce PLGA bioactive microcarriers to be loaded into 3D scaffold for tissue engineering applications. The innovative SEE-C process arrangement will be obtained by using a high pressure packed column operating in counter-current in which mass transfer between the liquid and the gaseous phases is improved by the internal packing elements. The process operating parameters such as, pressure, temperature and phase compositions (thermodynamic optimization) and flow rate ratios (fluidodynamic optimization) will be also study and optimized in order to increase encapsulation efficiency and reduce batch-to batch repeatability drawbacks.
- ✓ to produce different PLGA microcarriers and characterize their morphology, particle size and distribution and active compounds loading and their release profiles in different media. Among the active compounds proteins and growth factors (GF) will be also considered.
- ✓ to test the activity of PLGA microcarriers for the “*in situ*” sustained delivery of bioactive molecules in cell cultivation medium and/or when embedded in more complex 3D scaffold. Bioactive scaffold loaded with PLGA microcarriers will be also tested on dynamic cultivation by using a bioreactor for cell differentiation in dependence of active substance loading and release. Stem cells differentiation will be considered for this part of the study and ECM component productions and their evolution at different time points will be also evaluated.

Chapter 2. Continuous Supercritical Emulsions Extraction: a new technology for PLGA microcarriers production

2.1 Introduction

Poly-lactic-co-glycolic acid (PLGA) is a well-know biodegradable polymer that has received a great interest for the development of micro-particulate based formulations. PLGA microparticles can be administered by in-situ injection, achieving a precise and localized drug delivery which is more effective in many cases such as, for chemotherapy, hormone therapy, DNA/protein or vaccine delivery, as discussed in details in the previous chapter. Moreover, PLGA microparticles with a specific size and distribution have also been proposed for the use in tissue engineering as building blocks of implantable 3D scaffolds because of the several benefits offered such as, versatility of the release kinetics of encapsulated growth factors for cellular function orienting and directing [71]. PLGA microparticles can be also used as biodegradable support for cell culture and/or cell administration in the so-called “*injectable scaffolds*” which may affect stem cells lineage restriction and, after polymer degradation, allow a complete integration of the grafted cells in the host tissue [72-74].

The aim of this part of the work is to use the new SEE process operating in Continuous mode (SEE-C) to investigate the production of PLGA microparticles with an engineered size and distribution. This innovative process arrangement is obtained by using a high pressure packed column operating in countercurrent in which mass transfer between the liquid and the gaseous phases is improved by the internal packing elements. The analysis of the SEE-C operating parameters such as, pressure, temperature, phase composition and flow rate ratios is also proposed together with the comparison of SEE-C process performance with the ones of the corresponding batch operating mode processes (supercritical and conventional evaporation) in terms of process yield and PLGA particle size distribution. A detailed characterization of microparticles in terms of size distribution, morphology and solid state is proposed and a study on the PLGA microparticles degradation is performed to monitor any morphological difference between these biodegradable devices produced by SEE-C and the ones obtainable by conventional evaporation technology.

2.2 *Experimental Methods*

2.2.1 *Materials, Emulsion Preparation & Methods*

CO₂ (99.9%, SON, Naples, Italy), polyvinyl alcohol (PVA, Mol wt: 30000–55000, Aldrich Chemical Co.), ethyl acetate (EA, purity 99.9%, Aldrich Chemical Co., Milan, Italy) poly-(lactic/glycolic) acid (PLGA, 75:25 Mol wt; 60000-120000 Aldrich Chemical Co.) were used as received. To prepare single *o-w* emulsions (composition ratio 20:80 w/w), a known amount of polymer was dissolved into EA to form an organic solution. Then, the solution was added into a known amount of EA-saturated aqueous PVA solution (0.8% w/w in water) to form an emulsion using a high-speed stirrer (mod. L4RT, Silverson Machines Ltd., Waterside, Chesham Bucks, United Kingdom) operated at 2800 rpm for 3 min. The oily phase contained fixed PLGA amounts ranging from 5 to 10% w/w depending on the test performed. To prepare double *w-o-w* emulsions (composition ratio of 1:19:80 w/w/w), 1 mL of water/PVA solution (0.04% w/w in water) was added in EA/PLGA solution and sonicated for 2 min (mod. VCX130, Vibra Cell, Sonics & Materials, Inc., Newtown, CT, USA). This primary emulsion was, then, added into a known amount of EA-saturated aqueous PVA solution to form the secondary emulsion. In this case, the oily phase contained fixed PLGA amounts ranging from 2.5 to 10% w/w depending on the test performed.

2.2.2 *SEE apparatus*

SEE-batch operation layout (SEE) apparatus consisted of a 0.25 dm³ cylindrical stainless steel extractor. SC-CO₂ was delivered using a high pressure diaphragm pump (Milton Roy, model Milroyal B, Point Saint Pierre, France) and was bubbled into the extraction vessel at a constant flow rate (0.4 Kg/h), through a cylindrical stainless steel porous dispenser located at the bottom of the extractor. Temperature inside the extractor was controlled using an air-heated thermostated oven. A separator located downstream the extractor was used to recover the solvent of the *oily* phase; pressure in the separator was regulated by a backpressure valve. At the exit of the separator, a rotameter and a dry test meter were used to measure the CO₂ flow rate and the total quantity of CO₂ delivered, respectively. When the extraction process was complete, the microspheres suspension was removed from the bottom of the extraction vessel for further processing. A schematic representation of the SEE process layout is reported in **Figure 2.1a**.

2.2.3 SEE-C apparatus

A schematic representation of the SEE-C process layout is reported in **Figure 2.1b**. The P&D description is reported in **Figure 2.1c**. The apparatus consists of a packed column with an internal diameter of 13 mm, in which carbon dioxide (C) is fed from the bottom of the column using a high-pressure diaphragm pump (SC_P, mod. Milroyal B, Milton Roy, Pont Saint-Pierre, France), and the emulsion (E) is delivered from the top of the column using a high pressure piston pump (L_P, mod. 305, Gilson, Villiers-le-Bel, France). The column is formed by three AISI 316 stainless steel cylindrical sections of 30 cm height, connected by four cross-unions and is packed with stainless steel packings 4 mm nominal size with 1889 m^{-1} specific surface and 0.94 of voidage (0.16 inch Pro-Pak, Scientific Development Company, State College, PA, USA). The apparatus is thermally insulated by ceramic cloths and its temperature is controlled by six controllers (TC1-TC6, Gordon J/Series 93, Watlow, Milan, Italy) at different heights of the column. The extracted solvent is recovered in a separator (S) put downstream the top of the column in which the pressure is regulated by a backpressure valve (V5, 26-1700 Series, Tescom, Selmsdorf, Germany). A rotameter (R, mod. N5-2500, ASA, Sesto San Giovanni, Italy) at the exit of the separator measures the CO_2 flow rate delivered. The start-up of the extraction process begins delivering SC- CO_2 from the bottom of the column until the operating pressure is reached. Then, the emulsion delivery is started at the top of the column and the two flow rates are set at fixed values. The microparticles suspension was collected at the bottom of the column, washed several times with distilled water and, then, recovered by membrane filtration.

2.2.4 Morphology & Size Distributions

The droplets contained in the emulsion were observed using an optical microscope (mod. BX 50 Olympus, Tokyo, Japan) equipped with a phase contrast condenser. A Field Emission-Scanning Electron Microscope (FE-SEM mod. LEO 1525, Carl Zeiss SMT AG, Oberkochen, Germany) was used to study the morphology of the PLGA microparticles. A sample was mounted on a carbon tab previously stuck to an aluminium stub. Samples were coated with gold (layer thickness 250 \AA) using a sputter coater (mod.108 A, Agar Scientific, Stansted, UK). Droplet size distribution (DSD) and particle size distribution (PSD) were measured by dynamic light scattering (DLS, Mastersizer S, Malvern Instruments Ltd., Worcesterstershire, UK). The Mastersizer S software uses Mie theory to produce an optimal analysis of the light energy distribution and to obtain the size distribution of the particles.

Analyses were performed immediately after the preparation of the emulsion and of the microparticles suspension, using several milligrams of each sample. The volumetric particle size distributions curves were proposed in a cumulative form.

2.2.5 Solid state characterization

Diffraction patterns were obtained using an X-ray diffractometer (mod. D8 Discover, Bruker AXS, Inc., Madison, USA) with a Cu sealed tube source. Samples were placed in the holder and flattened with a glass slide to assure a good surface texture. The measuring conditions were as follows: Ni-filtered CuK radiation, $\lambda = 1.54 \text{ \AA}$, 2θ angle ranging between 5° and 70° with a scan rate of 3 s/step and a step size of 0.2° . Thermograms were obtained using a differential scanning calorimeter (DSC mod. TC11, Mettler Toledo, Inc., Columbus, USA). Fusion temperature and enthalpy were calibrated with an indium standard (melting point 156.6°C). The samples (5 mg) were accurately weighed, crimped in an aluminium pan and heated from 25 to 300°C at $10^\circ\text{C}/\text{min}$, under a nitrogen purge of 50 mL/min. X-ray and DSC analyses were performed in three replicates for each batch of material.

2.2.6 Microparticles degradation study

100 mg of PLGA microparticles were suspended in 20 mL of water, agitated at 50 rpm at 37°C . 10 μL of suspension were sampled every 4 days, dried and mounted on an aluminium stub for the morphological analysis by FE-SEM. The suspension pH was measured by a pHmeter (mod. pH 210, HANNA instruments, Italia).

2.2.7 Solvent residue analysis

The EA content in the recovered suspension of PLGA microparticles was analyzed to determine the efficiency of solvent removal from the emulsion. The EA residue was measured using a head space sampler (mod. 50 Scan, Hewlett & Packard, Palo Alto, CA, USA) coupled to a gas chromatograph interfaced with a flame ionization detector (GC-FID, mod. 6890 Agilent Series, Agilent Technologies Inc., Wilmington, DE). EA was separated using a fused-silica capillary column 30 m length, 0.25 mm internal diameter, 0.25 μm film thickness (mod. DB-1, J&W, Folsom, CA, USA). GC conditions were: oven temperature at 40°C for 8 min. The injector was maintained at 180°C (split mode, ratio 1:1) and Helium was used as the carrier gas (7 mL/min). Head space conditions were: equilibration time 60 min at 100°C , pressurization time 2 min, loop fill time 1 min. Head space samples were prepared in 10 mL vials filled with 3 mL of suspension. Analyses were performed on each sample in three replicates.

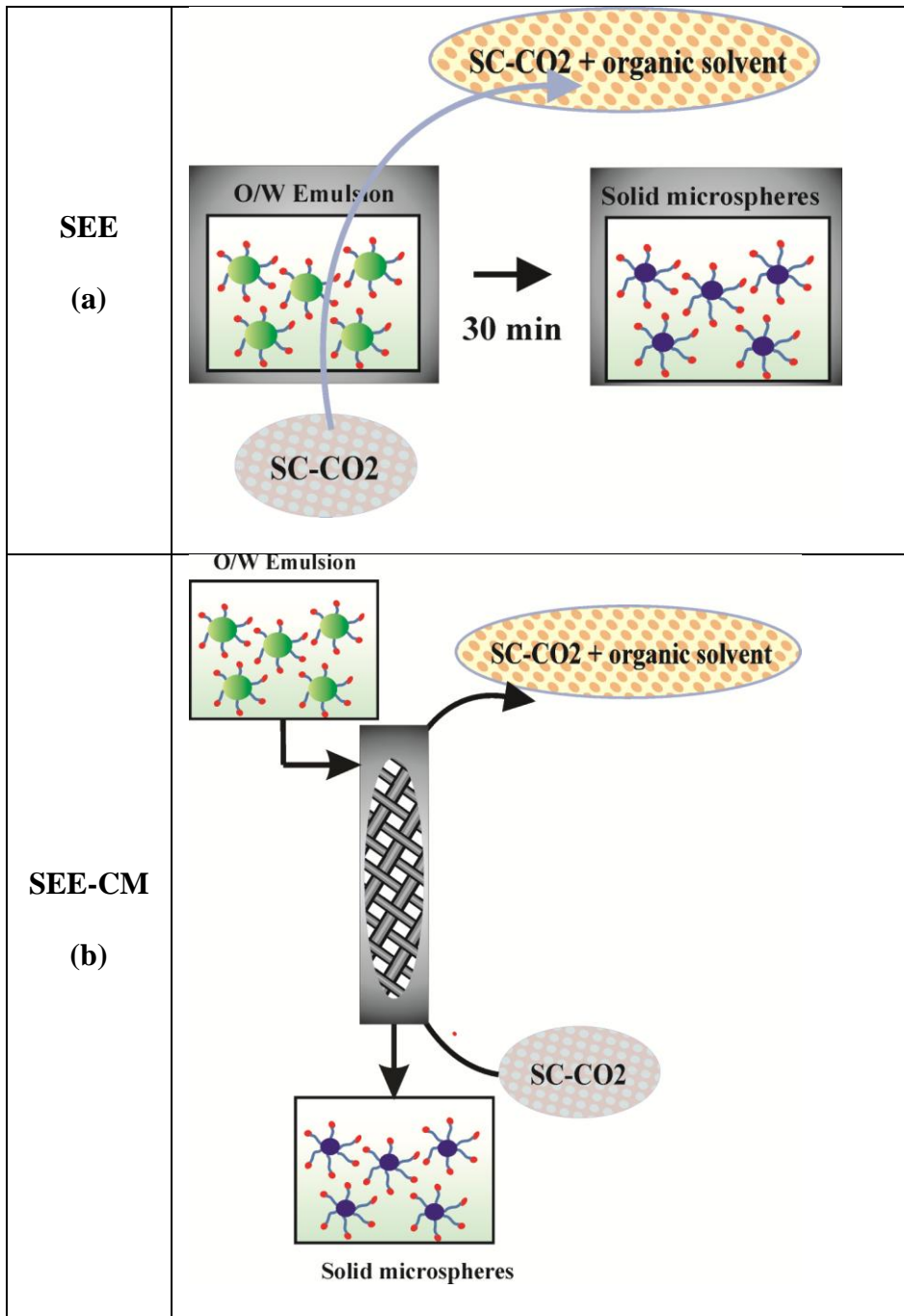


Figure 2.1a-b. Schematic representation of SEE and SEE-C processes layouts. SEE is an intrinsically batch process (a); SEE-C allows a continuous emulsion processing by using a countercurrent packed tower (b).

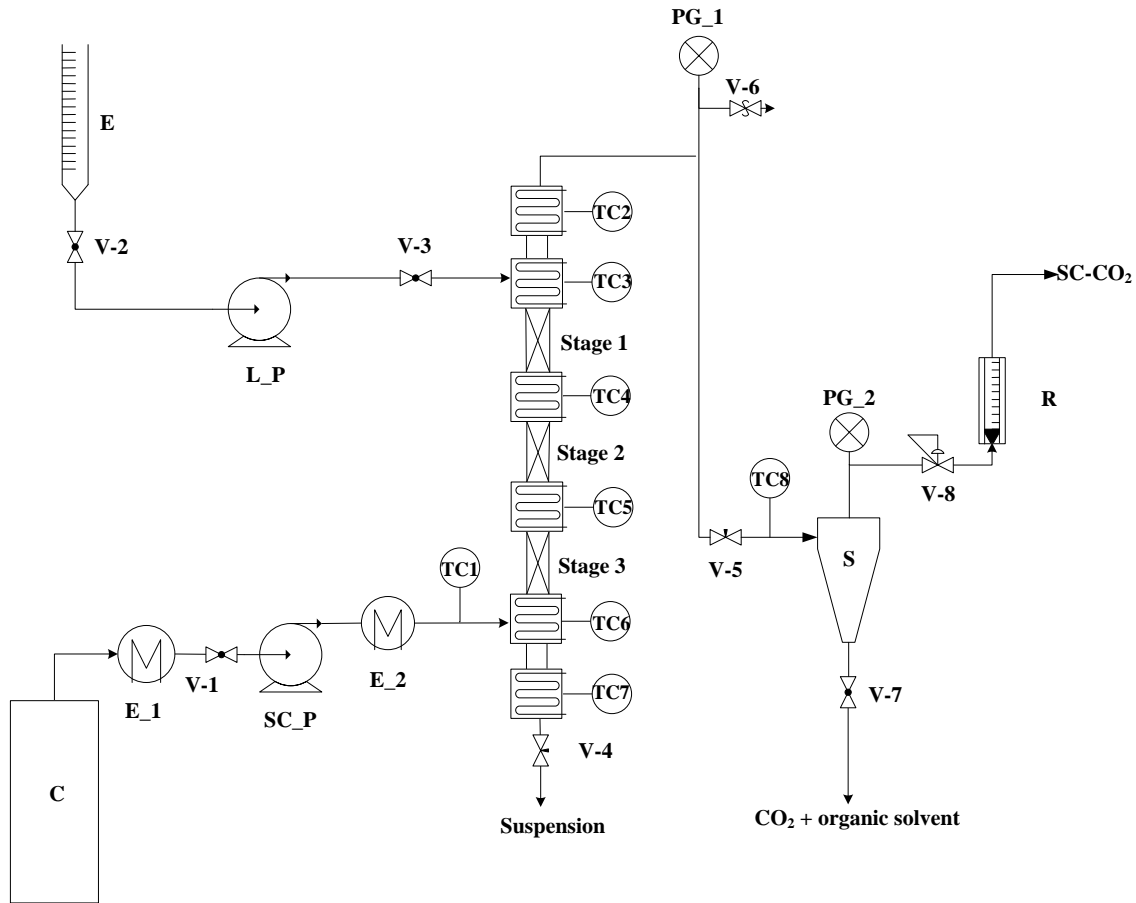


Figure 2.1c. SEE-C apparatus P&I description. C, CO₂ supply; E, emulsion supply; PG₁ and PG₂, pressure gauges; SC_P, diaphragm pump used for high pressure SC-CO₂; L_P, piston pump used for the emulsion; TC1-TC8, thermocouples/controllers; S, separator; R, rotameter; E₁ and E₂, heat exchangers; V1-V8, valves.

2.2.8 Correlations for flooding point calculation

Flooding point can be calculated using standard procedures based on the use of graphs reported in the literature. The first is the “*Generalized Pressure Drop Correlation*” (GPDC) [75], that describes the balance between the up-flowing gas momentum force and the gravitational forces acting on the liquid droplets; it is a function of the physical properties of the gas and of the liquid stream; therefore, mass flow rates, gas and liquid densities, viscosity of the liquid, as well as a packing factor must be known. The other two correlations tested are the “*Brunner correlation*”, that is the GPDC correlation modified by Brunner for towers operating with supercritical CO₂ [76] and the “*Random packing correlation*”(RPC) that is specific when random elements are loaded [77]. The correlation proposed by *Brunner* allows to calculate flooding points for packed columns with structured packings. Particularly, the gas

capacity factor on the ordinate is a measure of the gas velocity necessary to suspend a liquid droplet, and the flow parameter on the abscissa rates the kinetic energy of the liquid phase to the kinetic energy of the gaseous phase. The “*Random packing correlation*” depends on liquid and gas flow rates, surface area of packing per unit lower volume, fractional void volume of dry packing, liquid viscosity, local acceleration due to gravity, liquid and gas densities. This last correlation shows three separate curves: the intermediate curve can be used for random packings, the upper curve is used for stacked packings and the lower curve is for indicating an approximate lower limit when random packings are loaded.

2.3 *Results & Discussion*

2.3.1 *SEE-C parameters: pressure & temperature*

The extraction pressure and temperature conditions of 80 bar and 38°C were chosen for processing emulsions with an *oily* phase content of about 20% w/w. These conditions were selected to assure the complete miscibility of EA in SC-CO₂ [78-79]; whereas, at the same conditions, the solubility of water (the continuous phase) in CO₂ is of $0.53 \cdot 10^{-3}$ (as molar fraction), so very low and it can be neglected [80-82]. A temperature of 38°C is also compatible with the glass transition temperature of PLGA (co-polymer ratio 75:25, see also materials section) that is located at about 40°C [83].

Moreover, during the SEE continuous operation, a mass transfer between the two phases is activated, but, variations in the top and bottom product composition can be observed until steady state conditions have been obtained. As a consequence, another relevant process parameter, in the continuous operation, is the time required to obtain steady state composition in the column. So that, in some preliminary experiments, performed at the conditions described above and using an empty *o-w* emulsion (ratio 20:80), it was observed that after 30 min, the solvent residue in the water recovered at the bottom of the column became almost constant and lower than 300 ppm. Following these indications, the SEE-C experiments were always performed after reaching the steady state conditions by using an empty emulsion and a solvent residue values lower than 300 ppm were measured in all PLGA suspensions recovered in the following part of the work.

The use of packed towers is commonly not suggested for processes involving the presence of a solid phase; indeed, it should be expected that the solid precipitate from the

liquid phase and cover the packing surface, producing a reduction of the mass transfer and, then, the blockage of the column. However, in the SEE-C, this event was not observed. There are two good conditions to explain why this phenomenon does not significantly interfere with the continuous solvent elimination process. As the dimensions of the microparticles produced (related to droplet diameters) are always in the micronic range, they will show the tendency to remain suspended in the falling liquid film inside the column (i.e., particles residence time in the column is expected to be shorter than their sedimentation time); moreover, the presence of the surfactant on the particle surfaces will allow their easy slipping on the packing surfaces. The presence of surfactant around the microparticles suspension is also useful for their recovery at the bottom of the column since it avoids any other particle collapsing or aggregation. Moreover, the Joule-Thomson effect that follows the CO₂ lamination, induces a strong cooling effect on the microparticles suspension (2-4°C are normally reached), improving PLGA particles stability during their recovery.

2.3.2 SEE-C parameter: evaluation of flooding

In the classical interpretation of a liquid extraction process, mass transfer is concentrated at the interface between the two films formed by liquid and gas phase [84]. This schematization can be also applied to SEE-C process; therefore, mass transfer between the liquid and the dense gas can take place at the interface between the film of liquid moving downwards on the surface of the packing and the film of SC-CO₂ moving upwards in the column. In a countercurrent packed column, efficient mass transfer conditions are reached when the liquid flowing down over the packing begins to be held in the void spaces between the packing; this is called the *loading condition* and the pressure drop in the column begins to increase. Further increases in gas or liquid velocity will produce further increases of the pressure drop, until the liquid completely fills the void spaces in the packing, hindering the gas flow; therefore, the liquid cannot flow down through the column and it is forced to flow up, together with the gas stream. This condition is referred as *flooding* and the column is no more operative. Given a packed column, for a fixed gas rate, there is a definite liquid rate above which the column will flood; similarly, at any given liquid rate, there is a definite gas rate above which the column gives flooding. Moreover, the flooding point depends on the density difference between the two phases involved, as well as, when emulsions are used in the column, by the foam generated from the surfactant that reduces the free area for gas flow.

The flooding experiments at different CO₂ densities were performed on the apparatus previously described, using water as the liquid phase and supercritical carbon dioxide as the dense gas phase. For each experiment, gas flow rate and CO₂ density (i.e. pressure and temperature conditions) were fixed; whereas, the liquid velocity was increased by small steps to measure the increase of the pressure drop, until the flooding point was reached. We first measured the limit in density difference between the liquid and gas phase that allows countercurrent operation; the results are reported in **Figure 2.2** at fixed L/G ratios. For CO₂ densities lower than ~0.6 g/cm³ (below the dashed line), the gas to liquid (water) density difference allows the proper interaction of the two phases; for CO₂ densities larger than ~0.6 g/cm³ (above the dashed line), entrainment of the liquid phase increases rapidly until flooding occurs; small changes in the flow rates near the limit conditions lead to an unstable process. A similar value of the density difference was also found by Brunner and co-workers that, operating a continuous supercritical fractionation process of fish oil ethyl esters, found that the operating point at 0.603 g/cm³ was close to the flooding point [85]. Flooding velocities as a function of the liquid/gas ratio for different densities are reported in **Figure 2.3**: at constant L/G ratio, the flooding velocity decreases with the increase of CO₂ density.

For comparison purposes, CO₂ flow rates at flooding conditions were also calculated using the various correlations discussed in the methods section; the obtained values are listed in **Tables 2.1** and **2.2** at different L/G ratios and at different densities, respectively. The flooding values experimentally measured are also reported. Looking at the data, SC-CO₂ flooding flow rate (G_f) decreases with the increase of L/G for all literature correlations and the same trend has been found for the experimental values produced in this work. But, the G_f values calculated from the literature are from about 2.5 to 4 times larger than our experimental data; moreover, their variation with L/G is also less pronounced. Possible explanations for these differences are that literature correlations have been produced for processes using gases at ordinary pressure conditions, i.e. near the atmospheric pressure, where gas densities are very small compared to those of supercritical CO₂. The only exception is Brunner's correlation that has been developed for SC-CO₂; however, in that case, structured packings have been used that allow a larger void section through the column, to which correspond larger spaces for gas to flow up, with reduced interactions with the liquid. In our apparatus, instead, very small random packings are used.

When L/G is varied between 0.1 and 0.4, the corresponding limits for liquid flow rates are indicated in **Table 2.3**. Using the results discussed until now, efficient separations in the column are obtained with a flow rate of 1.4 Kg/h of CO₂ that corresponds to the 50% of the flooding experimental value, when operating at 80 bar, 38°C with a L/G ratio of 0.1.

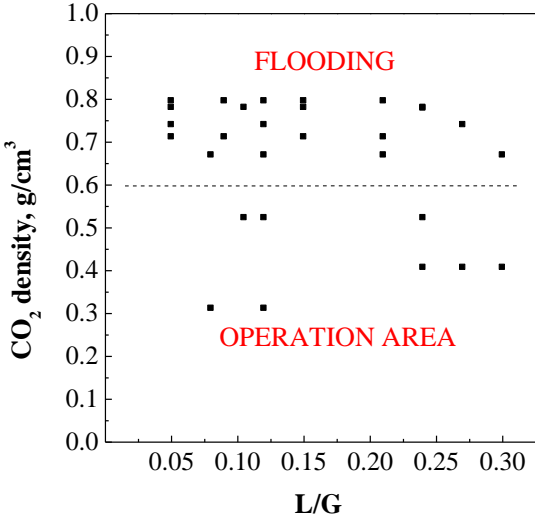


Figure 2.2. Effect of the gas density upon flooding for different L/G ratios (dashed line: boundary line between proper process conditions and flooding).

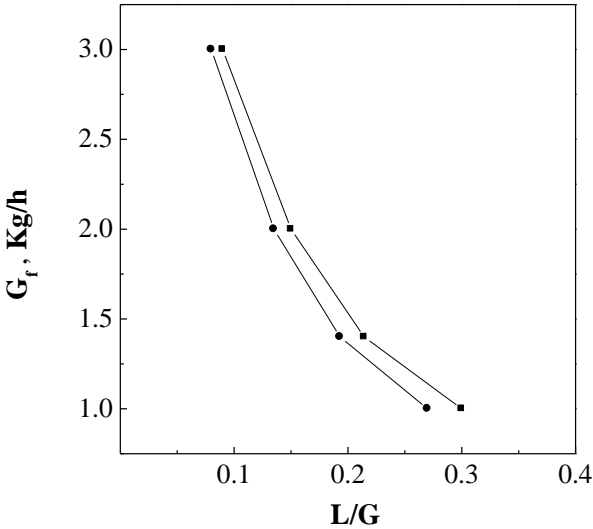


Figure 2.3. Flooding velocities as a function of the liquid/gas ratio (L/G) for different CO₂ densities: (■) P = 80 bar, T = 38°C, ρ = 0.31 g/cm³ and (●) P = 100 bar, T = 44°C, ρ = 0.52 g/cm³.

Table 2.1. Evaluation of the Gf conditions varying the L/G ratio between 0.1 and 0.4 at fixed T = 38°C and P = 80 bar ($\rho = 0.31 \text{ g/cm}^3$) using the correlations previously discussed.

L/G	G _f [Kg/h]			
	<i>GPDC</i>	<i>Brunner</i>	<i>RPC</i>	<i>This work</i>
0.1	10.25	11.26	7.50	2.82
0.2	8.68	9.38	6.64	1.40
0.4	7.09	7.51	5.21	1.00

Table 2.2. Evaluation of the flooding conditions varying the density at fixed L/G = 0.1, using the correlations previously discussed. CO₂ density of 0.31 g/cm³ correspond to 80 bar and 38°C; 0.52 g/cm³ to 100 bar and 44°C.

CO ₂ density (g/cm ³)	G _f [Kg/h]			
	<i>GPDC</i>	<i>Brunner</i>	<i>RPC</i>	<i>This work</i>
0.31	10.25	11.26	7.50	2.82
0.52	10.24	11.23	9.26	2.61

Table 2.3. Liquid and SC-CO₂ flow rates used at different values of L/G.

L/G	SC-CO ₂ flow rate [Kg/h]	liquid flow rate [Kg/h]
0.4	1.4	0.56
0.2	1.4	0.28
0.1	1.4	0.14

2.3.3 Droplets & microparticles size and morphology

It is known that the size of the particles is directly related to the emulsion droplet size and, therefore, depends on the emulsion formulation. Particularly, the increase of the oily solution viscosity, due to a higher polymer concentration in the solvent, can produce larger droplets when using the same dispersion shear force and surfactant concentration during the emulsion production [86]. Following this indication, SEE-CM experiments (in steady state conditions) were performed by processing 100 g of single (*o-w*) and/or double (*w-o-w*) emulsions in each run, varying the PLGA content in the oily phase from 5 to 10% w/w to obtain PLGA microparticles of increased mean size. All the distribution data of the droplets and of the microparticles produced are summarized in **Table 2.4**.

Optical Microscope images of two different emulsions (*o-w* single emulsion produced at PLGA concentration of 5% w/w and *w-o-w* double emulsion with a PLGA concentration of 10% w/w in the oily phase) are reported in **Figures 2.4a-b**, respectively. From the images it is clear that the emulsions were stable with non-coalescing droplets. The produced PLGA microparticles were spherical and non-coalescing as illustrated in the SEM images reported in **Figures 2.5a-b**. These images pertain to particles obtained from single (left side) and double (right side) emulsions prepared with PLGA concentrations in the oily phase of 5 % w/w (see **Figure 2.5a**) and of 10% w/w (see **Figure 2.5b**). All the SEM images reported have been taken at the same amplification and it is clear that the increase of the mean particle size from 1 to 3 μm when PLGA concentrations in the oily phase were increased from 5 to 10% w/w.

The PSD of the particles obtained from *o-w* emulsions containing 5% and 7.5% w/w of PLGA in the oily phase are also reported in a cumulative representation in **Figure 2.6**. The DSDs of the two emulsions processed by SEE-C are reported in the same figure, for comparison purposes. Droplets curves practically overlap, showing that the variation of PLGA concentration from 5 to 7.5% w/w in oily phase do not really influenced the droplets size that was similar. However, the PSD of the microparticles originated from the droplets containing 5% w/w of PLGA is sharper than the PSD of the microparticles from droplets containing 7.5% w/w of PLGA. This fact is due to the droplet shrinking factor (defined as the ratio between the particles and droplets mean sizes, $SF = MSS/MSE$) that also plays a relevant role in determining the final size of the microparticles. The droplets with a higher percentage of polymer have a lower possibility to shrink when the solvent is eliminated; therefore larger particles are produced [87]. Particularly, the obtained particles are about 60% and 33% smaller, respectively, than the original droplets.

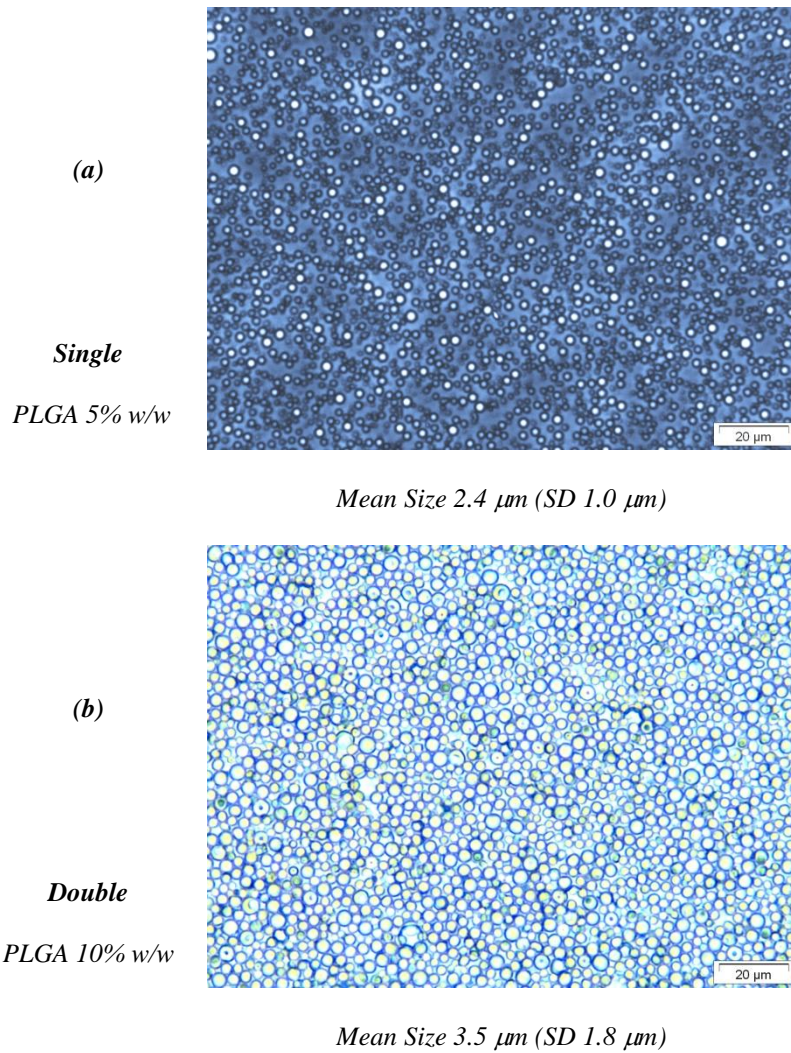


Figure 2.4a-b. Optical Microscope images of two emulsions: (a) single *o-w* (20:80; composition: EA plus PLGA 10% w/w; external water with PVA 0.8% w/w) and (b) double *w-o-w* (1:19:80; composition: internal water plus PVA solution 0.04% w/w; oil EA plus PLGA 10% w/w; external water with PVA 0.8% w/w).

Table 2.4. Dynamic laser scattering size distribution data of droplets (DSD) and of microparticles (PSD) produced at different PLGA concentrations in the oily phase using SEE-C of single (*o-w*) and double (*w-o-w*) emulsions. Legend: MS = mean size; SD = standard deviation; CV = coefficient of variation; SF = shrinking factor.

	Droplet Size Distributions (DSDs)				Particles Size Distributions (PSDs)			
	o/w			w/o/w	o/w			w/o/w
PLGA % w/w	5	7.5	10	10	5	7.5	10	10
MS (μm)	2.4	2.6	4.1	4.1	1.0	1.8	3.3	3.5
SD (μm)	1.0	1.2	2.1	2.1	0.4	0.8	1.6	1.8
CV _(SD/MS) (%)	41	46	51	51	40	44	48	51
SF(MD _S /MD _E)	--	--		--	0.41	0.67	0.80	0.85
D ₁₀ (μm)	1.1	1.2	1.5	1.5	0.4	0.7	1.1	1.2
D ₅₀ (μm)	1.8	1.8	3.0	3.1	0.7	1.3	2.3	2.6
D ₉₀ (μm)	2.7	2.7	4.9	5.1	1.2	2.1	3.8	4.6

DSDs of the emulsion containing 10% w/w of PLGA in the oily phase and PSDs of the related microparticles were also studied using single (*o-w*) and double (*w-o-w*) emulsions and the related size distribution curves are reported in the **Figure 2.7**. Double emulsions are more difficult to be processed by conventional solvent evaporation, since the emulsion is less stable and the produced microparticles are expected to be porous due to the entrapped internal water phase. Coalescence phenomena are frequent, as well as, the formation of concave particles due to the loss of the water internal phase and the formation of collapsed empty particles. PLGA concentration of 10% w/w in the oily phase produced droplets with almost the same distribution in the case of single and double emulsions. The PSDs cumulative curve of the microparticles generated from single emulsion showed a larger shift from the DSDs related curve, indicating a larger droplet shrinking (the gap between PSD/DSD at D50 values is 0.74 μm); whereas, when a double emulsion was processed, the size distribution curve of the generated particles showed a smaller shift (gap between PSD/DSD at D50 values is 0.49 μm).

The coefficient of variation (CV), defined as the ratio between standard deviation (SD) and mean size (MS), were evaluated for both droplet and particle distributions and its values are also reported in **Table 2.4**. The CV of the particle size distributions obtained by SEE-CM were in the range of 40-50 % and always lower or, at least, the same of the ones of the original emulsions, confirming the fine reproduction of the size distribution from droplets to particles of the supercritical continuous process.

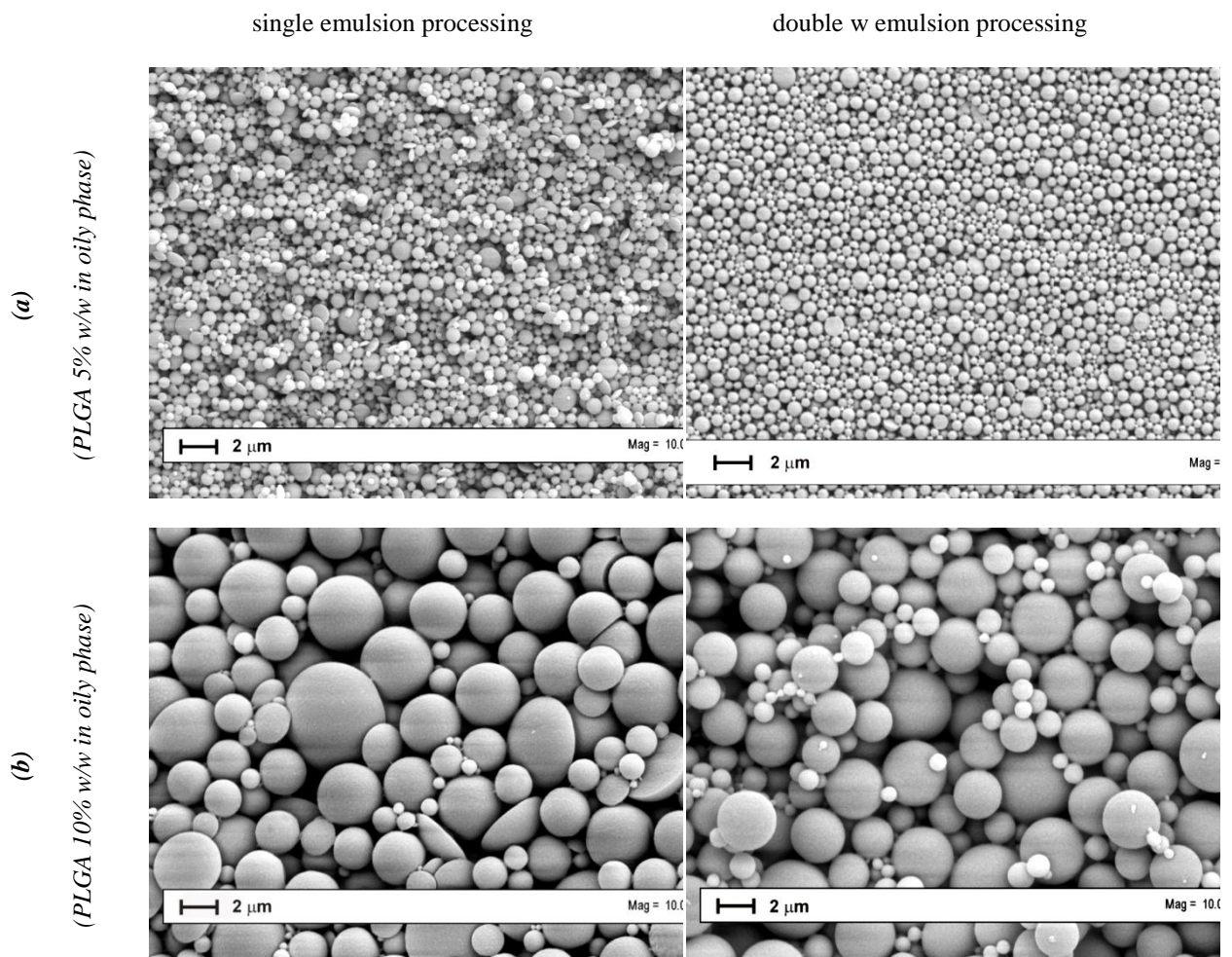


Figure 2.5a-b. SEM images of PLGA microparticles obtained by SEE-C by processing both single and double emulsions containing PLGA in concentration of (a) 5% w/w and (b) 10% w/w; Operating conditions: 80 bar and 38°C, L/G ratio 0.1.

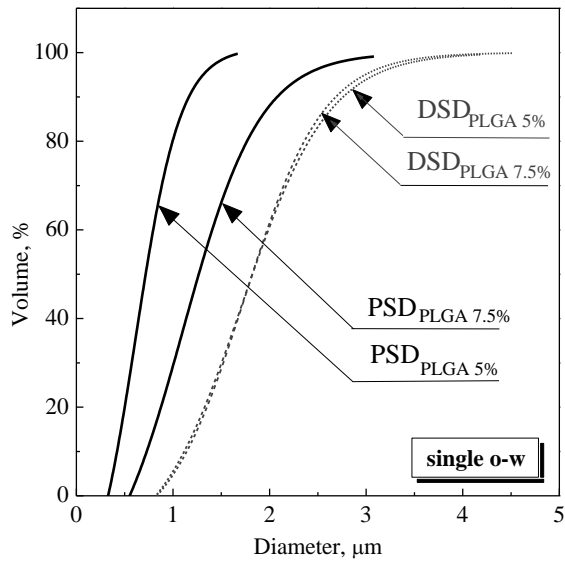


Figure 2.6. PSDs of PLGA particles produced from single (o-w) emulsions containing 5% and 7.5% w/w of PLGA in the oily phase. The DSDs of the two emulsions processed by SEE-C are also reported (dashed curves), for comparison.

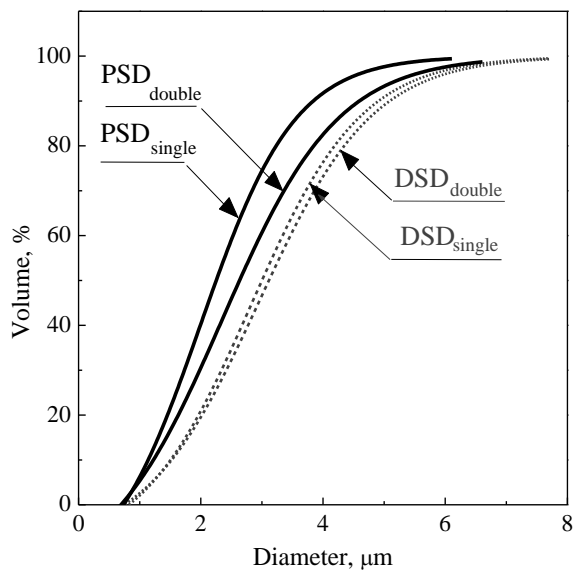


Figure 2.7. PSDs of PLGA particles produced from single and double emulsions containing 10% w/w of PLGA in the oily phase. The DSDs of the two emulsions processed by SEE-C are also reported (dashed curves), for comparison. The gap between PSD/DSD at D50 values for single emulsion is 0.74 μm); the gap between PSD/DSD at D50 values for double emulsion is 0.49 μm).

2.3.4 Comparison between SEE, SEE-C and evaporation

A comparison between the product obtained by SEE, SEE-C and conventional solvent evaporation process (SE) was performed using *w-o-w* emulsions that were processed using the three different technologies/process layouts. Mean sizes and distributions of PLGA microparticles obtained by SEE-C, SEE and by conventional solvent evaporation (SE) are reported in **Table 2.5**. In the same table the DSDs of the treated emulsions are also reported, for comparison purposes. **Table 2.5** data confirmed that the SEE-C allows the recovery of particles with an MSs and SDs slightly smaller than the ones produced by the SEE and smaller than the ones produced by the SE. The reason should be in the very short processing time of all the emulsions treated by SEE-C. Indeed, considering as a reference time, the residence time of the liquid phase in the packed column, the continuous processing requires a residence time of the emulsion/suspension in the column of about 5 min; whereas, 30 min are the residence time of the emulsion/suspension treated by SEE and the 4-6 hours are necessary to perform the conventional SE (often also at higher temperatures). With respect to the SEE standard layout, the SEE-C offers other advantages such as, complete absence of aggregated particles and minimized lost of particle in the CO₂ gas stream during the depressurization steps. Indeed, SEE usually shows a recovery percentage (defined as: *PLGA charged in emulsion/PLGA recovered after the processing *100*) variable from 40 to 60%; whereas, a recovering percentage of about 90% was measured in SEE-C.

Table 2.5. Dynamic laser scattering size distribution data of droplets contained in double *w-o-w* emulsions and related PLGA microparticles size distribution produced using standard SEE layout, SEE-C and solvent evaporation process (SE). Legend: MS = mean size; SD = standard deviation; CV = coefficient of variation.

	Droplets μm			Microspheres μm								
				SEE			SEE-CM			SE		
	MS (μm)	1.0	2.0	4.8	1.1	2.3	4.6	1.0	1.9	4.2	1.5	2.0
SD (μm)	0.5	0.8	2.4	0.4	1.0	2.1	0.5	0.8	2.1	0.8	1.0	2.4
CV (%)	50	40	50	36	43	46	50	42	50	53	50	52

2.3.5 *Microparticles solid state and degradation*

Thermal analyses (DSC) were performed on microparticles obtained by SEE-C and on raw PLGA, for comparison purpose. The obtained thermograms are reported in **Figure 2.8**. PLGA shows a glass transition between 39 and 45°C (onset 39.98°C; endset 45.32°C) and the decomposition that occurs at above 300°C. The produced microparticles show the same glass transition and degradation event of the unprocessed polymer. X-ray analyses were also performed on the untreated polymer and on PLGA microparticles to have information about the solid state of the produced materials. The X-ray patterns are reported in **Figure 2.9**; they indicate that both unprocessed polymer and microparticles are amorphous, confirming the fast polymer precipitation inside the droplets during the microparticle formation by SEE-CM.

2.3.6 *Proposed process mechanism*

Precipitation of PLGA inside the droplets is induced by SC-CO₂ extraction of the organic solvent of the oily dispersed phase. Although the detailed behavior of this process has not yet been defined, a possible mechanism can be described as follows; when emulsion and SC-CO₂ come in contact, the mass transfer of the organic solvent proceeds by two parallel pathways: (A) the diffusion of the organic solvent into water followed by extraction of the solvent from the aqueous phase to SC-CO₂; (B) the direct extraction upon contact between SC-CO₂ and the organic phase inside the droplet (see **Figure 2.10**). The path (A) is the only one used to describe the conventional solvent evaporation because, in that case, the amount of solvent evaporated at the liquid air interface is compensated by the solvent diffusing into the continuous phase from the droplet [88]. This path can be justified also in the SEE-C process by the fact that a thermodynamic equilibrium occurs into the solvent-rich and aqueous-rich phases. Moreover, at the operating conditions selected, very large solubility of the oily phase is assured in SC-CO₂; therefore, it may extract the solvent of the dispersed oily phase from the external water phase of the emulsion causing the subsequent diffusion of the solvent from the droplets to the continuous phase, to restore the thermodynamic equilibrium. This phenomenon may prevail, for example, in the case of EA because its solubility in water is particularly great (8.7% w/w at ambient conditions) [89].

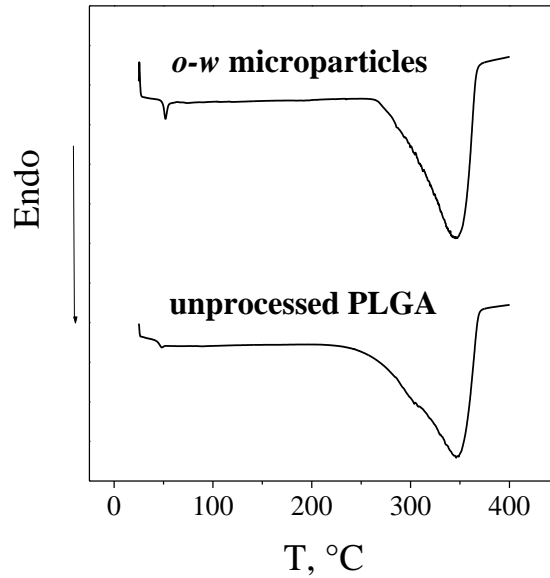


Figure 2.8. DSC traces of unprocessed and PLGA microparticles produced by SEE-C. The polymer glass transition did not change after SEE-C processing.

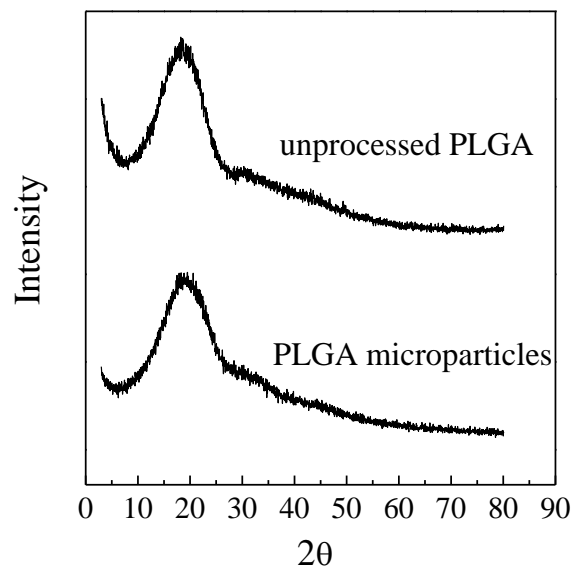


Figure 2.9. X-ray profiles of unprocessed and PLGA microparticles produced by SEE-C. The polymer is clearly amorphous in both case.

However, the co-existence of the path (B) in the SEE-C process should be confirmed by the process of *water in oil* emulsion reactions assisted by SC-CO₂ for the production of metal oxides [90-91]. In that case, the CO₂ was used not only as extracting agent of the organic external phase, but also, as a reagent that, reacting with the solute in the internal water phase,

forms metal oxides nanoparticles. In this particular application, the SC-CO₂ diffusion into the droplet is necessary for the reaction evolution and the results reported in the literature, indicated a very a fast reaction rate after SC-CO₂ diffusion into the droplets, through the surfactant shell.

Mattea et al., [92] also observed the behaviour of a dichloromethane drop (covered by surfactant) in water after its contact with SC-CO₂ at a given pressure, temperature and CO₂ molar fraction and reported possible swelling of the drops, after SC-CO₂ diffusion in it (that may suggest the direct extraction of the solvent), suddenly overcome by a rapidly drop shrinking, probably due to the dichloromethane diffusion out of the drop into the external water phase (that may also suggest the indirect solvent extraction). Both mass transfer paths, namely “*direct solvent extraction*” and “*indirect solvent extraction*” from the external phase, may concur in generating the polymer supersaturation inside the droplet and its fast precipitation. However an hypothesis about the possible prevailing mechanism in the SEE-C process cannot be attempted at the moment due to lack of experimental data in the literature.

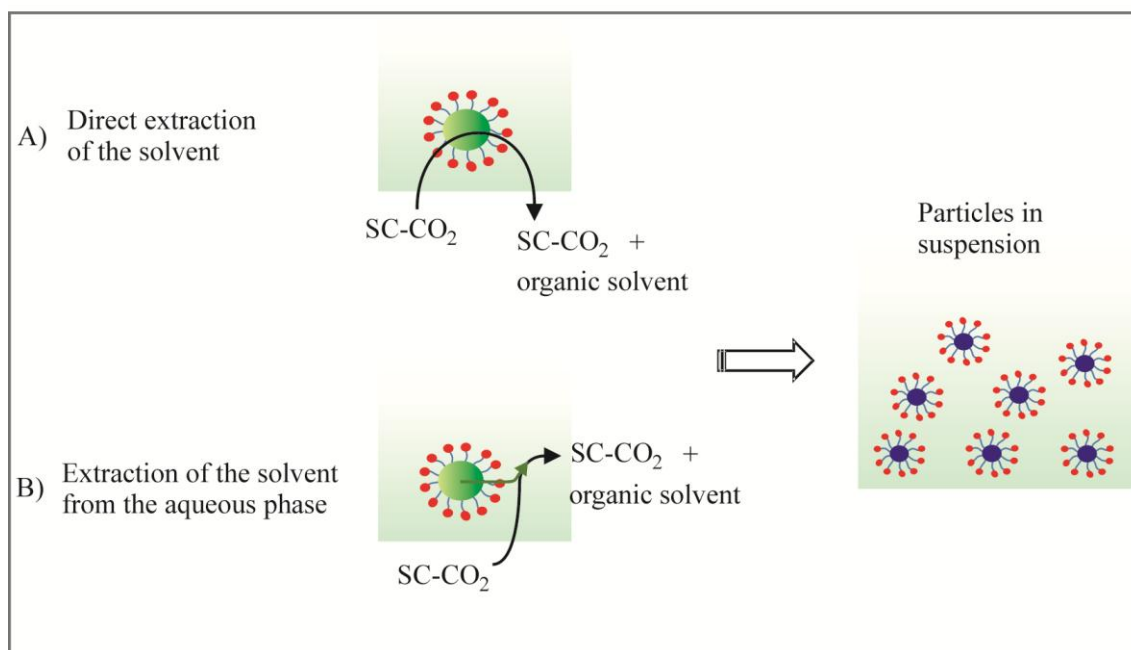


Figure 2.10. Schematic representation of the possible mass transfer pathways of the oily phase during the SEE-C process. Two parallel pathways: (A) diffusion of the organic solvent into water followed by subsequent supercritical extraction of the solvent from the aqueous phase; (B) direct supercritical extraction upon contact between SC-CO₂ and the organic phase into the droplet.

PLGA is well known for its bulk erosion properties [93]. In order to study the degradation of the microparticles produced by the supercritical process, two different batches of particles produced using single and double emulsions (with a fixed MS of 3 μm , \pm 0.75 μm) were suspended in distilled water at 37°C with an agitation of 50 rpm. The PLGA particles degradation starts in the first 48 hours, as indicated by the pH lowering of the suspension that decreased from 6.8 to 4.5. From each suspension, 10 μl were sampled every 7 days, dried and prepared for the morphological analysis by FE-SEM.

The microparticles produced by single emulsion showed a complete erosion in 60 days. The microparticles surface modification after 14 and 35 days are reported in **Figures 2.11 (a-b_left side)**. A smooth surface is still present on the particles sampled after 14 days of degradation. The progressive erosion starts to be evident after 35 days, when the microdevices became nanoporous.

The microparticles produced by double emulsion showed a complete erosion in 50 days. Their surface morphologies after 14 and 35 days are also reported in **Figures 2.11 (a-b_right side)**. A smooth surface can be still observed after 14 days of residence in distilled water (**Figure 2.11a_right side**); whereas, the circular structures observed on the microparticles surface should be due to the polymer precipitation on the internal water phase of the double emulsion. Nanoporous and near-collapsed particles can be observed after 35 days, indicating the polymer bulk depolymerization (**Figure 2.11b_right side**).

The overall period between 50-60 days, required for PLGA microparticles complete degradation in water coupled with a maximum pH lowering of the suspension to a value between 4.5 and 3.8 is in agreement with the literature data [94], which suggested a degradation time of 60 days for similar PLGA composition and particle sizes obtained by conventional solvent evaporation.

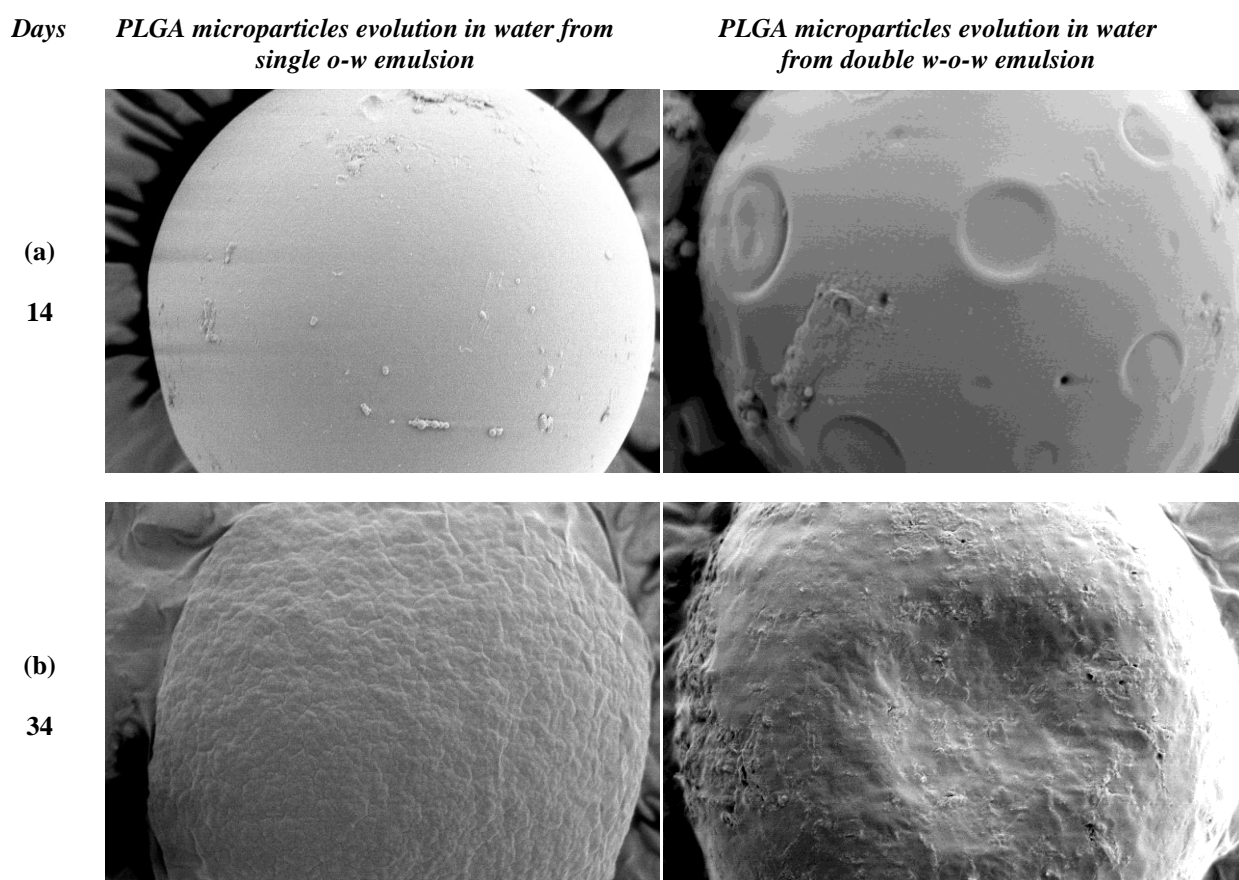


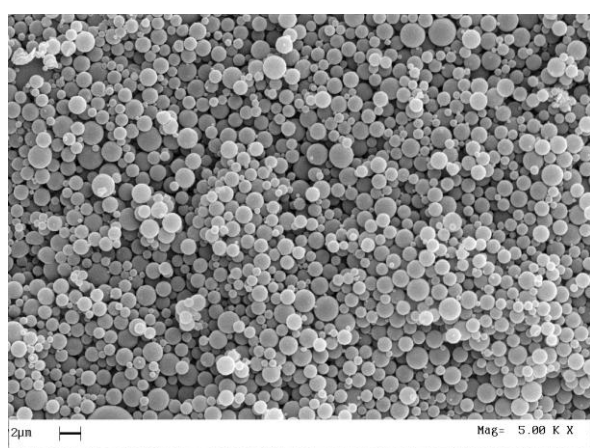
Figure 2.11a-b. SEM images (Mag = 50.00 K X) related to a morphological study of PLGA microparticles degradation in water after 14 (a) and 34 days (b), respectively. The particles have a diameter of almost 3 μm and were produced by SEE-CM using a single (left side) and double *w-o-w* emulsions (right side).

2.4. Others results on PLGA microcarriers charged with bioactive substances

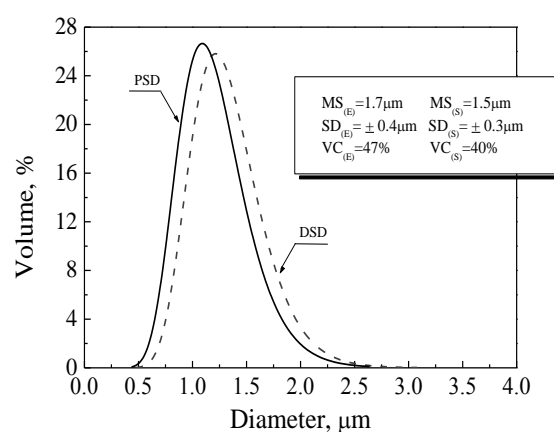
SEE-C technology was used to produce PLGA microdevices charged with several active principles, such as vancomycin hydrochloride (VH, a glycopeptide antibiotic) and hydrocortisone acetate (HA, a corticosteroid) [95]. Different emulsions were tested to optimize the VH loading at 5% w/w (theoretical drug loading) into PLGA microspheres that showed MSs of 1.5 μm (\pm 0.3 μm). An example of SEM images of the PLGA/VH microspheres obtained is reported in **Figure 2.12a**; whereas, the related distribution curve is reported in **Figure 2.12b**; the emulsion DSD from which they are generated are also reported for comparison purpose in the same Figure, as dashed line.

Optical microscope (OM) image of double *w-o-w* emulsion (1:19:80 composition) containing PLGA in concentration of 10% w/w in the oily phase (HA loading is 9% w/w of PLGA) is reported in **Figure 2.13a**; the droplets produced were non-coalescing and exhibited a MS of 3.4 μm ($\pm 0.8 \mu\text{m}$). The PLGA microspheres produced are illustrated in the SEM image reported in **Figure 2.13b**; they were spherical and showed a MS of 3.1 μm ($\pm 0.7 \mu\text{m}$). Drug encapsulation percentages of 87% for VH and of 85% for HA, respectively, were measured [96].

From an *o-w* emulsion obtained with acetone and aqueous glycerol, SEE-C process was also tested for the production of PLGA microspheres charged with retinyl acetate (RA) and β -carotene (CA). Microdevices with a MS of 6.5 μm ($\pm 1.7 \mu\text{m}$) were obtained with a good encapsulation efficiency of 70% for RA and 60% for CA, respectively. Examples of two emulsions are illustrated in the OM images reported in **Figure 2.14a-b**; whereas, SEM images of the obtained PAMs are reported in **Figure 2.15a-b**, respectively [97].



(a)



(b)

Figure 2.12a-b. SEM image of the PLGA/VH microspheres obtained by SEE from *w-o-w* emulsion. Mean Size: 1.5 μm ($SD \pm 0.3 \mu\text{m}$), Variation Coefficient: 40% (a). Particle Size Distribution (PSD) curve of PLGA/VH microspheres obtained by SC-CO₂ extraction (continuous line) and Droplets Size Distribution (DSD) curve of the droplets in the emulsion before SC extraction (dashed line) (b).

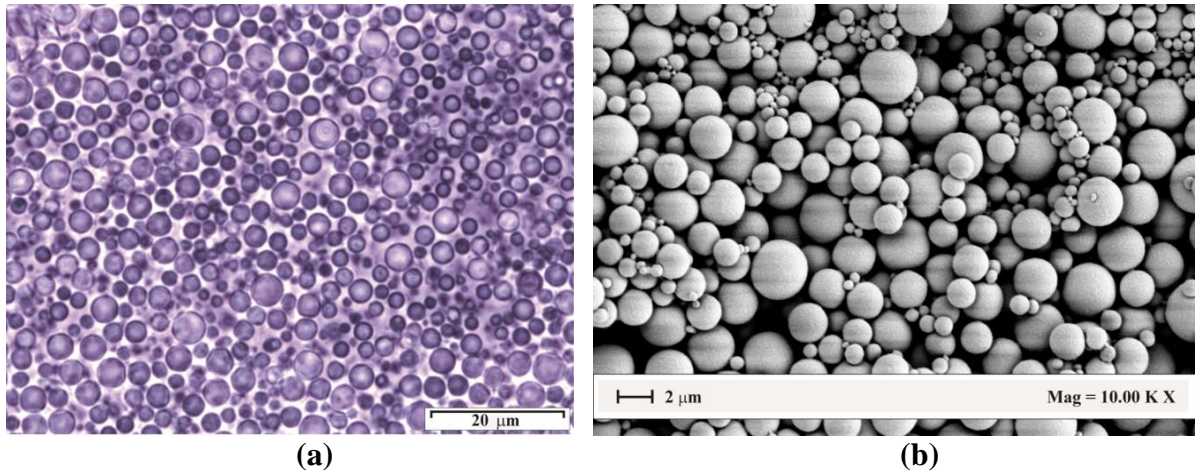


Figure 2.13a-b. Optical Microscope image of a double *w-o-w* emulsion (1:19:80 composition) containing PLGA in concentration of 10% w/w in the oily phase (HA is 9% w/w of PLGA) (a). SEM image of PLGA microspheres charged with HA (loading 6 % w/w) produced by SEE-C operating at 80 bar and 38°C, L/G ratio 0.1 (b).

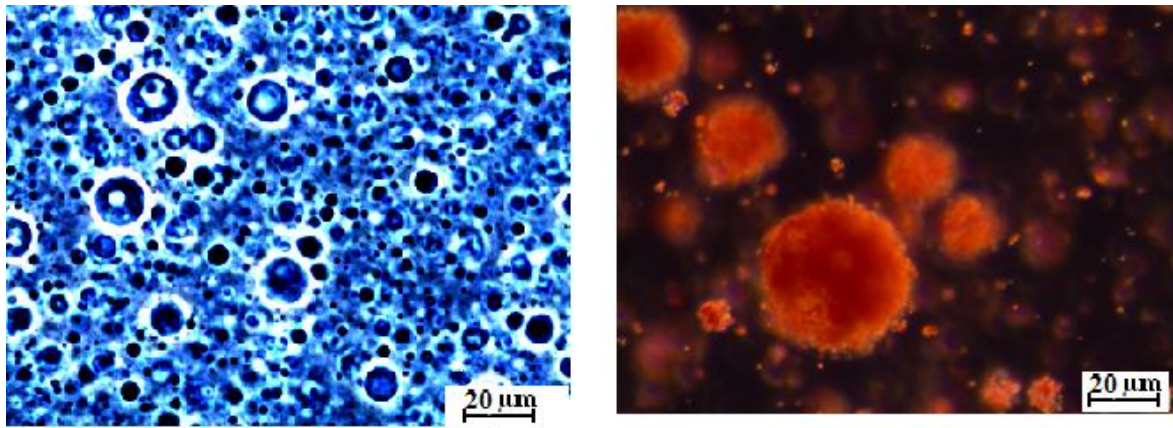


Figure 2.14a-b. (a): Emulsion o-w ratio 20/80, Oil: 45% PLGA with 3% RA; Water 80% glycerol, 20% water and 0.6% PVA. (b): Emulsion o-w ratio 20/80, Oil:45% PLGA and 6% β -carotene; Water 80% glycerol, 20% water and 0.6% PVA

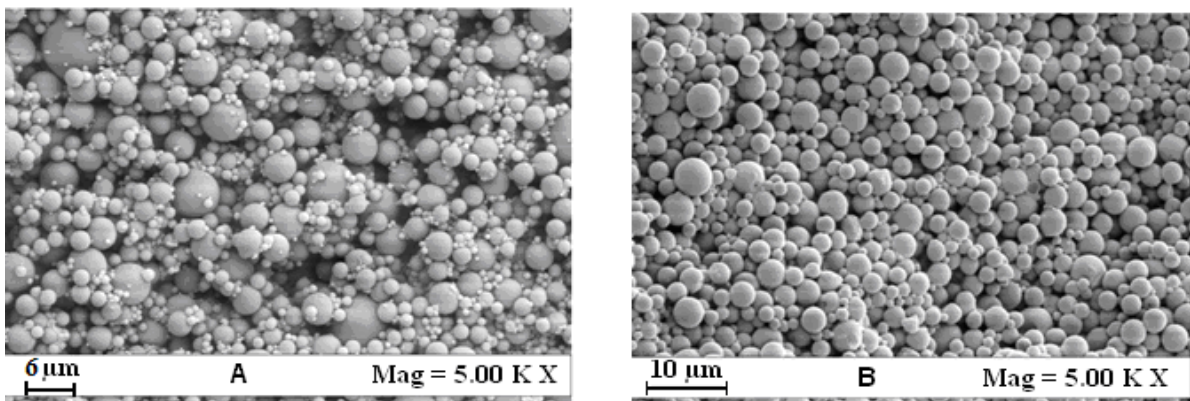


Figure 2.15a-b. SEM images of the PAMs produced (a): PLGA with 3% w/w of RA; PLGA with 6% β -carotene (b).

2.5 Conclusions & Perspectives

The successful upgrade of the batch SEE process to a continuous operating mode (SEE-C) was illustrated. Greater product uniformity, higher throughput with smaller plant volumes and elimination of batch-to batch repeatability problems were the important advantages observed. The measurement of droplet-to-particle shrinking factors and the monitoring of microdevice degradation in a aqueous media demonstrated that the internal structure of the PLGA microdevices, is almost the same of the ones produced by conventional evaporating process; however, the faster solvent extraction will have a significant effect on the size distribution of the precipitated particles which are always smaller than (or at least reproduce exactly) the size of the originally droplets, avoiding the aggregation phenomena that occur during conventional slower processes. SEE-C allowed also higher encapsulation efficiencies especially when double emulsions were treated.

Chapter 3. PLGA microdevices by SEE for Retinoic acid sustained release: evaluation of the kinetics constants

3.1 Introduction

All *trans*-retinoic acids (atRA) show a high therapeutic potential in the treatment of several diseases and, recently, they have also been included in anti-cancer therapeutical schemes [98]. However, atRA are very labile at ambient conditions and their degradation is a typical radical reaction, catalyzed by light, transition metals or free radicals [99]. Due to their short half-life and hydrophobicity, retinoids parenteral administration is very difficult and to date no commercial formulations are available. Different formulations have been investigated to overcome retinoids fast metabolization and to achieve their locally sustained release: encapsulation into injectable microspheres [100], emulsions [101], nanodisks [102], solid lipid nanoparticles (SLNs) [103] and nanoparticles [104]. Retinoids encapsulation in *poly-lactic-co-glycolic acid* (PLGA) microparticles could be interesting for drug controlled release and/or targeting after local administration [105-106] and/or for tissue engineering application [107]. Emulsion evaporation with methylene chloride produced PLGA particles ranging from 10 to 90 μm , with a maximum atRA loading efficiency of 59% in correspondence to a drug content of 2.3% w/w. It is also worth of mention that dichloromethane is still the most widely used oily phase solvent thanks to its high volatility; however, due to its carcinogenic nature, several efforts were made to replace it with ethyl acetate [108]. An atRA encapsulation efficiency of 47% was also reported for PLGA microspheres produced using chloroform [109]. Controlled release of retinol from silica particles was also reported by solvent evaporation of double *oil-water-oil* emulsions. In this case, the highest encapsulation efficiency was of 30% [110]. Recently, some authors reported the production of PLGA microspheres containing vitamin B₁₂ prepared by emulsion extraction using an innovative emulsion composition formed by acetone (as the solvent for the oily phase) and aqueous glycerol. Acetone was then “extracted” with water [111].

The aim of this part of the study is to produce PLGA microparticles with high retinyl acetate (RA) encapsulation efficiency by using less toxic solvents (acetone & aqueous glycerol) applying Supercritical Emulsion Extraction technology (SEE). This technology will

be tested both in batch (SEE-B) and in continuous (SEE-C) operating layouts. The microdevices produced by SEE will be also compared with the ones obtainable by conventional liquid-liquid extraction (LEE) process. Detailed characterization of the microspheres will be also proposed, comparing the morphologies, size distributions and physico-chemical properties (solid state, solvent residue) of the different products obtained. Different RA loading and corresponding release profiles will be also evaluated in modified media (*n*-propanol/water) and kinetic constants will be calculated by fitting the experimental data with a mathematical model that takes into account either diffusion and degradation contributions.

3.2 *Experimental Methods*

3.2.1 Materials

CO₂ (99.9%, SON, Naples, Italy), polyvinyl alcohol (PVA, MW: 30,000–55,000, Aldrich Chemical Co.), acetone (AC, purity 99.9%, Aldrich Chemical Co.), glycerol (GLY, purity 99%, Aldrich Chemical Co.) retinyl acetate (RA, Aldrich Chemical Co.), poly(lactic-co-glycolic) acid (PLGA, 75:25 MW: 20000, Resomer RG 752S, Boehringer) were used as received.

3.2.2 Emulsions formulation & Liquid Emulsion Extraction (LEE)

Emulsions with different *o-w* ratio of 20:80 and 10:90, respectively, were prepared. Oily phase was prepared dissolving fixed amount of the polymer (45% or 55% w/w of the oily phase) and drug (3 or 6 or 10 % w/w of the polymer) into acetone. Water phase was prepared dissolving PVA (0.6% w/w of the water phase) into aqueous glycerol solution (80:20 glycerol/water). The oily phase was added into the water phase using a high-speed stirrer (mod. L4RT, Silverson Machines Ltd., Waterside, Chesham Bucks, UK) at 4000 rpm for 3 min. 20 g of emulsion was charged in a beaker and the solvent was extracted adding dropwise 60 g of aqueous-glycerol (ratio 50:50 water/glycerol), the resulting solution was stirred for 80 min at 400 rpm; subsequently, 60 g of pure water were added dropwise and the extraction was performed at the same stirring conditions for other 100 min.

3.2.3 SEE: apparatuses & microdevices characterization

Schematic representation of the two SEE process layouts (batch and continuous operating mode) and detailed descriptions of the morphology and size evaluations of the produced microspheres were already reported in Chapter 2.

3.2.4 *Solid state characterization*

Thermograms of powder samples were obtained using a differential scanning calorimeter (DSC mod. TC11, Mettler Toledo, Inc., Columbus, USA). Fusion temperature and enthalpy were calibrated with an indium standard (melting point 156.6°C). The samples (± 5 mg) were accurately weighed, crimped in an aluminium pan and heated from 25 to 300°C at 10°C/min, under nitrogen purge of 50 mL/min. Diffraction patterns were obtained using an X-ray diffractometer (mod. D8 Discover, Bruker AXS, Inc., Madison, USA) with a Cu sealed tube source. Samples were placed in the holder and flattened with a glass slide to assure a good surface texture. The measuring conditions were as follows: Ni-filtered CuK radiation, $\lambda = 1.54 \text{ \AA}$, 2θ angle ranging between 5° and 70° with a scan rate of 3 s/step and a step size of 0.2°. DSC and X-ray analyses were performed in three replicates for each batch of material.

3.2.5 *Solvent residue analysis*

The acetone residue was measured using a head space sampler (mod. 50 Scan, Hewlett & Packard, Palo Alto, CA, USA) coupled to a gas chromatograph interfaced with a flame ionization detector (GC-FID, mod. 6890 Agilent Series, Agilent Technologies Inc., Wilmington, DE). Acetone was separated using a fused-silica capillary column 30 m length, 0.25 mm internal diameter, 0.25 μm film thickness (mod. DB-1, J&W, Folsom, CA, USA). The oven temperature in the GC was set to 40°C for 8 min. The injector was maintained at 180°C (split mode, ratio 1:1) and Helium was used as the carrier gas (7 mL/min). Head space conditions were: equilibration time 60 min at 100 °C, pressurization time 2 min, loop fill time 1 min. Head space samples were prepared in 10 mL vials filled with 3 mL of suspension.

3.2.6 *Drug loading & release*

Drug loading was measured by dissolving a known mass (5 mg) of microspheres in 2mL of acetone. Samples were stirred for 1 h at 100 rpm to ensure the complete dissolution of the polymer. Pure RA was also tested to verify its stability in acetone; no drug degradation was observed. The concentration of drug in the resulting solution was determined by HPLC (mod. Agilent Tech. 1200 series). The column was C₁₈ (3.9 x 250 mm), packed with 10 μm particles size. Elution was performed with methanol/water (98:2 v/v) at a flow rate of 1 mL/min. 20 μL were injected and the absorbance of the eluting compound was monitored at 324 nm. The amount of measured drug was then converted in the effective drug loaded into microspheres as in the follows: $100 \times (\text{weight of monitored drug} / \text{weight of sample taken for}$

analysis). The encapsulation efficiency was calculated as $100 \times (\text{effective loading}/\text{theoretical loading})$. Since the solubility of RA in *n*-propanol-water solution (30:70 v/v) is about 0.03 mg/mL, for each release test, 100 mg of microspheres were suspended in 500mL of this solution continuously stirred at 100 rpm in a 35°C incubator to maintain adequate sink conditions. The concentration of the released drug in the external medium was continuously detected by a UV probe at 324 nm (mod. Cary 50, Varian Palo Alto, CA).

3.3 Results & Discussion

3.3.1 Selection of the operating conditions

When acetone, water, and glycerol are mixed together, the phase diagram of the ternary system shows a two phase region due to phase separation and to obtain a stable emulsion, the ternary mixture composition should lie in this region. To verify the influence of the position of the operating points on the emulsion stability, two different *oil-water* ratios were prepared of 20/80 and 10/90, with a given composition of the oily phase (acetone with 45% w/w of PLGA plus 3% of RA) and the water phase (glycerol/water 80/20 with 0.6% w/w of PVA). **Figure 3.1** reports the ternary acetone-water-glycerol diagram in which two red dots indicate the position of the operating points selected for emulsions formulation. One point is located in the Phases I region (i.e., in the area of complete miscibility between the three components) and the second near the border of Phase II (i.e., in the two phases region). The emulsion with the *o-w* ratio of 20/80 (point 1, in **Figure 3.1**) was stable and led to well defined PLGA microspheres after the oily phase removal; whereas, the emulsion with the *o-w* ratio of 10/90 (point 2, in **Figure 3.1**) produced only large polymer aggregates. These results mean that the emulsion with the *o-w* ratio of 10/90 is not stable and in the following part of the study only the *o-w* ratio of 20/80 is used.

3.3.2 Comparison with the conventional liquid extraction

In this study, the comparison of the extraction processes (liquid and supercritical) is proposed based on the characteristics of the microspheres obtained by SEE-B and by conventional liquid extraction (LEE). The same emulsions (*o-w* ratio 20:80) have been processed with the two technologies and the morphology of microspheres produced by SEE-B was in all cases spherical and no coalescing; however, collapsed particles were often produced by LEE. All SEE experiments were performed operating at 80 bar, 36°C, since at this process conditions, acetone is completely miscible in SC-CO₂ [112]; whereas, the

solubility of the glycerol-water external phase in SC-CO₂ is extremely small [113-114]; therefore, a selective extraction of the oily phase from emulsions, is expected. Other operating conditions used, were already described in Chapter 2. Solid PLGA/RA products obtained after SEE-B treatment of these emulsions are reported in the SEM images illustrated in Figure 3.2 (a-b), respectively.

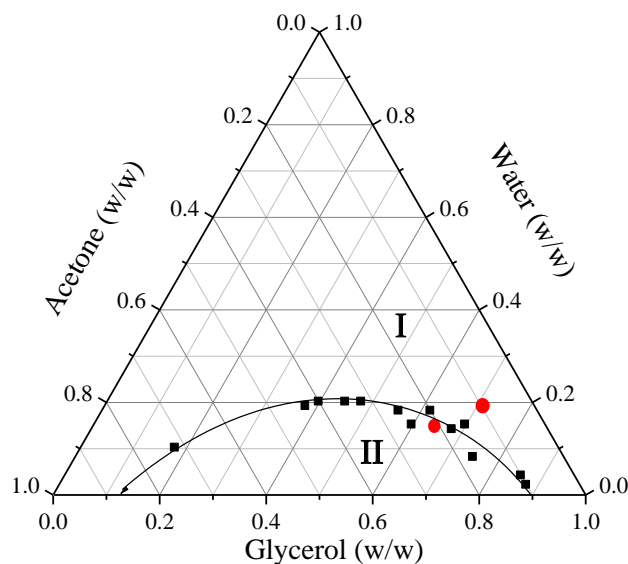


Figure 3.1. Phase diagram of water-glycerol-acetone ternary system with the representation of operating points I: *o-w* 20/80 and operating point II: *o-w* 10/90. Experimental data adapted from Matsumoto *et al.*, 2008.

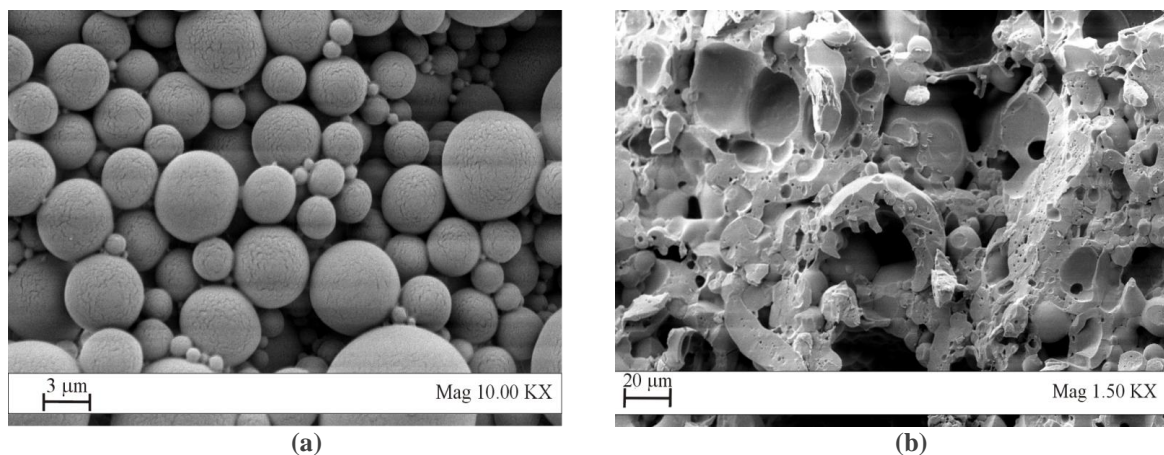


Figure 3.2 a-b. SEM images of the microparticles obtained by SEE using emulsions with different *o-w* ratios; (a) well shaped microspheres using an *o-w* ratio of 20/80; (b) collapsed and connected microspheres using an *o-w* ratio of 10/90. *Oily phase*: acetone with 45% PLGA and 3% RA w/w (theoretical loading); *water phase*: glycerol-water 80:20 with 0.6% w/w of PVA.

An example of the different results obtained, is illustrated in the SEM images reported in **Figure 3.3 (a-b)**, that are related to microparticles obtained from emulsions prepared with PLGA concentrations of 45% and RA content of 6%. The water phase was formed by glycerol-water (80:20) with 0.6% w/w of PVA. The SEM image in **Figure 3.3b**, shows large aggregates of microparticles. This phenomenon can be due to an inadequate amount of the extraction agent or an insufficient absorbing rate of the solvent leached from the solidifying microspheres, that may generate intra-particle adhesion [115]. On the contrary, the enhanced mass transfer characteristic of SC-CO₂, generates a faster extraction avoiding particles adhesion, as confirmed by SEM image of microspheres reported in **Figure 3.3a**. Distribution data, encapsulation efficiency and solvent residues of the produced microspheres are summarized in **Table 3.1**. For example, starting from an emulsion with a Droplet Mean Size of 4.1 μm (SD ± 2.2), microspheres with a mean size of 3.6 μm (SD ± 1.9) were obtained by SEE-B and with a mean size of 4.3 μm (SD ± 2.3) were produced by conventional LEE. The encapsulation efficiency into PLGA microspheres was 80% when operating with SEE-B and 73% when the conventional extraction process was used. Both encapsulation values can be considered excellent and indicate that the emulsion formulation proposed is stable.

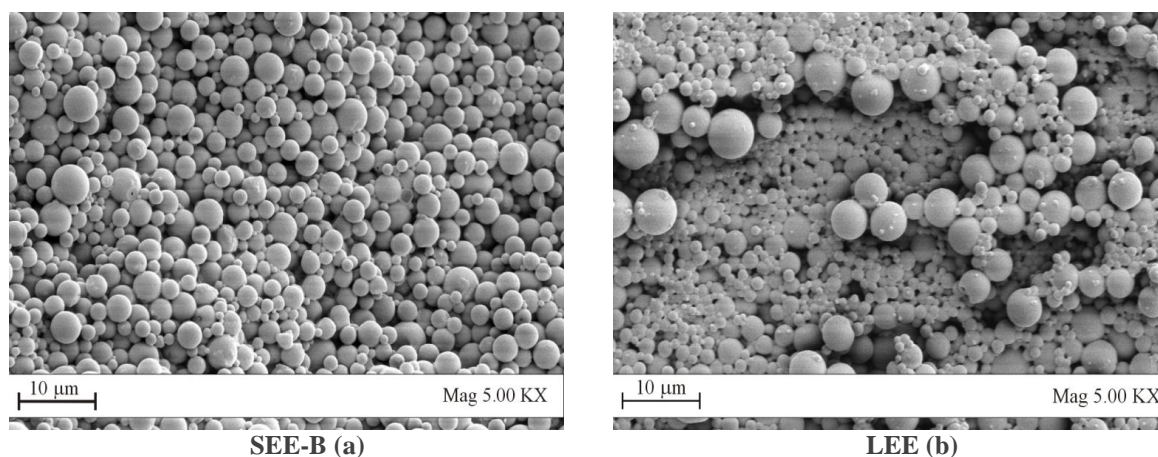


Figure 3.3a-b. SEM images of PLGA/RA microspheres produced by: (a) SEE-B; (b) conventional Liquid Extraction (LEE). Emulsion (*o-w* ratio 20/80) composition: *oily phase*, acetone with PLGA 45% w/w; *water phase*, glycerol-water 80:20 and 0.6% w/w of PVA.

Table 3.1. Results of liquid emulsion extraction (LEE) and supercritical extraction (SEE-B) proposed in term of PSDs produced using an *o-w* emulsion (ratio: 20:80).

PLGA content in oil (%)	45		
Teoretical drug loading (%)	3		
Distribution data	DSDs	PSDs	
Process layouts	---	LEE	SEE-B
MS (μm)	4.1	4.3	3.6
SD (μm)	± 2.2	± 2.3	± 1.9
Recovery (%)	----	65	56
Solvent Residue (ppm)	----	50000	3591
Effective drug Loading (%)	----	2.2	2.4
Encapsulation efficiency (%)	----	73	80

Solvent residue monitored after SEE-B processing was 3591 ppm and was significantly lower than the value found after the conventional LEE that produces suspensions with an acetone residue of the order of 50000 ppm. As a consequence, more complex downstream processes are required for particle recovery such as, prolonged washing with pure water, as well as, acetone/glycerol/water mixture separation to recover the pure solvents. Also the processing time is different because SEE-B process requires only 60 min against the 160 min of the LEE, to process the same quantity of emulsion.

3.3.3 *Batch vs. continuous operation*

Emulsions with *o-w* ratio of 20:80 were formulated fixing the PLGA concentration in acetone at 45% w/w and varying the RA theoretical loading from 3, 6 and 10 % w/w. They were treated using the two different SEE layouts: batch (SEE-B) and continuous (SEE-C). All the PSDs data of the microspheres recovered using the two processes layout and other significant process information are reported in **Table 3.2**. The DSDs data of the emulsions treated are also reported, for comparison purposes. Microsphere size and distribution are the first parameters considered for the comparison. Looking at the PSDs data of the microspheres produced by SEE-B and SEE-C, it is evident that they are similar and the process layout does not have a significant effect on the PSDs. Indeed, starting from an emulsion with a Droplet Mean Size of 3.5 μm (SD ± 1.9), microspheres with a mean size of 3.2 μm (SD ± 1.4) were obtained by SEE-B and with a mean size of 3.3 μm (SD ± 1.9) were produced by SEE-C. The drug encapsulation efficiency measured for all the microdevices produced were very good and ranged between 80 and 90%.

Table 3.2. Results of different SEE process layouts batch (B) and continuous (C) proposed in term of PSDs of the microspheres produced using an *o-w* emulsion (ratio 20:80).

PLGA content in oil (%)	45								
Theoretical drug loading (%)	3			6			10		
Distribution data	DSDs	PSDs		DSDs	PSDs		DSDs-	PSDs	
Process layouts	---	SEE-B	SEE-C	---	SEE-B	SEE-C	---	SEE-B	SEE-C
MS (μm)	3.5	3.2	3.3	4.9	3.5	3.2	6.2	5.9	4.3
SD (μm)	± 1.9	± 1.4	± 1.9	± 2.2	± 1.4	± 1.6	± 4.1	± 3.6	± 2.3
Processing Time (min)	---	60	10	---	60	10	---	60	10
Recovery (%)	---	56	85	---	48	90	---	60	89
Solvent Residue (ppm)	---	3591	1075	---	4100	1025	---	3600	980
Effective drug Loading (%)	---	2.4	2.7	---	5.1	5.2	---	8.7	8.8
Encapsulation efficiency (%)	---	80	90	---	85	87	---	87	88

As indicated in a previous chapter, the two process layouts can show different recovery efficiency, phase mixing and, therefore, processing time. Indeed, the batch process allowed the recovery of maximum 56% of the charged material because part of the microsphere suspension was lost in the gas stream released during the final depressurization step and part was not recovered from the walls of the precipitator. On the contrary, the continuous process allowed the recovery of about 85-90% of the charged material. The solvent residue after the continuous process was about 1000 ppm, a considerably lower value than the ones measured in the batch SEE operations that ranged between 2000 and 4000 ppm. This result confirms that the continuous process produces a better contact between the two phases (emulsion/SC-CO₂), enhancing mass transfer. The final remarkable result is the processing time: i.e., considering as a reference time, the residence time of the liquid phase in the packed column, the continuous processing requires a residence time of the emulsion/suspension in the column of only 10 min; whereas, about 60 min is the residence time of the emulsion/suspension treated by SEE-B and 160 min are necessary to perform the conventional liquid-liquid extraction.

3.3.4 *Microspheres size tailoring and solid state characterization*

PLGA concentration in the acetone oily phase was varied between 45 and 55% w/w at a fixed drug concentration of 3% w/w and the influence on microspheres size distribution and loading efficiency was studied, in the case of the continuous SEE process. The emulsion *o-w* ratio and the composition of the water external phase was maintained constant, as previously reported. The PSDs data of the produced microspheres are reported in **Table 3.3**, together

with the DSDs data of the corresponding emulsions, for comparison purposes. The variation of PLGA concentration in the oil phase, in the range explored, always produced emulsions with stable and non-coalescing droplets, as illustrated in the optical microscope image reported in **Figures 3.4a-b**. The correspondent microspheres obtained after SEE-C operation are reported in the SEM images shown in **Figures 3.4c-d**. Microspheres with a mean size of 3.2 μm (SD ± 1.4) were obtained at the PLGA percentage of 45% w/w and with a mean size of 4.0 μm (SD ± 2.1) at the PLGA percentage of 55% w/w charged in the oily phase, respectively.

Table 3.3. DSDs and PSDs of microspheres produced by SEE-C using an *o-w* emulsion (ratio 20:80; PLGA concentration: 45% and 55% w/w; drug loading: 3% w/w).

PLGA content in oil (%)	45		55	
Theoretical drug loading (%)	3			
Distribution data	DSD	PSD	DSD	PSD
MS (μm)	3.5	3.3	4.5	4.0
SD (μm)	± 1.9	± 1.9	± 2.4	± 2.1
Recovery efficiency (%)	--	85	--	90
Solvent Residue (ppm)	--	1075	--	1006
Effective drug Loading (%)	--	2.7	--	2.5
Encapsulation efficiency (%)	--	90	--	83

Thermal analysis (DSC) was performed on the produced microspheres and on raw PLGA and RA, for comparison purposes. The corresponding thermograms are reported in **Figure 3.5**. PLGA (75:25) shows a glass transition that remains relatively constant (onset 39.98°C; endset 45.32°C) in all the observed samples and the polymer decomposition occurs above 300°C. Raw RA shows an endothermic peak at about 58°C, due to its melting. The PLGA/RA microspheres show the same degradation event of the unprocessed polymer confirming that the supercritical process does not modify the polymer structure; whereas, the characteristic peak of RA is no longer visible in the microspheres, even when the drug effective loading was 8.8% w/w. This fact suggests that the drug is dissolved into the PLGA matrix. X-ray analyses were performed to obtain information about the solid state of the produced materials. The diffraction patterns of microparticles are reported in **Figure 3.6**. The XRD of raw polymer and RA are also reported, for comparison. XRD analyses show that all the particles obtained are amorphous due to the fast polymer precipitation inside the droplets during the oily phase extraction.

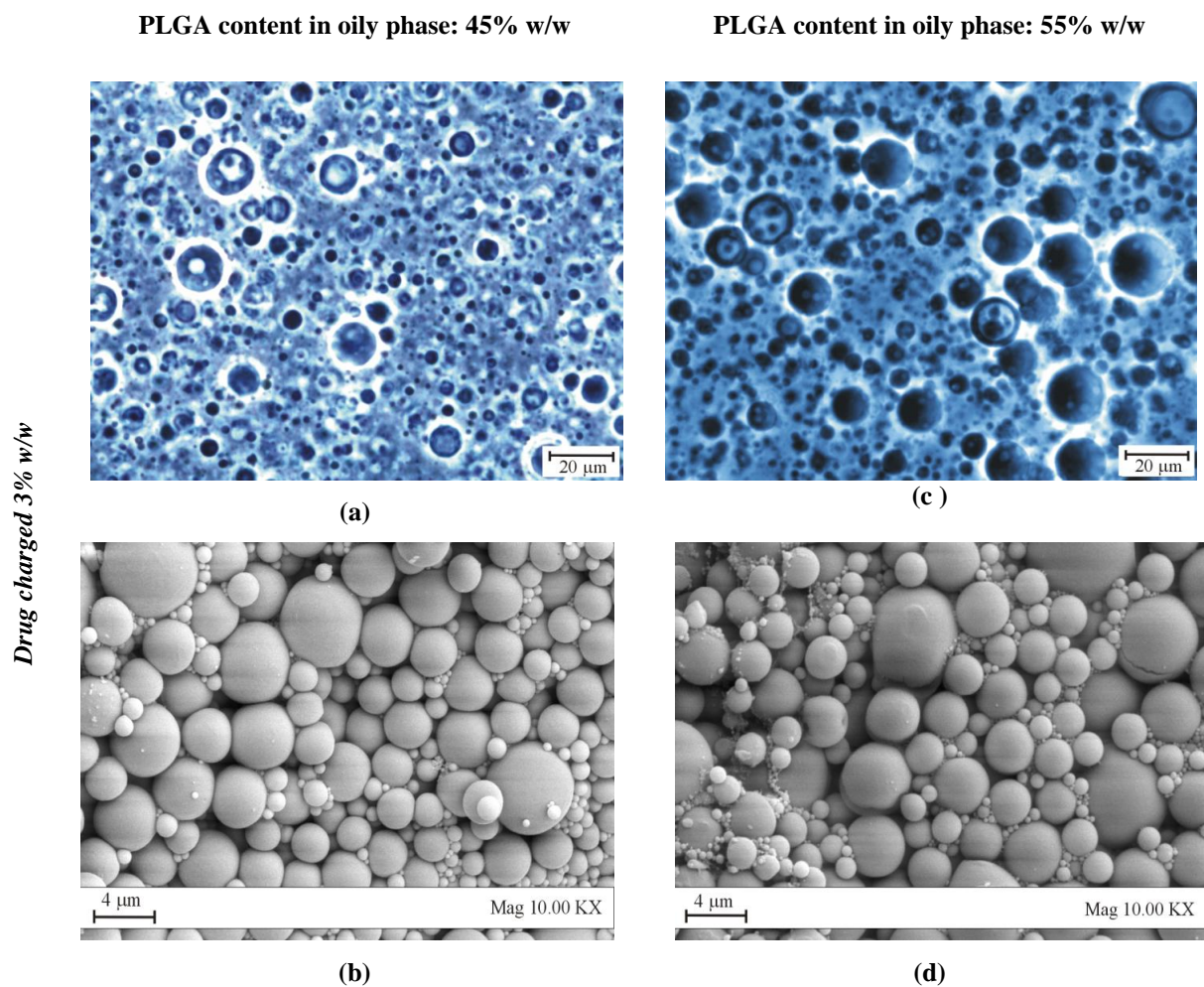


Figure 3.4a-d. Optical microscope images of the emulsions and SEM images of the related microspheres produced by SEE-C using emulsions (*o-w* ratio 20/80) with different PLGA content in the oily phase of 45 (a-b) and 55% (c-d) w/w, respectively. The theoretical drug loading was of 3% RA w/w (effective loading 2.7 and 2.5 % respectively); *water phase*, glycerol-water 80:20 and 0.6% w/w of PVA.

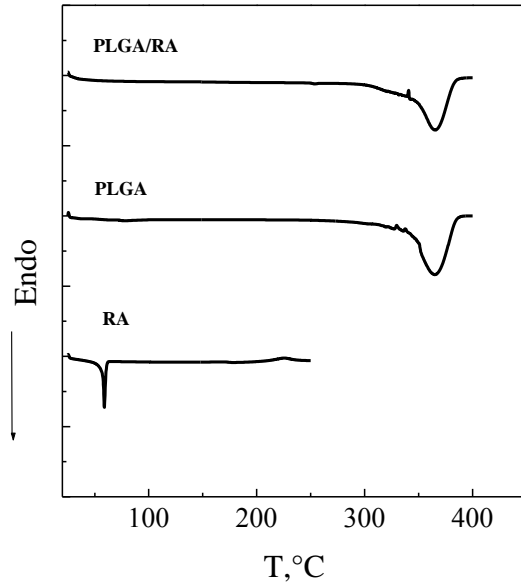


Figure 3.5. DSC traces of PLGA/RA microspheres produced by SEE with a MS of 4.3 μm ($\text{SD} \pm 2.3 \mu\text{m}$) and effective RA loading of 8.8% w/w. Traces of untreated PLGA and RA are also reported, for comparison.

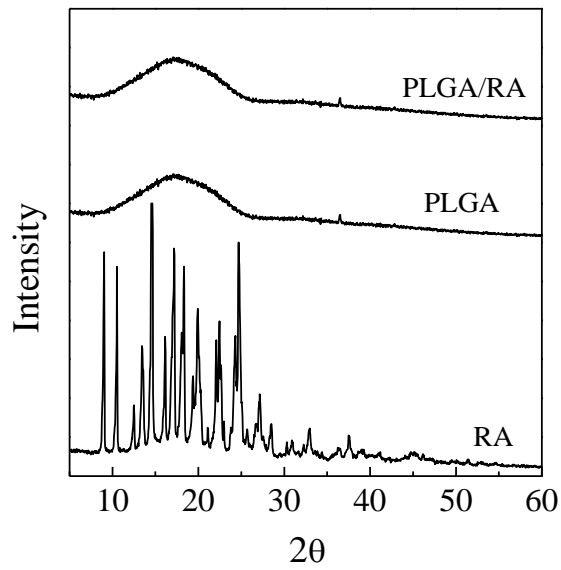


Figure 3.6. XRD patterns of PLGA/RA microspheres produced by SEE with a MS of 4.3 μm ($\text{SD} \pm 2.3 \mu\text{m}$) and effective RA loading of 8.8% w/w. Patterns of untreated PLGA and RA are also reported, for comparison.

3.3.5 Drug release study

PLGA microspheres produced by SEE-C and with RA effective loadings of 2.7, 5.2 and 8.8% w/w, were tested for drug release studies in a modified media [116] of water/n-propanol (70:30) at 35°C (microspheres distribution data are reported in **Table 3.2**). The release profiles are illustrated in **Figure 3.7**; in the same figure the dissolution rate of pure RA is also reported. Drug release was monitored only for 6 days, since RA degradation in the external medium was observed when longer times were used. Release profiles obtained at different loadings show that, when the RA content is increased, a slower drug release is obtained: i.e., 90% of RA is released in 6 days when the drug loading is 2.7% w/w; whereas, in the same time, only 40% and 10% of the drug is released when the charge is 5.2% and 8.8% w/w, respectively.

It is known from the literature, that drug release from PLGA can be described in two steps; the first one reflects the diffusion controlled mass transfer of the drug accessible at the solid/dissolution medium interface and the second step reflects the release of drug entrapped in the polymer during its bulk degradation [117-118]. The release behavior at different drug loadings observed in this study can be explained considering the low solubility of RA in the release medium (see measured solubility data in the Methods section). Indeed, as suggested by *Lee* [119], when the concentration of the drug in the polymer microsphere is higher than its equilibrium solubility in the external medium, two moving fronts can be established (diffusion followed by bulk erosion) and they are synchronized (the second front will be influenced by the first one). In our case, the diffusion front is very slow and can move towards the internal of the particles only when the concentration in the solid phase decreases to values lower than the equilibrium value; as a consequence, the higher is the drug concentration in the polymer, the slower is the movement of the diffusion front [120].

An attempt to describe this PLGA release mechanism (diffusion/degradation controlled) was also performed using the mathematical model proposed by *Corrigan and Li* [121] that takes into account the two different release steps with the following **equation (1)**:

$$F_{tot} = F_D + F_{deg} \quad (1)$$

where F_{tot} is the total fraction of drug released at a given time; F_D is the initial diffusion contribution of drug accessible at the solid/dissolution medium interface (mass percentage)

and F_{deg} is the contribution of drug (mass percentage) entrapped in the polymer, whose release depends only to the polymer bulk degradation. The authors also assumed that the drug is dispersed as a separate phase into the polymer. As a consequence, the component F_D can be described as:

$$F_D = F_{Dinf} (1 - e^{-K_d t}) \quad (2)$$

where F_{Dinf} is the diffusion contribution at infinite time and K_d is the first order constant associated with the diffusion controlled release that can be directly proportional to the apparent diffusivity of the drug in the system. K_d is equal to $DAC_s/F_D H_l$ where D and C_s are the diffusion coefficient and the solubility of the drug respectively, A is the surface area of drug available for dissolution and H_l is the apparent aqueous diffusion boundary layer thickness. The apparent diffusivity takes into account the drug transfer through the polymer and the drug transfer through the external medium [122].

The second component of the equation (1), F_{deg} , is related to polymer bulk erosion and can be described by **equation (3)**:

$$F_{deg} = (1 - F_{Dinf}) \left(\frac{e^{Kt - Kt_{max}}}{1 + e^{Kt - Kt_{max}}} \right) \quad (3)$$

where t_{max} and K are, respectively, the time of the maximum drug release rate and the first order rate constant of drug release, mediated by polymer degradation. Therefore, the fractional drug release versus time profile can be described by **equation (4)**:

$$F_{tot} = F_D (1 - e^{-K_d t}) + (1 - F_D) \left(\frac{e^{Kt - Kt_{max}}}{1 + e^{Kt - Kt_{max}}} \right) \quad (4)$$

Equation (4) allows the estimation of the parameters K_d , F_D , K and T_{max} by a non linear least square fitting. The calculated parameters obtained by fitting the experimental data with **equation 4** are reported in **Table 3.4**. The model also gives a fair good representation of the RA release profiles, as can be seen from the continuous curves reported in **Figure 3.7**.

Looking at the kinetic parameters reported in **Table 3.4**, it can be observed that K_d values decrease by increasing the drug loading (from 0.0085 to 0.0011 days⁻¹ with a drug loading of 2.7 and 8.8%, respectively); this behavior should mean that increasing the loading

of a low solubility drug, the apparent diffusivity of the drug will decrease and, therefore, the release kinetic constant is slower. On the contrary, the F_{Dinf} values increase from 0.56 to 0.96 when the drug loading is increased from 2.7 to 8.8%. F_{Dinf} represents the fraction of drug released by simple diffusion; i.e., this trend is reasonable considering that increasing the drug loading, diffusion becomes the prevalent phenomenon, controlling the drug release. T_{max} values were directly evaluated from the experimental curves and fixed to 1.5, 3.2 and 3.5 days. The timing of the maximum drug release rate should be explained taking into account that bulk erosion front follows the diffusion front, as stated before; therefore, when the diffusion front is delayed (by higher drug loading of the low soluble drug) also the T_{max} value increases. Finally, the bulk erosion kinetic constant K was calculated at 0.68 days^{-1} and was maintained constant in all data fitting because it should be independent from the drug loading, being only related to the depolymerization reaction.

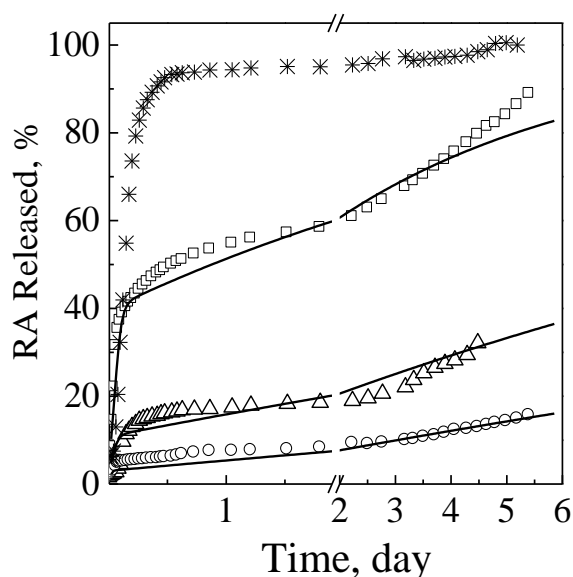


Figure 3.7. Release profiles from PLGA microspheres with effective RA loadings of 2.7% (\square), 5.2 % (Δ), 8.8 % (\circ). The release profile of pure RA is also proposed, for comparison (*). Curve fittings obtained using equation (4) are reported, as continuous line.

Table 3.4. Best fit model parameters estimated from RA release profiles obtained from PLGA microspheres.

Effective drug Loading (%)	F_d	K_d [day ⁻¹]	K [day ⁻¹]	T_{max} [day]	R^2
2.7	0.56 (± 0.01)	0.0085 \pm (0.0005)	0.68	1.5	0.97
5.2	0.89 (± 0.003)	0.002 \pm (0.001)	0.68	3.2	0.93
8.8	0.96 (± 0.001)	0.0011 \pm (0.00002)	0.68	3.5	0.94

3.4 Conclusions & Perspectives

Supercritical fluids emulsion extraction technology offers a new strategy in the biopolymer microsphere production with a better particle size control also when labile compounds, such as retinyl acetate, are processed. Taking advantage of the enhanced mass transfer of the supercritical solvent, spherical PLGA microspheres, with less residual solvent respect to the conventional process, can be successfully produced with an excellent drug encapsulation. The upgrade of SEE technology into the continuous process layout (SEE-C) allows a higher throughput with smaller plant volumes, eliminating all the batch-to batch repeatability drawback. This technology can be proposed as a process innovation that may allow the fast production of tailored PLGA/drug microspheres with an excellent control of drug release.

Chapter 4. PLGA-PAMs produced by SEE-C: Study on Bioactive Signal Release in Myoblast Culture

4.1 Introduction

Cell therapy promises to become a major therapeutic option in regenerative medicine, although relevant questions about cell homing, survival and differentiation into the host tissue are still open. *Pharmacologically Active Microcarriers* (PAMs) may contribute to face these problems since these biocompatible and/or bioresorbable microdevices can deliver a specific bio-signal (such as growth factors) they are loaded with [123-125], inside to a more complex 3D scaffold with cells onboard. In this configuration they may also act as transient microdevices influencing cell fate into the host tissue, as recently reported [126-127].

Poly-lactic-co-glycolic acid (PLGA) has received great interest as a hydrolytically degradable and bioresorbable polymer [128] for the development of nano- and micro-devices to be used in tissue engineering [129] being among the few biopolymers approved by the Food and Drugs Administration (FDA) for injectable/implantable use in human body. As an example, PLGA microcarriers have been reported as a moldable scaffold for cartilaginous tissue engineering [130-132] and when RGDS peptides were immobilized onboard they were able to promote chondrocyte attachment, proliferation, viability and sulfated glycosaminoglycans secretion [133].

In this light, considerable scientific efforts have been made for the development of robust and reproducible technologies to manufacture these PLGA microcarriers, in order to better control their size distribution, as well as, their bioactive molecule loading and release. The most common method to encapsulate biomolecules such as, peptides or proteins, into PLGA microspheres is the use of double *water-oil-water* emulsions followed by solvent evaporation. This technique is easy to set up at the laboratory scale but its success is hampered by the limited efficiency and the lack of batch-to-batch reproducibility in encapsulation of the bioactive molecules [134]. Moreover, due to the long evaporation step required, the encapsulated protein may form insoluble precipitates when exposed to the water/organic solvent interfaces of emulsion [135-136], or may diffuse to the continuous

external aqueous phase leading to protein loss [137], although this last problem can be partially cleared adding hydrophilic components, such as glycerol, that participate to the formation of a stable internal phase of double emulsification [138].

The aim of this work is to produce high quality PLGA-PAMs to be used for sustained release of bioactive signals in a culture medium. Different *water-oil-water* emulsions, obtained using ethyl acetate as oily phase solvent, will be prepared and processed by SEE-C for the production of microdevices with controlled size and distinct bioactive protein (bovine serum insulin) loading; they will also be characterized in terms of morphology, size and protein encapsulation efficiency. The insulin release profile in different media (phosphate saline buffer and cell culture medium) will be monitored and fitted using a mathematical model to give a better description of the two different release steps (diffusion and degradation) that are typical of the PLGA devices. Finally the H9c2 cell line (rat embryonic ventricular myoblasts) [139] will be cultured in presence of insulin-loaded PLGA-PAMs to monitor cell viability and proliferation as sustained by bioactive insulin release in serum-free culture medium.

4.2 *Apparatus, Materials and Methods*

4.2.1 *Materials*

CO₂ (purity 99.9%) was purchased from SON (Naples, Italy). Poly (lactic-co-glycolic) acid (PLGA 50:50; RESOMER[®] RG 504H; Mol wt: 38000-54000; inherent viscosity 0.45-0.60 dl/g) was supplied from Boehringer Ingelheim (Germany). Polyvinyl alcohol (PVA, Mol wt: 30,000–55,000), Insulin from bovine pancreas (INS, purity 99.9%) and glycerol (GLY, purity 99%) were obtained by Sigma-Aldrich Co. (Milan, Italy). Trifluoroacetic acid (TFA) and HPLC grade acetonitrile were purchased by Carlo Erba Reagents (Milan, Italy).

4.2.2 *Emulsion Formulations*

The *water-oil-water* emulsion ratio was fixed at 1:19:80. Particularly, a fixed amount of insulin was dissolved into an aqueous/TFA GLY solution (250 µl of GLY and 750 µl of water with 0.1% TFA) with PVA concentration of 0.04% w/w and 1 mL of this solution was added into the oily phase formed by ethyl acetate (EA) and PLGA at 10% w/w. Insulin is only sparingly soluble in water and it is mandatory to set the pH below the protein isoelectric point (pI=5.5), therefore, an acid environment obtained with TFA was used at pH 2.5 to assure that ion-pairing takes place with all basic insulin functionalities. The primary *w₁-o* emulsion was obtained by ultrasonication with a digital ultrasonic probe (mod. S-450D, Branson Ultrasonics

Corp., Danbury, CT, USA) at 50% of amplitude for 90 sec. The secondary w_1-o-w_2 emulsion was obtained mixing the primary emulsion with an outer water phase of saturated aqueous PVA solution (0.6% w/w in water) by high-speed homogenizer (mod. L4RT, Silverson Machines Ltd., Waterside-Chesham Bucks, UK). An external ice bath was always used to keep the emulsion temperature lower than 10°C. All the emulsions were prepared with filtered or autoclaved solutions.

4.2.3 Production by SEE-C Technology in GMP sterile conditions

SEE-C apparatus was already described in details in Chapter 2. However, procedures for sterile PAMs collection were developed in this part of the work: i.e., during the runs, the PAMs suspension is continuously collected at the bottom of the extraction column, washed with sterilized water by centrifugation and then lyophilized. At the end of each run, the column is washed with pure acetone and sterilized water to eliminate any processing residue from the internal packing surface and also to sterilize it. Ultrafiltered or autoclaved gas and liquids coupled with standardized operative procedures in a continuous operation apparatus assured PAMs sterility.

4.2.4 Droplets & PAMs characterization

The droplets in the emulsions were observed using an optical microscope (mod. BX 50 Olympus, Tokyo, Japan) equipped with a phase contrast condenser. Microspheres shape and morphology were analyzed by Field Emission-Scanning Electron Microscope (FE-SEM mod. LEO 1525, Carl Zeiss SMT AG, Oberkochen, Germany).

The specimens were prepared by mounting the dry sample on aluminium stubs and coating it with a gold-palladium film (layer thickness 250Å) using a sputter coater (mod. 108 A, Agar Scientific, Stansted, UK). Droplet Size Distributions (DSDs) and Particle Size Distributions (PSDs) were measured by a dynamic light scattering (DLS, mod. Mastersizer S, Malvern Instruments Ltd., Worcesterstershire, UK). Analyses were performed immediately after the preparation of emulsions and microdevices suspensions, using several milligrams of each sample. Mean size was measured ten times for each sample and the distributions proposed are the mean of the replicates. Droplets and particle size are expressed as volume Mean Diameter (MD, μm) and Standard Deviation (SD) of values collected.

4.2.5 Protein loading determination

The amount of protein loaded into the microspheres was monitored using the procedure described by *Bilati et al.* [140]. Briefly, 10 mg of dried microspheres were dissolved in 600 μL of acetonitrile in centrifuge tubes and sonicated until the complete transparency of the solution. Then, 1400 μL of water containing 0.1% TFA (0.1% aqueous TFA solution) were added dropwise to the corresponding centrifuge tube to dissolve insulin. The remaining undissolved PLGA was separated by centrifugation at 2000 rpm for 2 minutes. The resulting clear supernatant solution was directly analyzed at room temperature by HPLC (model 1200 series; Agilent Technologies Inc.) equipped with a LiCrosphere C18 column (250 \times 4.6 mm), packed with 5 μm particles size of 100 \AA pore size. The mobile phase was composed of acetonitrile/water mixture (32:68 v/v) containing 0.1% v/v TFA. The flow rate was 0.9 mL/min, the injection volume of the test sampled was 20 μL and the detecting wavelength was 214 nm. The amount of insulin in solution was calculated by means of a calibration curve and then converted in the effective insulin loading as the amount (mg) of insulin charged in PLGA-PAMs (g). Encapsulation efficiency (EE) is the ratio of the final insulin loading to the nominal one. A known amount of pure insulin was also tested to verify its stability in water with 0.1% TFA and no protein degradation was observed. Each sample was assayed in quadruplicate and a good reproducibility was observed.

4.2.6 In Vitro protein release studies

In vitro release kinetics of insulin from PAMs were evaluated by suspending accurately weighed 20 mg of dried microspheres in 2 mL of Phosphate-Buffered Saline (PBS, 100 mM, pH 7.4) or 2 mL of Dulbecco's Modified Eagle Medium (DMEM) used for cell culture, in a centrifuge tube. The tubes were then placed in an incubator at 37°C and stirred continuously at 50 rpm. At fixed time intervals, the samples were centrifuged at 4000 rpm for 15 minutes and the supernatant was completely withdrawn and replaced with fresh media to maintain sink conditions. The amount of released protein was determined by measuring the protein concentration in the supernatant using HPLC method. Release experiments were performed in triplicate and the proposed curves are the mean profiles obtained. The percentage of released insulin was defined as the mass of protein released divided by the total mass of the charge.

4.2.7 PAMs Sterilization & Cell Culture

Microspheres sterility is assured by a good manufacture practice protocol adopted during their production by SEE-C. However, before their use in cell cultivations, an additional

soaking in 1% v/v penicillin/streptomycin (PEN/STR) was performed for 15 min; PLGA microspheres were then recovered by centrifugation and washed with PBS. Rat embryonic ventricular myoblasts (H9c2 cell line) were used to test cell viability and proliferation as sustained by bioactive insulin release from PLGA microspheres in serum-free culture medium. An optical microscope image of the cells is reported in **Figure 4.1a**. Cells were routinely grown to 80% confluence at 37°C in an atmosphere of 5% CO₂ prior to passage and seeding for experiments in a standard medium formed by DMEM with 1% of L-glutamine solution (GLU, 0.1 ug/mL) supplemented with 10% v/v of fetal bovine serum (FBS) and 1% v/v PEN/STR. The Alamar blue (AB) test was used to monitor cell viability and proliferation by direct addition to culture medium at different time points (24 and 72 h). The redox reaction where AB is reduced by the cells was measured by fluorescence readings (Ex/Em = 540/590 nm) in a multilabel multiplate Infinite M200 reader (TECAN, Cernusco sul Naviglio, MI, Italy) [141].

Cell viability and proliferation were monitored in a DMEM serum free medium added with insulin-loaded microspheres (see **Figure 4.2b**). Each sample was assayed in 10 replicates.

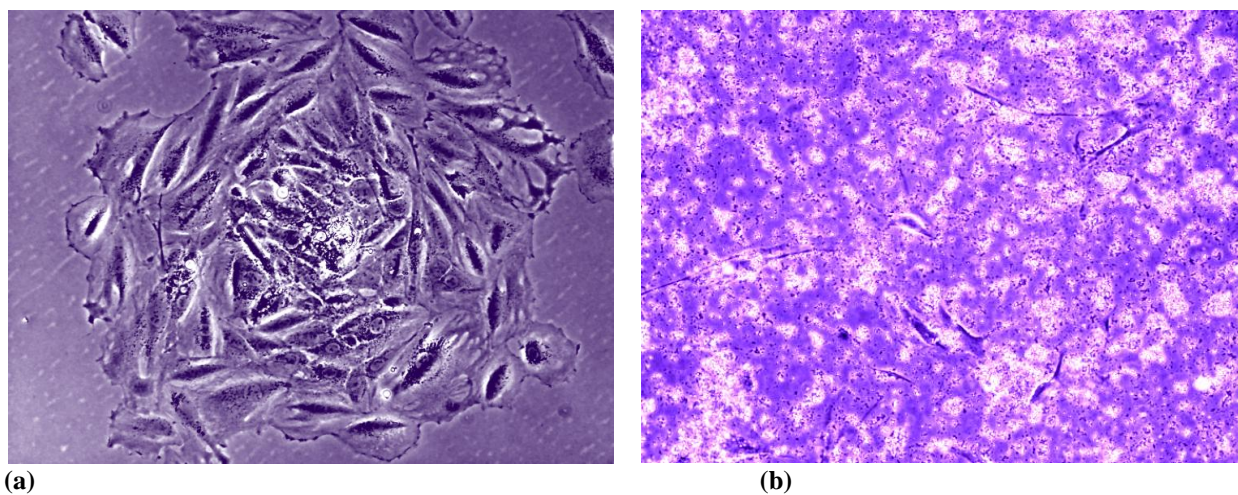


Figure 4.1a-b. OM image of 80% confluent embryonic ventricular myoblasts (cell line H9c2) obtained from rat cultivated in a standard medium(a); PLGA microspheres were suspended in the cell medium with cells stuck at the bottom of the culture flask (b).

4.3 Results & Discussion

To ensure selective extraction of ethyl acetate from the oily phase of the emulsion, SEE-C operative conditions, in terms of pressure and temperature, were chosen taking into account the high pressure vapor-liquid equilibrium diagram (VLE) of the binary system ethyl acetate/CO₂. Temperature of 37°C and pressure of 80 bar were selected to work above the critical point of the binary mixture considered, as described in detail in Chapter 2.

4.3.1 PLGA-PAMs loaded with Insulin

Bovine serum insulin was loaded into PLGA microdevices as a model compound to be used as a cell medium supplement (substituting for fetal bovine serum). Indeed, insulin has been reported to have the same positive effect of IGF in myoblast cultures and to interact with the same cell receptors [142]. As a consequence, theoretical loading values of 5 and 10 mg/g were selected because close to the ones used for the encapsulation of growth factors into biopolymer microdevices.

A w_1 - o - w_2 double emulsion (see “Apparatus, Materials and Methods” section for the exact composition) with a fixed PLGA content in the oily phase of 10% w/w and insulin theoretical loading of 5 mg/g was prepared by varying the stirring rate during the formation of the secondary o - w_2 emulsion from 2800 to 1400 rpm for 3 min; different droplets with MDs of 3 μm ($\pm 1.2 \mu\text{m}$) and 5 μm ($\pm 2.3 \mu\text{m}$), respectively, were obtained. The emulsions were processed by SEE-C just after their preparation, obtaining two batches of PAMs with different MDs of 2 μm ($\pm 0.9 \mu\text{m}$) and 3 μm ($\pm 2.2 \mu\text{m}$), respectively, because of droplets shrinkage between 33% and 40% of their volume. Examples of the produced PLGA-PAMs are reported in **Figures 4.2a-c**, where FE-SEM images of the obtained microdevices are illustrated. In both cases, the insulin encapsulation efficiency was of 60%, leading to the production of PLGA-PAMs with an insulin content of 3 mg/g of PLGA. Another batch of PAMs was produced with a MD of 3 μm ($\pm 1.9 \mu\text{m}$) but loading the double amount of insulin (10 mg/g). In this case, the encapsulation efficiency was of 58%, leading to PAMs with an insulin content of 6 mg/g. A batch of empty PLGA-PAMs with a MD of 2 μm ($\pm 0.7 \mu\text{m}$) was also produced to be used for the toxicity and control tests; in this case, an o - w emulsion with a PLGA content in the oily phase of 10% w/w and obtained using a stirring rate of 2800 rpm was processed by SEE-C. The PSDs curves of the three different PLGA-PAMs batches charged with insulin are illustrated in **Figure 4.3**. It can be observed that decreasing the stirring rate from 2800 rpm to 1400 rpm during the emulsions generation, the derived particle mean size increases and

distribution slightly enlarges. The encapsulation efficiencies (EE) and insulin loadings (theoretical, TL, and effective, EL) are summarized in **Table 4.1**. They can be considered very good and higher than the values reported in the related literature especially when ethyl acetate was used as oily phase solvent; indeed, ethyl acetate is normally considered a solvent that leads to the worst encapsulation efficiency due to the high tendency of droplets to coalesce during the solvent evaporation step and, therefore, not suggested for microspheres production. Indeed, especially when a double emulsion must be used to encapsulate a water soluble compound, the use of dichloromethane (that is a more toxic solvent) is recommended [143-144]. However, using the SEE-C technology, good encapsulation efficiencies were obtained with respect to the conventional processes, also using ethyl acetate (that is a less toxic solvent if compared with dichloromethane) in the emulsion formulation. Moreover, when a double emulsion is processed for microspheres production, the coalescence between the inner and outer water phase may produce the leakage of the load water soluble molecules. In the emulsions used in the present work, glycerol was added to the internal water phase to increase the inner phase viscosity and reduce the insulin diffusion to the outer water phase, as suggested by some authors [145]. The presence of glycerol, into the inner phase, coupled with the very fast SEE-C processing are considered responsible of the very good encapsulation efficiencies obtained.

Table 4.1. Characteristics of the PLGA-PAMs produced by SEE-C technology: Mean Diameter (MD) and Standard Deviation (\pm), theoretical (TL) and effective (EL) insulin loading and encapsulation efficiency (EE); percentage amount of insulin released in DMEM media after 72 h (that corresponds to the period selected to monitor the cell growth on PAMs).

PAMs_MD μm	TL mg/g	EE %	EL mg/g	Insulin released at 72 h %
1.8 (\pm 0.9)	5	62 (\pm 2.9)	3 (\pm 0.03)	50.1
3.2 (\pm 2.2)	5	60 (\pm 1.5)	3 (\pm 0.02)	27.5
2.8 (\pm 1.9)	10	58 (\pm 3.4)	6 (\pm 0.07)	73.4

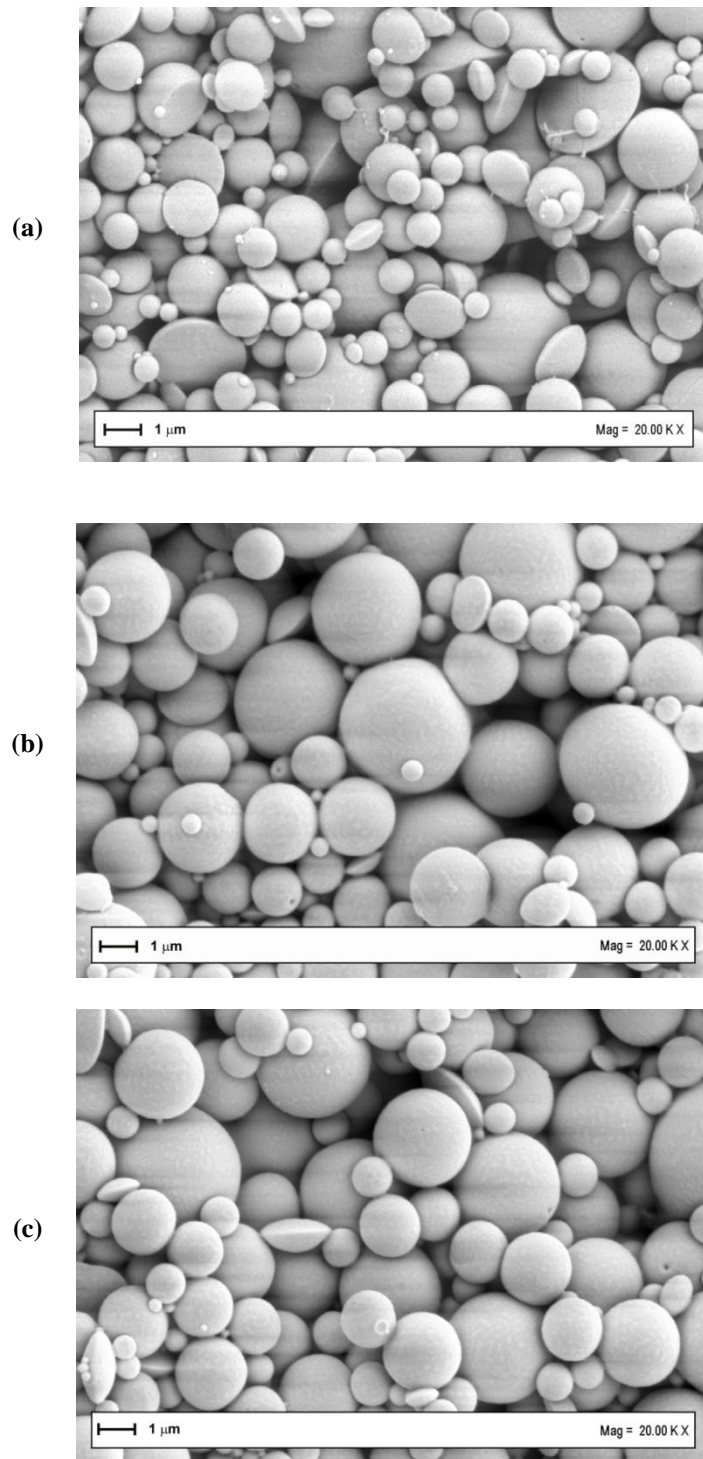


Figure 4.2a-c. FE-SEM images of PLGA-PAMs obtained after the emulsion processing by SEE-C at 80 bar and 37°C. (a) PAMs with MD of 2 μm and loading of 3 mg/g; (b) PAMs with MD of 3 μm and loading of 3 mg/g; (c) PAMs with MD of 3 μm and loading of 6 mg/g.

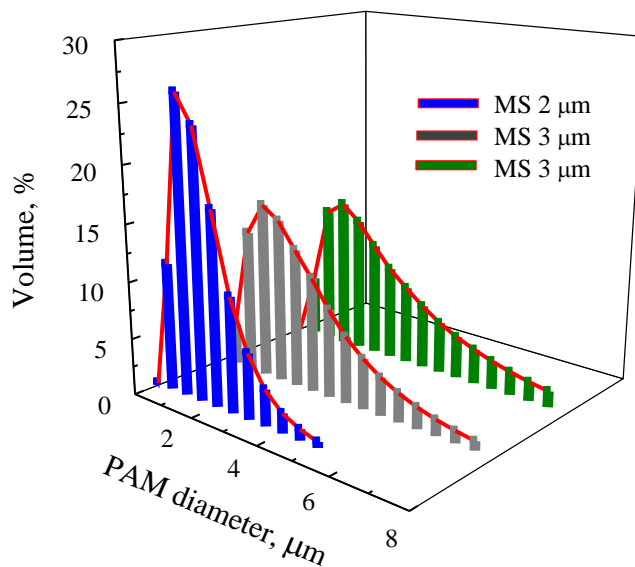


Figure 4.3. PSDs of the insulin-loaded PLGA-PAMs batches tested.

4.3.2 *In Vitro* Insulin Release Study from PAMs

It is known from the literature that drug release from PLGA can be described in two steps; the first one reflects the diffusion controlled mass transfer of the drug accessible at the solid/dissolution medium interface and the second step reflects the release of drug entrapped in the polymer by its bulk degradation, as discussed in Chapter 3. PLGA-PAMs of different MDs (2 and 3 μm) and protein loadings (3 and 6 mg/g) were tested to monitor the insulin release profiles at 37°C in two different release media: PBS and DMEM. The PBS medium is the one recommended by the US Pharmacopeia for the drug release study; therefore, was used to compare our release profiles (and the calculated kinetic constants) to the ones reported in the literature of PLGA microspheres with a polymer composition of 50:50 and charged with water soluble compounds. The release profiles in DMEM medium were also studied in order to understand the amount of insulin released from PAMs at fixed time during the cell culture.

The release profiles of PAMs with different MDs of 2 and 3 μm and loaded with 3 mg/g of insulin in PBS are reported in **Figure 4.4a**. Fittings curves are also illustrated as dashed lines. Both sizes showed in PBS a fast release in the first days, followed by a more sustained release up to the subsequent 28 days. Microspheres with mean size of 2 μm released 80% of the total amount during the first day, whereas, microspheres with mean size of 3 μm released 50% of molecule loaded in the first day. When a higher insulin loading of 6 mg/g was tested

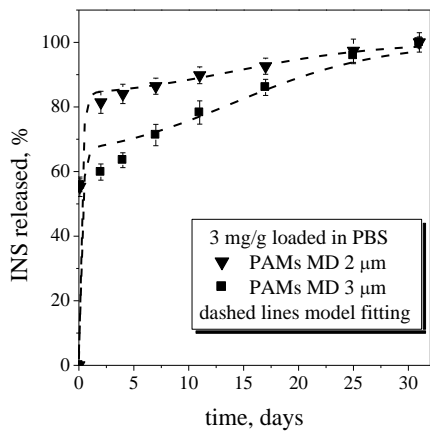
from microspheres with a mean size of 3 μm , an even faster release was observed and almost the 90% of the charge was released in the first day (see **Figure 4.4b**). Insulin release, in the following days, was slower for microspheres with a larger size (3 μm); whereas, higher loadings (6 mg/g) generated a faster release. This last behavior is in agreement with the results proposed by *Corrigan and Li* [121] reporting that the highest loading gave the fastest protein release throughout the same period and can be expected when the diffusion controlled mass transfer is prevalent. The release profiles produced in DMEM medium are reported in **Figures 4.5a-b**. In this case, microspheres with mean size of 2 μm released the 35% of the total amount during the first day; whereas, microspheres with mean size of 3 μm released in the same time interval only the 9% of the load (insulin loaded 3 mg/g). Increasing the insulin loading to 6 mg/g (microspheres mean size of 3 μm), again a more fast release was observed and the 70% of the charge was released in the external media in the first day. In DMEM medium, the overall release was almost completed in 24 days. It's worth noting that a slower release was observed in DMEM with respect to PBS; this behavior can be explained considering their different composition and the possibility that in DMEM the protein release by desorption is delayed [146]. Moreover, the shape of the insulin release profiles obtained in DMEM illustrated a multistep release mechanism with as initial fast release of the protein adsorbed at the microspheres surface, followed by its sustained release from the internal polymer layers largely enhanced by the depolymerization reaction. From the release kinetics obtained in DMEM it can be also observed that the controlled diffusion mechanism seems to be predominant in the first part of the release, where the curve profiles are clearly separated and larger microspheres sizes generated a slower release. The erosion mechanism seems to superimpose in the second part of the observed release, where the profiles overlap.

An attempt to describe the observed release profiles was also performed using the equation previously discussed in Chapter 3. The model proposes a simplified mechanism to describe an overall release profile (typical of PLGA) that takes into account the diffusion controlled mechanism probably predominant in the first part of the release and a the diffusion/erosion ones that also involves the depolymerization reaction.

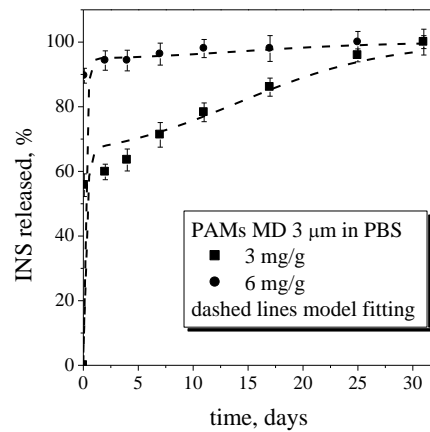
The calculated parameters obtained by fitting the experimental data are reported in **Table 4.2**. The model also gives a fair good representation of the insulin release profiles, as can be seen from the dashed curves reported in **Figures 4.4a-b** and **Figures 4.5a-b**. Looking at the kinetic parameters reported in **Table 4.2**, for the release profiles monitored in PBS, it

can be observed that K_d decreases its values by increasing the PAMs sizes at fixed insulin loading of 3 mg/g (from 4.20 to 3.80 days⁻¹ for PAMs sizes of 2 and 3 μm , respectively); whereas, with the increase of PAMs loading to 6 mg/g K_d increases its value to 5 days⁻¹. This behavior is in agreement with the K_d expected behavior and should mean that increasing the loading, the apparent diffusivity will increase and, therefore, the release kinetic constant is higher; trends in K_d with microspheres size can be explained by the decrease in specific surface area and, thus, the amount of surface insulin available. The K_d values were in fairly good agreement with the ones proposed by *Corrigan and Li* [121] for the release of ovalbumin from PLGA microspheres with similar size and loading in PBS. Similar K_d values trend was also observed for the release profiles performed in DMEM; however, in this case the calculated K_d values were 0.32 and 0.13 days⁻¹ for PAMs sizes of 2 and 3 μm charged with 3 mg/g of insulin, respectively, so one order of magnitude smaller respect to the ones calculated for the release profiles in PBS.

For the release profiles monitored in PBS, the F_D values decrease from 0.82 to 0.63 when the PAMs size is increased from 2 to 3 μm (loading 3 mg/g of insulin); F_D represents the fraction of protein released by simple diffusion; therefore, this trend is reasonable considering that increasing the PAMs size, the diffusion pathway increases slowing the related release kinetics and, therefore, reducing the overall fraction of protein released by diffusion contribution. On the contrary, F_D values increases to 0.94 when the insulin loading is increased to 6 mg/g for PAMs with a MD of 3 μm . The increase in F_D with increased loading was attributed to the high concentration of drugs dispersed, which effectively increases the proportion of drug linked/adsorbed to the particle surface-liquid interface and is consistent with the observations of *Gallagher and Corrigan* [147]. The same trend, but less marked, was observed for the F_D values calculated in DMEM medium. T_{max} is the timing value of the maximum drug release rate and it was directly evaluated from the experimental curves and fixed at 14 and 11 days for all the curves obtained in PBS and in DMEM, respectively. Finally, the bulk erosion kinetic constant K was fixed at 0.15 days⁻¹ for all the release performed in PBS and at 2.5 days⁻¹ for all the ones performed in DMEM. These values were maintained constant in all data fitting for the two different media because K should be independent from the PAMs size or loading and mainly related to the PLGA depolymerization reaction.

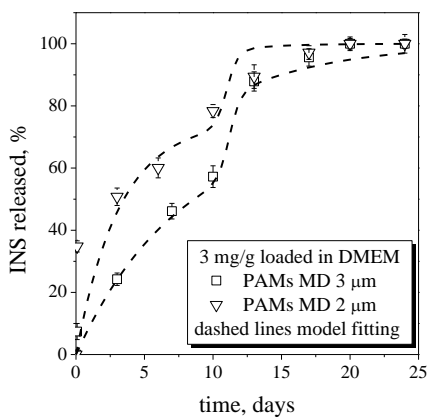


(a)

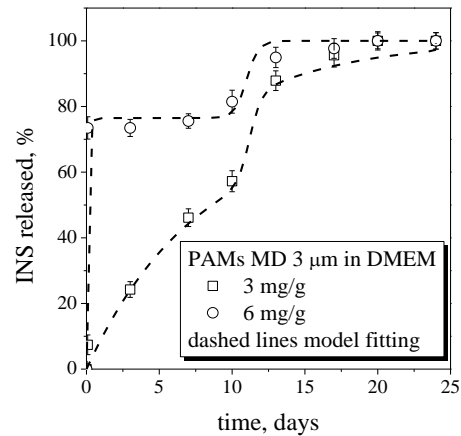


(b)

Figure 4.4a-b. Comparison between the release profiles (days) of insulin from PLGA-PAMs suspended in PBS with: (a) different MDs of 2 and 3 μm and charged with the same loading of 3 mg/g; (b) different loadings of 3 and 6 mg/g and with the same MD of 3 μm . Dashed lines are model fittings.



(a)



(b)

Figure 4.5a-b. Comparison between the release profiles (days) of insulin from PLGA-PAMs suspended in DMEM with: (a) different MDs of 2 and 3 μm and charged with the same loading of 3 mg/g; (b) different loadings of 3 and 6 mg/g and with the same MD of 3 μm . Dashed lines are model fittings.

Table 4.2. Best fit model parameters estimated from insulin release profiles obtained from PLGA-PAMs of different sizes and protein loadings and in different media: phosphate buffer solution (PBS) and Dulbecco's Modified Eagle Medium (DMEM).

Medium	PAMs_MD μm	EL mg/g	F _D	K _d (day ⁻¹)	K (day ⁻¹)	T _{max} (days)	R ²
PBS	2	3	0.823	4.20	0.15	14	0.98
	3	3	0.628	3.80	0.15	14	0.95
	3	6	0.943	5.00	0.15	14	0.88
DMEM	2	3	0.750	0.32	2.50	11	0.87
	3	3	0.732	0.13	2.50	11	0.99
	3	6	0.765	0.81	2.50	11	0.89

4.3.3 Cells Viability, Adhesion & Growth on PAMs

A number of 1000 cells/well were seeded and cultivated for 72 h to fit the Alamar Blue (AB) calibration curve. H9c2 myoblasts were cultivated in standard medium (see *Materials & Methods* section) with or without 20 mg/mL empty PLGA microspheres. A comparable number of H9c2 cells (w/o PLGA microspheres = 4100 ± 600 , w PLGA microspheres = 3700 ± 800 , 10 replicates, $p < 0.05$) was observed either in presence or absence of these devices, confirming their lack of toxicity when produced by SEE-C.

Serum-free medium was used to evaluate H9c2 cell proliferation as sustained by bioactive insulin release when PLGA microspheres with a mean diameter of 3 μm and 3 mg/g of insulin load were tested. Loaded microspheres were added in scalar dilutions in order to obtain a theoretical insulin release up to 4, 8, 16 and 34 ug/mL, respectively, after 72 h. 1000 cells/well were seeded and cultivated for 72 h in these different dilutions and their number at 72 h is illustrated in **Figure 4.6**. As a control, cells were also cultivated in a serum free media with empty microspheres and, in this case, no cell proliferation was observed (see control results highlighted in red on **Figure 4.6**). On the other hand, a significant proliferation, consistent with the expected increasing insulin release was observed for the cells grown in serum-free media added with loaded microspheres. Particularly, best cell growth was observed at insulin concentration of 16 ug/mL; whereas, higher insulin concentration values seemed to have an adverse effect on the cell growth (cell number decreased from 8600 to 5500 when the insulin concentration released was 34 ug/mL). This result is in agreement with

data reported in literature, where about 10 $\mu\text{g/mL}$ is the recommended concentration using insulin as a growth supplement [148].

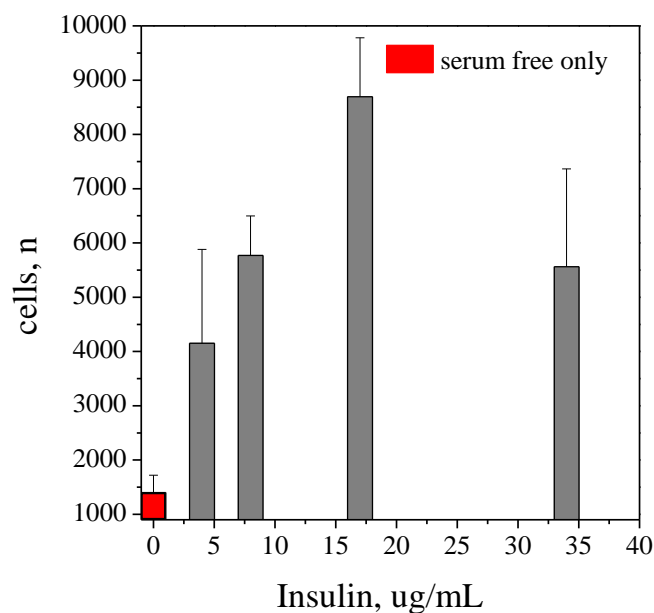


Figure 4.6. Number of cells growth after 72 h of incubation with different PLGA-PAMs amounts (MD of 3 μm , insulin loading of 3 mg/g) against the insulin concentrations delivered in the serum free medium. The number of cell growth after 72 h in serum free media without PAMs is reported in red, for comparison.

PAMs of different sizes but with the same loading showed different release kinetics, as reported previously. To evaluate the effect of the different release kinetics on cell growth, two different serum free media were prepared by adding a calculated amount of PLGA-PAMs with different MDs of 2 and 3 μm (insulin loading of 3 mg/g) to reach fixed insulin concentrations between 15-17 $\mu\text{g/mL}$ after 72 h of release. The numbers of cell growth in these different media are illustrated in **Fig. 4.7**. Insulin concentrations in serum free medium ranging between 15-17 $\mu\text{g/mL}$ allowed cell growth in all cases; however, the number of cells growth on PAMs of 2 μm was lower. The observed behaviour was probably due to the static condition of the cell cultivation, where PAMs with smaller size were observed to stick easier on the multiwell lateral surface probably preventing or reducing the insulin release. The observed behaviour should be taken into account for dynamic cell culture into a medium added with PAMs .

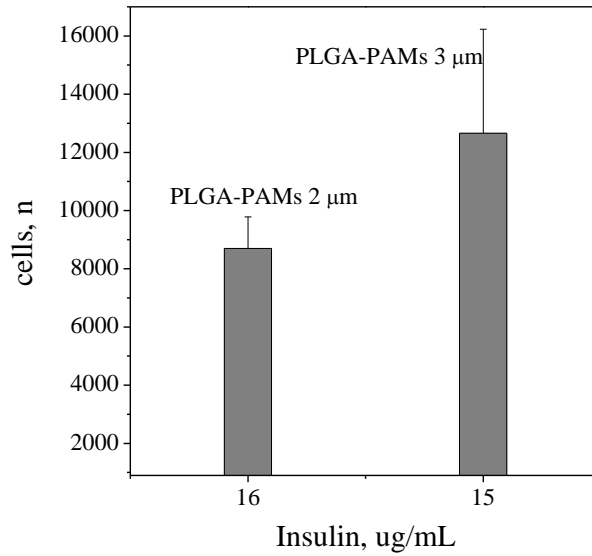


Figure 4.7. Cell growth on PLGA-PAMs of different size 2 and 3 μm (insulin loading of 3 mg/g) into serum free media with a fixed insulin concentration ranging from 15-17 ug/mL released after 72 h.

4.4 Conclusions

At the optimized operating conditions, a double w_1-o-w_2 emulsion can be easily converted in PLGA microspheres loaded with insulin by SEE-C technology. The process is completed in 5 min of residence time in the high pressure column, and biopolymer microdevices with controlled particle size and good encapsulation efficiencies can be obtained. The produced microspheres allowed a sustained insulin release, in cell culture medium, and were able of delivering bioactive insulin to sustain myoblasts growth in a serum-free medium. The results indicate SEE-C technology as a promising tool in the field of tissue engineering/regenerative medicine; indeed, these microdevices can be charged in more complex 3D scaffold with cell onboard for local signal delivery.

Chapter 5. Synergistic effect of sustained release growth factors from PLGA-PAMs and dynamic bioreactor flow on hMSC osteogenic differentiation in 3D alginate scaffolds

5.1 Introduction

New challenges of the regenerative medicine are the treating of bone injuries by seeding and growing a cell source on a 3D scaffold and implanting the scaffold and cells into the injury site [149]. Current changes in bone tissue engineering techniques are cell-containing scaffolds cultured *in vitro* prior of their implantation in order to promote cell proliferation and to allow for differentiation from stem cells into target cells. However, *in vitro* static culture techniques of 3D tissue engineering scaffolds showed several limitations including oxygen and nutrient gradients with lowered concentrations toward the centre of the scaffold, leading to cell death [150]. A bioreactor is often used to overcome this limitation of nutrient transfer. It is a culturing system designed to support or expand a population of cells through dynamic culture in a controlled environment. Different bioreactors systems have been proposed in bone tissue engineering, including spinner flasks [151-153], rotating wall bioreactors [154], and perfusion systems [155-158]. Spinner flask and rotating wall bioreactors are effective at creating a homogenous media solution surrounding the exterior, but do not effectively perfuse media into the interior of the scaffold. Perfusion systems effectively provide media (at laminar flow regimes) throughout the scaffold, enhancing nutrient transport. In addition, it exposes cells to fluid shear stresses shown to be influential in osteogenic differentiation of stem cells and mineralization of the extracellular matrix [159-160]. Indeed, *in vivo* bone constantly remodels in response to mechanical stresses and it was hypothesized that these stresses are mainly transmitted to bone cells via fluid shear stresses [161] and that they experience *in vivo* shears from 8 to 30 dynes/cm² [162-163].

Mesenchymal stem cells (MSCs) are a multipotent stem cell population present in bone marrow, cartilage, and adipose tissue. They are easily differentiated into osteoblasts, chondrocytes, or adipocytes [164-165]. Therapies involving MSCs include direct

transplantation of an MSC population, growth factor loaded scaffolds for MSC recruitment, or implantation of scaffolds containing an *in vitro* cultured MSC population [166-168]. During MSCs differentiation, biological and mechanical cues induce specific pathways dictating whether the cell remains multipotent or differentiates into a specific cell type. Recently, *Yeatts et al.* [169] demonstrated that human mesenchymal stem cells (hMSCs) can undergo osteoblastic differentiation into osteoblasts when cultured in the tubular perfusion system (TPS) bioreactor. The system cultures cell-encapsulated alginate bead scaffolds in a dynamic flow environment. It improves the supply of convective oxygen and nutrient transport within a 3D scaffold compared to static culturing conditions. In addition, it adds mechanical stimuli via the shear flow of the media, shown to improve osteoblastic differentiation. After *in vitro* culture, the beads can form an aggregated construct for *in vivo* implantation. TPS flow rate was also optimized to apply a shear stress between 1 to 3 dynes/cm².

hMSCs respond favourably towards several biochemical signals. Particularly, it is reported that biopolymer scaffolds modified with growth factors (GFs) including fibroblast growth factor-2 (FGF-2), vascular endothelial growth factor (VEGF), or bone morphogenetic protein-2 (BMP-2) [170] could enhance *in vivo* bone growth. For example, VEGF, an angiogenic growth factor, has been used to enhance endothelial cell proliferation and encourage vessel sprouting aiding in the vascularization of an implanted construct [171-172]; whereas, BMP-2 has been widely investigated for its role in enhancing *in vivo* bone growth and *in vitro* osteoblastic signaling [173-176]. In this case, bioactive 3D scaffold capable of a locally controlled release of specific growth factors may provide an innovative tool capable of an additional level of cell environment regulation not possible with an inert scaffold.

In this part of work, the TPS bioreactor was used to cultivate bioactive tissue-engineered scaffolds, with the idea to provide *in situ* controlled release of GFs that will enhance differentiation of hMSCs not possible with an inert 3D scaffold. To provide proof of concept, bioactive alginate scaffolds were loaded with hMSCs and growth factor-encapsulated PLGA-PAMs (specifically h-VEGF and h-BMP-2) produced by SEE-C technology. Alginate was selected as a hydrogel because of the ease of spherical bead scaffolds formation and because they can be tightly packed in the TPS growth chamber. The aim of this study was to determine the effect of different locally released GFs from PLGA-PAMs on the osteoblastic differentiation of hMSCs when cultured in alginate scaffolds in a dynamic TPS bioreactor.

5.2 *Materials & Methods*

5.2.1 *PLGA-PAMs production by SEE-C technology*

Water-oil-water emulsion ratio was fixed at 1:19:80. Particularly, a fixed amount of GFs was dissolved into a BSA solution with PVA concentration of 0.04% w/v and this solution was added into the oily phase of ethyl acetate (EA) and PLGA at 10% w/w. The primary w_{1-o} emulsion was obtained upon 90 second sonication by digital ultrasonic probe at 50% of amplitude (mod. S-450D, Branson Ultrasonics Corporation, Danbury, CT, USA). This primary emulsion was, then, immediately poured into a known amount of EA-saturated aqueous Tween 80 solution (0.6% w/w in water) used as outer water phase, to form the secondary emulsion by a high-speed homogenizer (mod. L4RT, Silverson Machines Ltd., Waterside, Chesham Bucks, United Kingdom) for 6 min at 10°C in an ice bath with a stirring rate of 2800 rpm. The emulsions were processed by SEE-C immediately. All the emulsions were prepared with filtered or autoclaved solutions.

SEE-C apparatus was already described in detail in Chapter 2. Ultra filtered or autoclaved gas and liquids coupled with standardized GMP operative procedures in a continuous operation apparatus assured PAMs sterility (see also method section of Chapter 4). An additional PAMs passage in Pen/Strep (1% w/V) followed by washing in PBS was also performed.

5.2.2 *Morphology & size distributions*

The droplets formed in the emulsion were observed using an optical microscope (OM, mod. BX 50 Olympus, Tokyo, Japan) equipped with a phase contrast condenser. Microspheres shape and morphology were investigated by field emission-scanning electron microscopy (FE-SEM, mod. LEO 1525, Carl Zeiss SMT AG, Oberkochen, Germany). Samples of powder were placed on a double-sided adhesive carbon tape previously stuck to an aluminum stub and coated with a thin gold film (layer thickness 250Å) using a sputter coater (mod.108 A, Agar Scientific, Stansted, United Kingdom). Droplet size distributions (DSD) and particle size distributions (PSD) were measured using a Mastersizer S apparatus (mod. Mastersizer S, Malvern Instruments Ltd., Worcesterstershire, United Kingdom), based on the dynamic light scattering (DLS). Mastersizer S software uses Mie theory to produce an optimal analysis of the light energy distribution and to obtain the size distribution of the particles. Analyses were performed immediately after the preparation of the emulsions and of the microsphere suspensions, using several milligrams of each sample, appropriately diluted

with distilled water. The distributions proposed in this paper are the mean of several DLS analysis. Droplets and particle size are expressed as volume MS (mean size, μm) \pm SD (standard deviation) of values collected.

5.2.3 BSA & GFs release and loading

The amount of BSA loaded into PAMs was determined by dissolving 10 mg of dried PAMs in 600 μL of acetonitrile in centrifuge tubes and sonicated until the solution was complete transparency. Then, 1400 μL of water were added to the corresponding centrifuge tube to dissolve proteins and peptides. The remaining undissolved PLGA was separated by centrifugation at 2000 rpm for 2 minutes. The resulting clear supernatant solution was directly analyzed at room temperature by high-performance liquid chromatography (HPLC, mod. 1200 series; Agilent Technologies Inc.) equipped with a LiCrosphere C18 column (250 \times 4.6 mm), packed with 5 μm particles size of 100 Å pore size. The mobile phase was composed of acetonitrile/water mixture. The flow rate was 0.9 mL/min, the inject volume of the test sampled was 20 μL and the detecting wavelength was 225 nm. The amount of BSA in solution was calculated by means of a calibration curve and then converted in the effective loading as the amount (mg) of protein charged in PLGA-PAMs (g). The BSA loading was assumed as a reference for the GFs loading.

GFs release profiles were monitored in vitro using an ELISA-based assay. 20 mg of PLGA-PAMs were suspended in 2 mL of Dulbecco's Modified Eagle Medium (DMEM), in a centrifuge tube. The tubes were then placed in an incubator at 37°C and stirred continuously at 50 rpm. At fixed time intervals, the samples were centrifuged at 4000 rpm for 15 minutes and the supernatant was completely withdrawn and replaced with fresh medium to maintain sink conditions. Released VEGF concentrations from collected samples were then measured with an ELISA assay (PeproTech, Rocky Hill, NJ). Release experiments were performed in triplicate and the proposed curves are the mean profiles obtained. The percentage of released VEGF was defined as the mass of GFs released divided by the mass of the load.

5.2.4 h-MSC Culture

Human mesenchymal stem cells (p \leq 5) were purchased from Lonza (Walkersville, MD) and cultured before the study in a control medium containing High Glucose DMEM with L-Glutamine (Gibco, Carlsbad, CA), supplemented with 10% fetal bovine serum (FBS, Invitrogen), 1% v/v penicillin/streptomycin (Gibco), and 0.1 mM nonessential Amino Acids (Invitrogen) following the protocol set by the manufacturer with a medium change every 4

days. Cells were stored in a cell culture incubator at 37°C and 5% of CO₂ and passaged every 6-7 days using trypsin/ethyldiaminetetraacetic acid (EDTA, Invitrogen). The osteogenic medium was formulated as described in the literature by supplementing control media with 100nM dexamethasone (Sigma, St. Louis, MO), 10mM β-glycerophosphate and 173 mM ascorbic acid (Sigma) [177]. Cell samples were counted on a standard hemocytometer after their mixing with trypan blue (Sigma). Four counts were made for each sample.

5.2.5 Alginate bead production loaded with PAMs and h-MSC

2% w/w alginate solutions (Sigma Aldrich) were prepared by adding alginic sodium salt from brown algae (Sigma) dissolved into 0.15M NaCl (Sigma) and 0.025M HEPES (Sigma) in deionized water. The alginate solution was then sterilized via autoclave. hMSCs were removed from tissue culture flasks using trypsin/EDTA and pelleted via centrifugation at 500 g for 5 min. The cell pellet was resuspended in HEPES buffer. Meanwhile, the GF-loaded PLGA-PAMs was also resuspended in HEPES buffer solution by sonification in ice water. PAMs/ HEPES suspension was poured into the sterile alginate solution and thoroughly stirred with a magnetic stir bar. Next, the cell suspension was added to the PAMs/alginate mixture and carefully stirred until fully integrated. A syringe and 16 1/2G needle were used to create the PAMs-hMSC-loaded alginate scaffold beads by a slow drop wise suspension into a stirred solution of 0.1M calcium chloride (Sigma), which immediately crosslinked the alginate to form beads. Beads were allowed to stabilize for 15 min. Roughly 100,000 hMSCs and 8 ug of growth factor were incorporated into each alginate bead.

5.2.6 Perfusion Bioreactor for Dynamic Environment

The tubular perfusion bioreactor (TPB, see Images on **Figures 5.1a-b**) bioreactor was used as a dynamic fluid conditioner. It consists of a tubular growth chamber and medium reservoir connected via a tubing circuit, as described in a previous work [178]. The medium's flow was driven by an L/S Multichannel Pump System (Cole Parmer, Vernon Hills, IL) at 3 mL/min. The circuit consists of platinum-cured silicone tubing (Cole Parmer) connected using silver ion-lined connectors (Cole Parmer). The growth chamber has high gas permeability to allow for easy exchange of carbon dioxide and oxygen and is made of platinum-cured silicone tubing (Cole Parmer) with an inner diameter of 6.4 mm, an outer diameter of 11.2 mm and a wall thickness of 2.4 mm and. After loading, the autoclaved tubing was fully assembled inside a cell culture hood and then placed in a cell culture incubator at 37C and 5% CO₂. 70 mL

milliliters of the osteogenic medium were loaded into separate flasks for each growth chamber. The medium was withdrawn and replaced every 4 days. Briefly, the beads were divided into four different groups, depending on their GFs loaded PAMs and placed into four growth chambers. At each experimental timepoint, beads residing in the top most chambers were removed for further analysis and the empty chamber replaced.

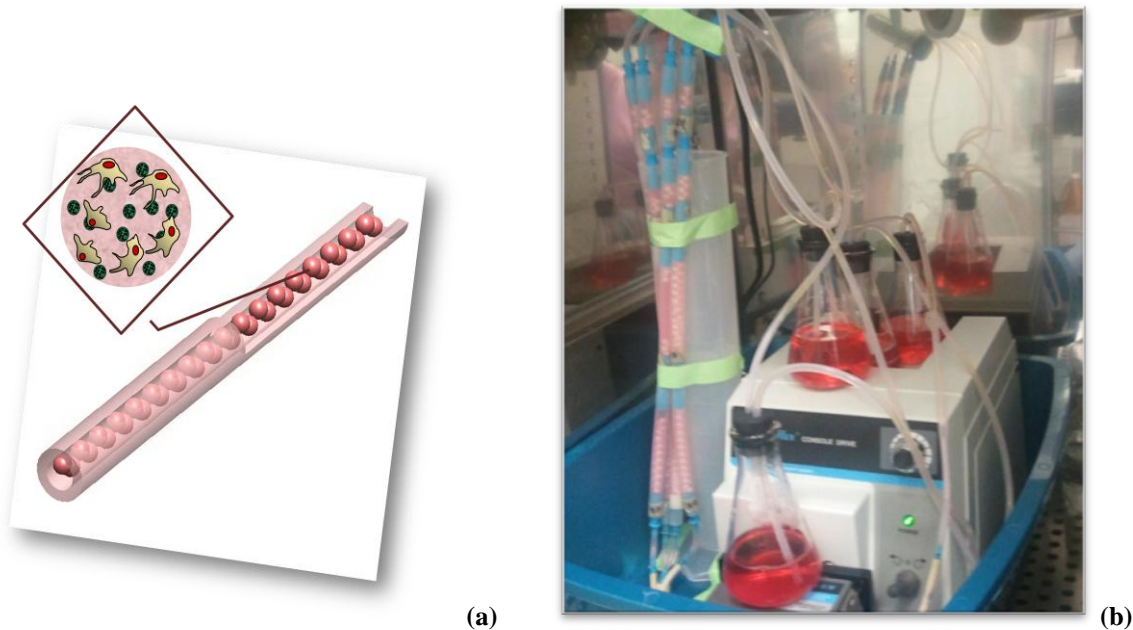


Figure 5.1a-b. Schematic representation of the bioactive scaffold charged in a tubular bioreactor (a). Image of the bioreactor with the four chambers (b).

5.2.7 *Static Environment*

As a control, beads were also placed into a static environment. The same number of beads was incubated at 37°C, 5% CO₂ in 6-well plates with 1mL of osteogenic media per bead. Analysis was carried out on the static beads on the same time points.

5.2.8 *Immunohistochemistry*

At different time points of culture (1, 7, 21 days) alginate beads were recovered from dynamic and static culture conditions. They were fixed in 4% paraformaldehyde (Sigma) for 3 hours, followed by an overnight incubation in sodium cacodylate (Sigma). The beads were then placed in cassettes and dehydrated for histological processing in a series of ethanol dilutions (75%, 90%, 100%). The samples were then embedded in paraffin (Fisher Scientific), sectioned using a Microtom (Lica) into 5-micron-thick sections and placed on glass slides

(Fisher Scientific). The samples were deparaffinized in Ctrisolv (Fisher Scientific) and rehydrated in ethanol.

Specifically, osteoblastic differentiation was monitored using immunohistological staining of protein markers, including alkaline phosphatase (ALP), an early differentiation marker, and osteocalcin (OCN) and osteopontin (OPN), both late differentiation markers. Generally, the samples underwent standard immunostaining protocol for antigen retrieval, endogenous peroxidase and protein blocks. They were incubated for an hour with rabbit monoclonal ALP, mouse monoclonal osteocalcin, mouse monoclonal osteopontin (AbCam, Cambridge, MA), respectively, followed by broadband polyclonal biotinylated secondary antibody (Abcam, Cambridge, MA).

For the von Kossa staining of the sections, the samples were incubated in 2.5% (w/v) silver nitrate for 20 min under UV light, followed by 5% (w/v) sodium carbonate for 5 min, and 0.1% Nuclear Fast Red (Poly Scientific). Lastly, the samples were dehydrated again in the same series of ethanol dilutions.

5.2.9 Live-dead assay

Cell viability was assessed using a live-dead assay (Invitrogen) following standard protocols. Beads were first soaked in PBS for 60 min to remove FBS and the medium. Dead controls were soaked in 70% methanol (Sigma) instead of PBS. Beads were then placed in 48-well plates and incubated in 2 mM ethidium homodimer and 4 mM calcein AM (Molecular Probes) for 30 min. Fluorescent images were then taken of the entire bead using a fluorescent microscope (Axiovert 40 CFL with filter set 23; Zeiss, Thornwood, NY) equipped with a digital camera (Diagnostic Instruments 11.2 Color Mosaic, Sterling Heights, MI). Live-dead images of whole beads, not cross sections, were obtained.

5.2.10 Statistical Analysis

All samples were completed in triplicate. Data were analyzed using single-factor analysis of variance followed by Tukey's Multiple Comparison Test assuming normal data distribution with a confidence of 95% ($p < 0.05$). Mean values of triplicates and standard deviation error bars are reported on each figure as well as relevant statistical relationships.

5.3 Results & Discussion

5.3.1 SEE-C operative conditions for PLGA-PAMs manufacturing

The SEE-C pressure and temperature conditions in the high pressure column were of 8 MPa and 38°C with an SC-CO₂ flow of 1.4 kg/h and an L/G ratio of 0.1; these conditions were used because already optimized, as discussed in Chapter 2. At these SEE-C conditions the processed emulsions were converted in a PLGA-PAMs water suspension in less than 5 min of residence time in the column, preventing any aggregation phenomena between particles. Each run allowed the recovery of the 98% of the charged biopolymer and assured an excellent batch to batch reproducibility.

5.3.2 PLGA-PAMs: size, loading & in vitro GFs release study

Four w_1 - o - w_2 double emulsions (see “Apparatus, Materials and Methods” section for the exact composition) with a fixed PLGA content in the oily phase of 10% w/w and GFs theoretical loading of 10 ug/g were prepared. BSA was always used as GFs stabilizer in the emulsion internal water phase with a concentration of 2.5 mg/g of PLGA. Droplets with a MDs of 3 μ m (\pm 0.9 μ m) were always obtained and processed by SEE-C just after their preparation producing four batches of PAMs with a MDs of 2.1 μ m (\pm 0.6 μ m). In all cases, the droplets shrunk almost 30% in diameter. Examples of results obtained are reported in **Figures 5.2a-d**, depicting optical microscopy (OM) images of the emulsions treated and FE-SEM images of the related PAMs. Four different batches were produced for the present study: B1, only BSA- but no growth factor-loaded PAM; B2, BSA- and hBMP-2-loaded PAM; B3, BSA and hVEGF-loaded PAM; and B4, BSA- an 50:50 mix of hBMP-2 and hVEGF-loaded PAM. hBMP-2 was selected because it plays an important role in development of bone and cartilage and has been found to be involved in inducing osteogenesis; whereas VEGF is traditionally known to stimulate vasculogenesis and angiogenesis and is also secreted during osteoblastic differentiation.

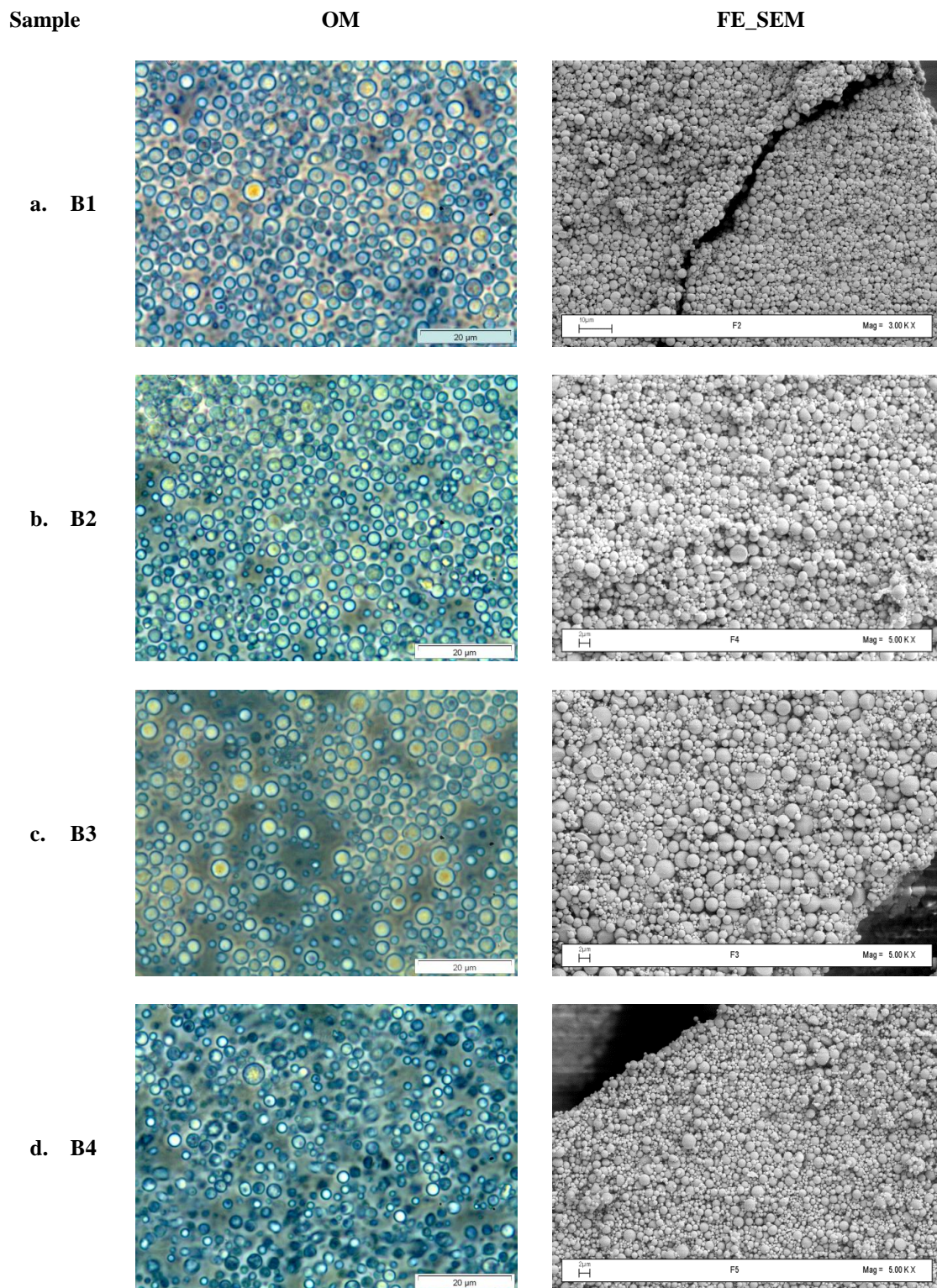


Figure 5.2a-d. Optical microscope (OM) images of emulsion and FE-SEM image of the microspheres obtained by SEE-C. B1, only BSA charged PAMs; B2, BSA and h-Bone Morphogenic Protein 2 (h-BMP-2) charged PAMs; B3, BSA and h-Vascular Endothelial Growth Factor (h-VEGF) PAMs; B4, BSA and GFs mix (ratio 1:1) charged PAMs.

The PSD curves of the four different PLGA-PAMs batches are illustrated in **Figure 5.3**; their overlapping confirms the high reproducibility of the SEE-C technology for the production of nanostructured microdevices. In all cases, the BSA encapsulation efficiency was 80%, leading to the production of PLGA-PAMs with a protein content of 2 mg/g of PLGA. As a consequence, the GF loading was assumed to be 8 ug/g of PLGA. The release profile of GFs from PAM was monitored in DMEM medium is reported in **Figure 5.4**. A burst almost the 20% of the GF was observed during the first day, followed by a more gradual and linear release over the following 16 days. The entire amount of GF was released within 22 days, so the encapsulated GFs in alginate bead scaffolds will provide a good *in situ* GF delivery to the onboard hMSCs for 20 days..

5.2.3 Scaffold characterization and bioreactor conditions

100 alginate beads with a mean diameter of 0.46 mm were produced per experimental group (hVEGF, hBMP2, and 50:50 mix of each). Each bead was loaded with 100,000 hMSCs and 8 ug of GF-encapsulated PAM. Therefore, an average amount of 80 ng of hBMP2 or hVEGF were encapsulated into each beads for the groups B2 and B3, respectively. However, 40 ng of each GFs were present into the bead belonging to B4 group.

A schematic representation of the bioactive scaffold is shown in **Figure 5.5a**. A viability stain was performed on the bead at the end of the cultivation period as seen in **Figure 5.5b**, where green represents live cells and red stains dead cells. **Figures 5.6a-b** shows two different enlarged sections of the alginate beads after hematoxylin and eosin (H&E) staining as observed using a phase-contrast condenser. In the two images, it is evident that the hMSCs (pink) and the PAMs (white spots) are uniform distributed in the alginate matrix.

The internal structure of a freeze-fractured scaffold was also confirmed using SEM at different enlargements, as seen in **Figures 5.7a-c**. Particularly in **Figure 5.7b**, it is evident that the PAM is uniformly distributed in the alginate matrix, while a single hMSC is highlighted by a red circle in **Figure 5.7c**.

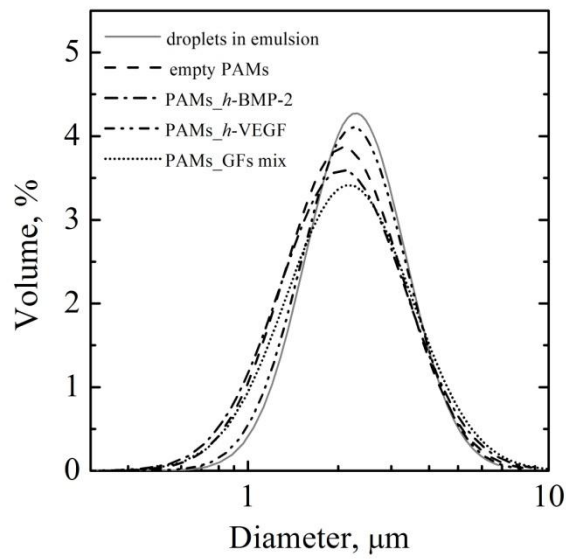


Figure 5.3. Particle Size Distribution curves of the PAMs produced by SEE-C; the size distribution curve of the droplets in emulsion is also reported in grey, for comparison purpose.

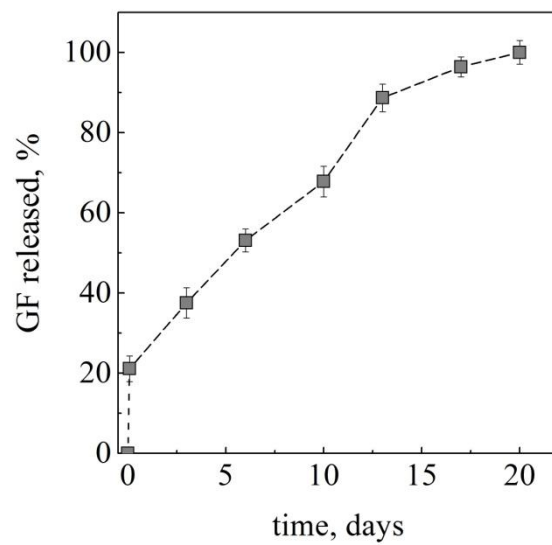
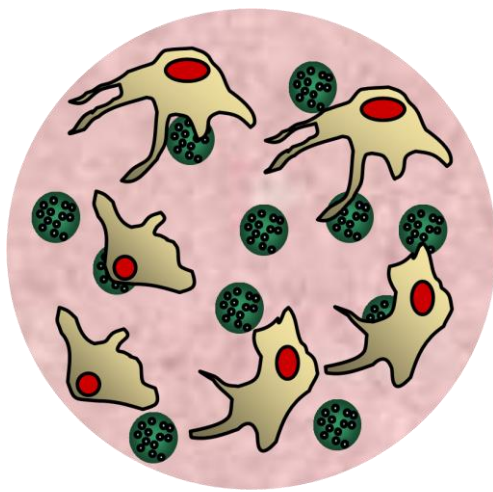
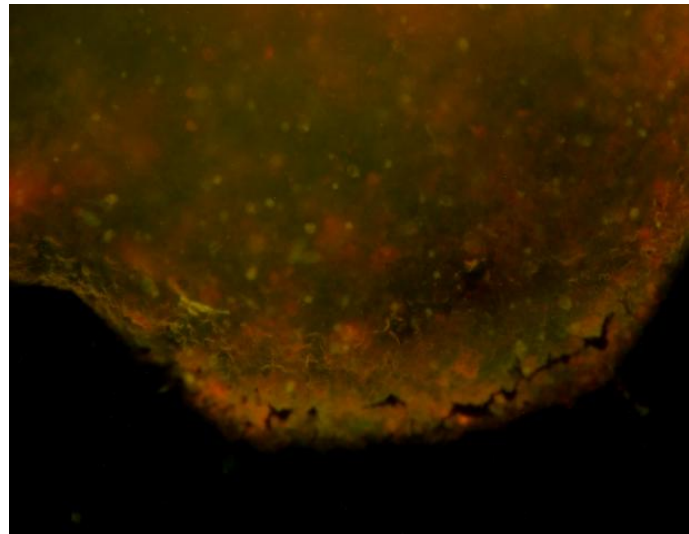


Figure 5.4. Release profiles (days) of GFs from PLGA-PAMs suspended in DMEM medium.

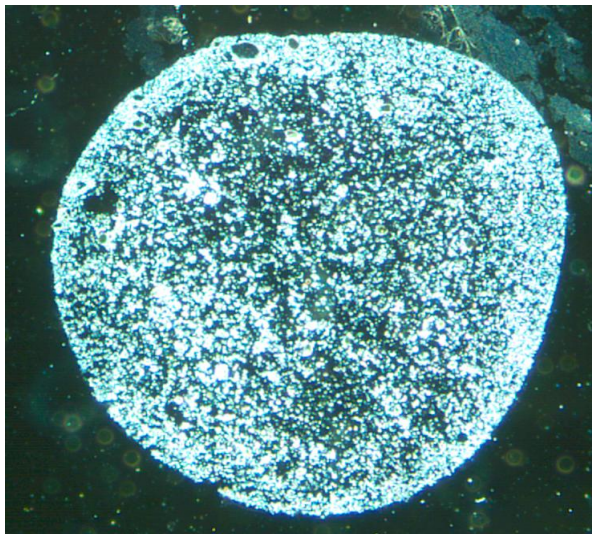


a.

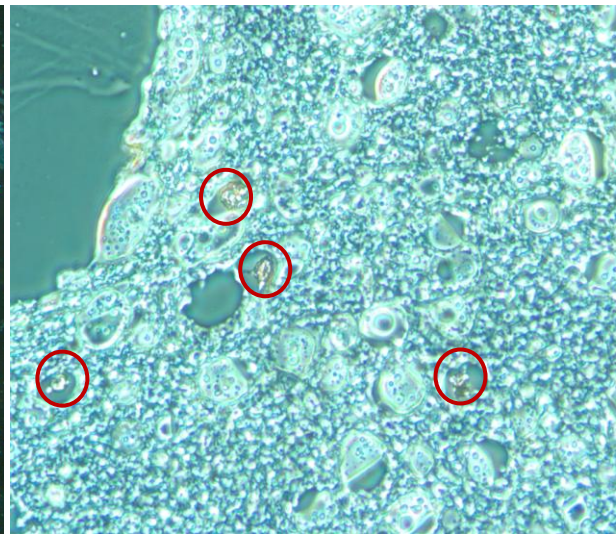


b. 10 X

Figure 5.5a-b. A schematic representation of the bioactive scaffold with the PAMs (green), the cells (yellows and red) and the alginate gel (pink) (a); live & dead image of part of a bead taken from 28 days of cultivation with an enlargement of 10 X; the PAMs were stained in red (b).



a. 2.5 X



b. 40 X

Figure 5.6a-b. OM images of alginate beads sections reported with two different enlargements; sections of the alginate beads after Hematoxylin and Eosin staining observed at optical microscope with a phase contrast condenser; in the two images are evident the h-MSC in pink and the PAMs (as a white spots) uniformly distributed in the alginate matrix.

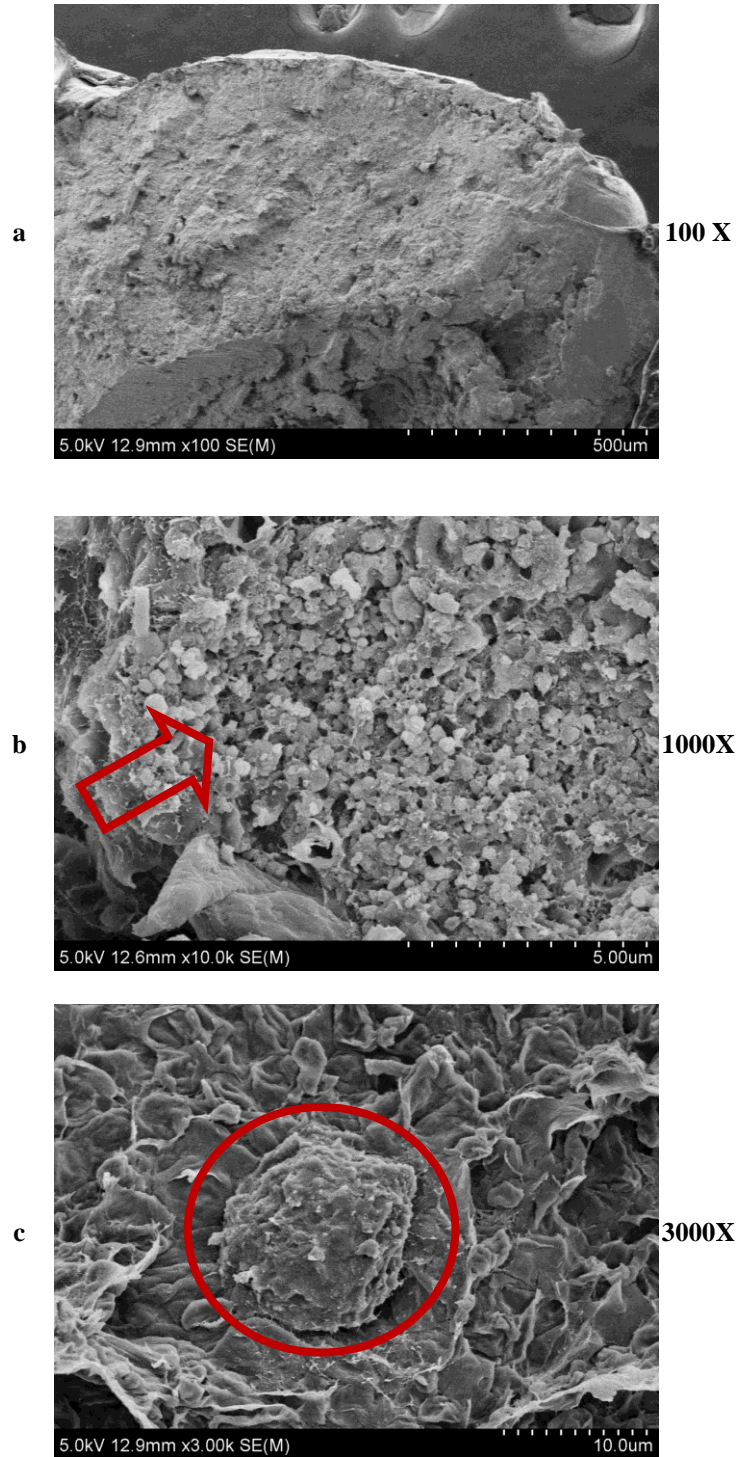


Figure 5.7a-c. FE-SEM images at different enlargements of the alginate beads fractured after its freezing in liquid nitrogen. PAMs are uniformly distributed in the gel matrix. The h-MSG is highlighted by a red circle.

Beads of each group were packed into four different TPS growth chambers. Each growth chamber was set to have an internal volume of 9 cm^3 and was charged with 60 beads (with a volume of 0.05 cm^3 each) in order to have an equivalent CSTR volume of 6 cm^3 and a packing density of 0.33. Separate flasks each containing 60 mL of the osteogenic media were connected to the chambers and a volume of 0.1 mL of medium was calculated for each bead. A continuous flow rate of 3 mL/min provided media to the cells throughout the study, with osteogenic media changed every 4 days. In these conditions, a Sherwood number (that represent the ratio between the convective to diffusive mass transfer) of 13 was assured into the TPS bioreactor, as calculated in a previous study. The bioreactor was kept at a sterile 37°C incubator with 5% CO_2 . As a control, beads were also incubated at static conditions in 6-well plates with the same volume of osteogenic media per bead. To determine flow velocities and calculate shear stresses a 2D steady-state Navier-Stokes model was used by COMSOL Multiphysics Ver. 3.5. Initial flow into the growth chamber was modeled assuming fully developed flow. Walls of alginate beads were modeled as no slip and the medium was assumed to have a dynamic viscosity of 0.78 centipoise and a density of 0.993 g/cm^3 . Boundary shear stresses were calculated using the formula $\tau = \mu (\delta v / \delta y)$, where μ is the dynamic viscosity of the media, v is the velocity of fluid at the bead surface and y is the height of the boundary layer [179]. Based on the mathematical analysis the average shear stress at the surface of the beads in this study was of $0.98 (\pm 0.08) \text{ dyn/cm}^2$ for the 3 mL/min flow. For long-term culture in the bioreactor, shear stresses of 0.15 dyn/cm^2 have been reported to enhance osteoblastic differentiation [180].

5.3.4 *Immunoassay for cell differentiation monitoring*

Alginate beads were recovered from dynamic and static culture at different time points (days 1, 7 21 and 28). At each experimental time point, beads were removed for immunostaining analysis and the empty chambers replaced. The following proteins were stained to monitor cells differentiation: alkaline phosphatase, osteocalcin, and osteopontin. In addition, von Kossa staining was used to study mineralization and calcification of the cells.

Figures 5.8a-d shows OM images of beads after immunostaining for ALP of all the four experimental groups on day 7. ALP is considered an early osteogenesis marker and is involved in making inorganic salts available for later calcification. Its peak expression occurs between day 6 and 8 of culture. Cross-sectional images of alginate scaffolds revealed strong ALP activity in cell clusters formed in beads when cultured with hBMP-2. ALP expression

was also observed in beads belonging to the B4 group (both hBMP2 and hVEGF). However, in this case, less cell clustering were observed. Less evident protein activity was observed on day 7 in the bioactive scaffolds containing hVEGF and in the scaffolds contained the empty PLGA-PAM (control group).

Figures 5.9a-d shows osteopontin (OPN) staining completed for all the four groups on day 21. OPN is a cellular structural protein in mature osteoblast produced between days 14 and 28 and represents late osteoblastic differentiation. Cross-sectional images of alginate scaffolds revealed substational OPN activity in beads belonging to the B2 group (hBMP-2) on day 21, whereas, this protein was clearly stained into the group B4, only later at days 28th.

Figures 5.10a-d show osteocalcin (OCN) staining completed for all four groups on day 21. OCN is also considered marker of late osteogenic maturation that is produced between day 14 and 28. The images revealed a strong production of OCN and further confirmed the formation of cell clusters in the beads belonging to the B2 group (hBMP-2). OCN activity was also observed in B4 group, but less cell clusters were again observed. Low expression of OCN was observed in the bioactive scaffolds containing hVEGF and empty PAM (control group), on the same day. **Figures 5.11a-d** depict OM cross-sectional images of beads cultivated until day 21 and stained with von Kossa to observe the calcium deposition by hMCSs in the scaffolds. Images from day 21 demonstrated that the calcium deposition occurred in all experimental groups. However, a more homogeneous and intense calcium deposition was observed in the beads loaded with hBMP-2 encapsulated PAM.

The immunostaining assays confirmed that osteoblastic differentiation of hMSCs was enhanced in the bioreactor compared to when cultured in static conditions and revealed that hBMP-2 released in alginate scaffolds has a great influence of the on hMSC differentiation. In this sense, hBMP-2 sustained released and TPS cultivation may have a synergistic effect on hMSC differentiation; indeed due to their encapsulation in the alginate, only a portion of the cell population is exposed to the shear that could be too low to influence early differentiation, but may be high enough to affect late term differentiation and matrix deposition.

ALP_Day 7th

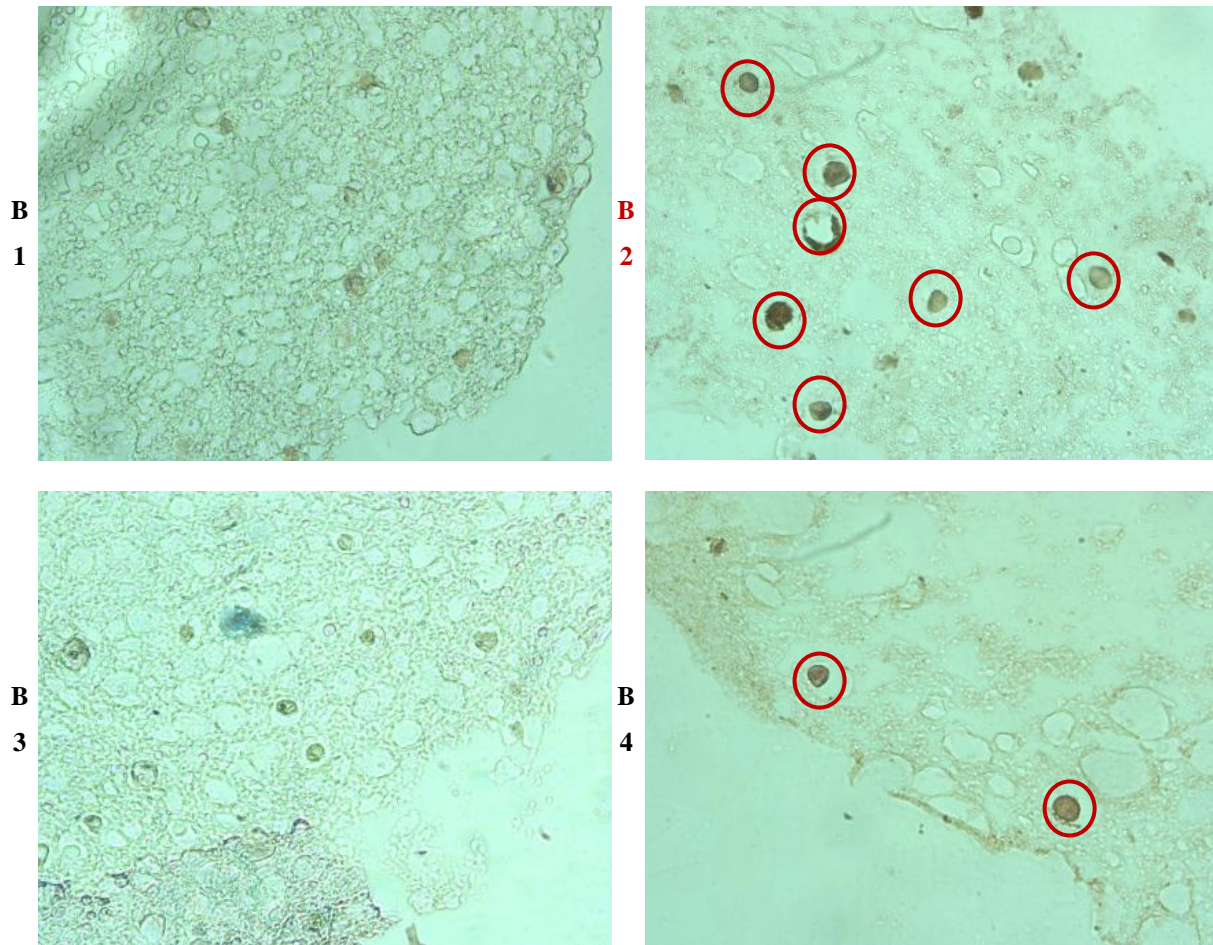


Figure 5.8a-d. Alkaline phosphatase staining of alginate beads after 7 days of culture in a TPS. All the images are made with the 40 X objective. B1, empty; B2, h-BMP-2; B3, h-VEGF; B4, GFs mix (ratio 1:1). ALP activity is marked in brown and appeared well stained in the group B2 and B4, revealing a great influence of h-BMP-2 released into the scaffold on the earlier cell differentiation.

OPN_Day 21st

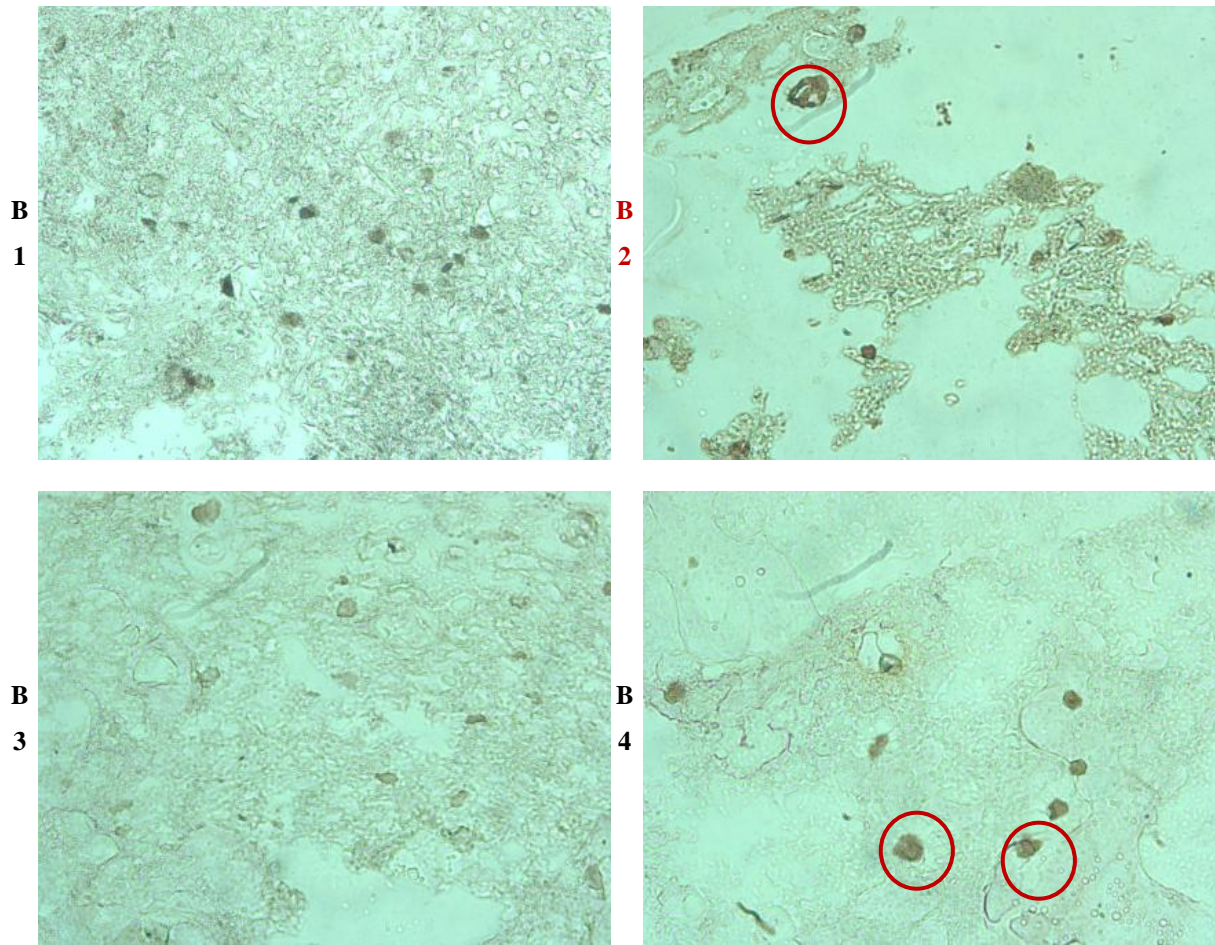


Figure 5.9a-d. Osteopontin (OPN) staining of alginate beads after 21 days of culture in a TPS. All the images are taken using a 40 X objective. B1, empty; B2, h-BMP-2; B3, h-VEGF; B4, GFs mix (ratio 1:1). OPN activity is marked in brown and appeared well stained in the group B2 and B4.

OCN_Day 21th

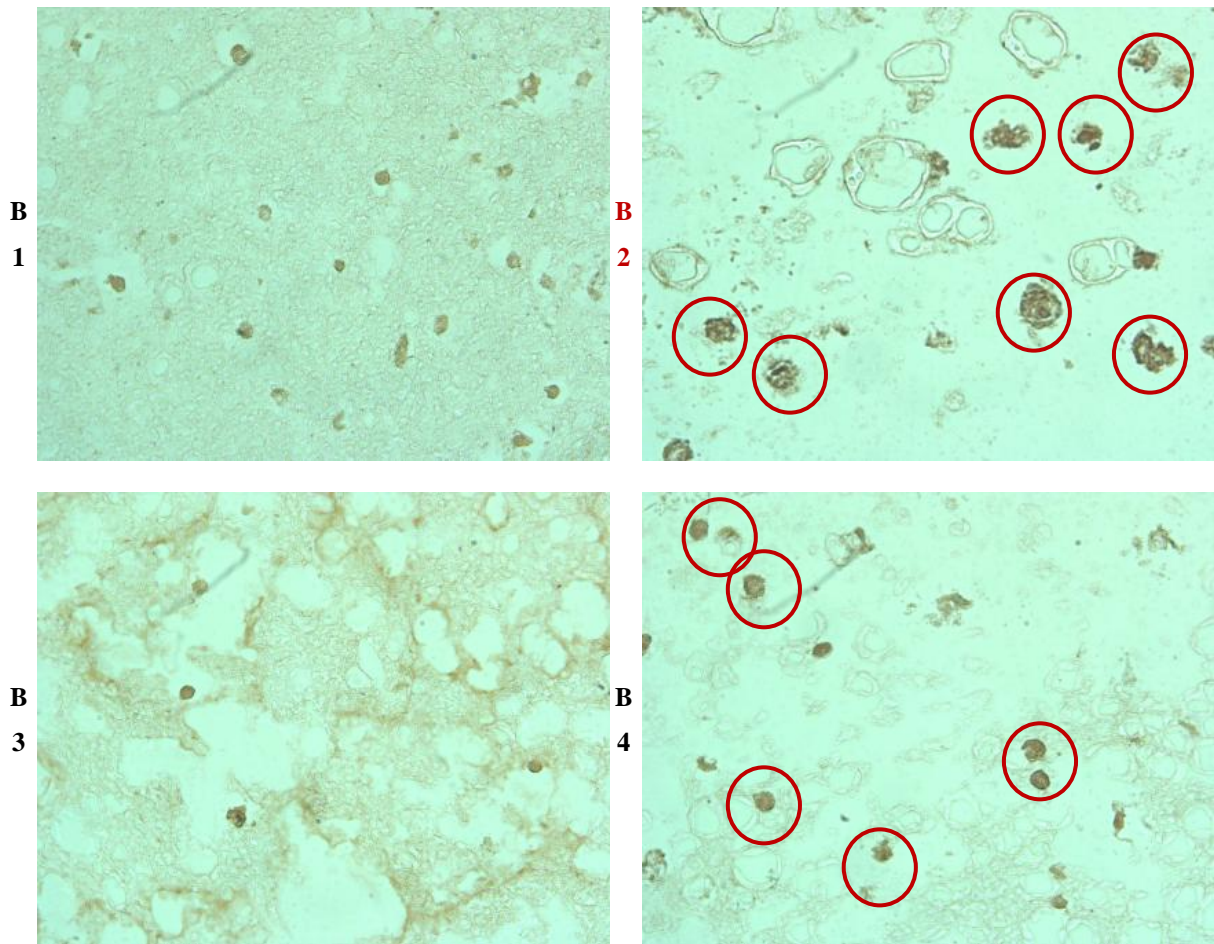


Figure 5.10a-d. Osteocalcin (OCN) staining of alginate beads after 21 days of culture in a TPS. All the images are taken using a 40 X objective. B1, empty; B2, h-BMP-2; B3, h-VEGF; B4, GFs mix (ratio 1:1). OCN activity is marked in brown and appeared well stained in the group B2 and B4, confirming the great influence of h-BMP-2 released into the scaffold on the earlier cell differentiation.

Von Kossa_Day 21st

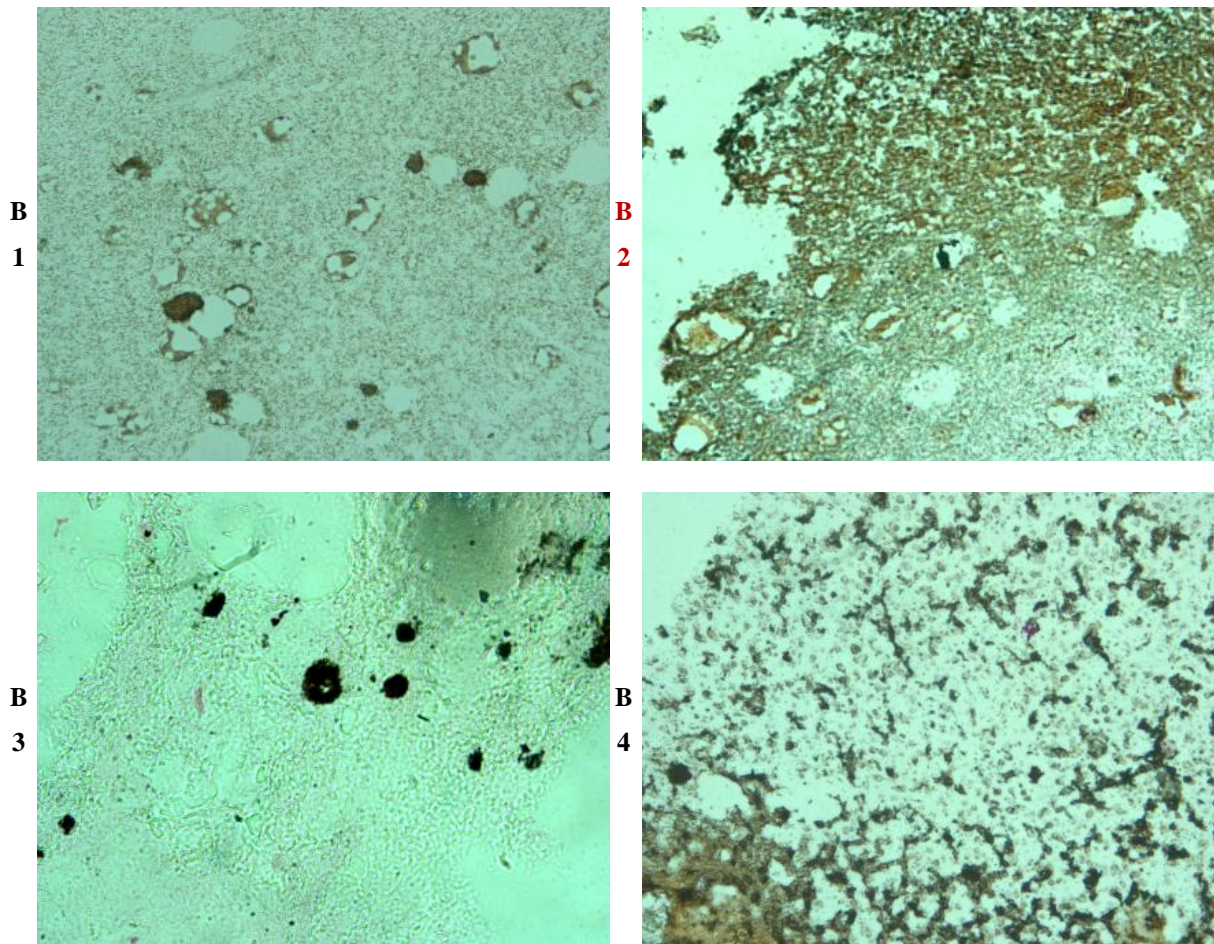


Figure 5.11a-d. Von Kossa staining of alginate beads after 21 of culture in a TPS. All the images are taken using a 40 X objective. B1, empty; B2, h-BMP-2; B3, h-VEGF; B4, GFs mix (ratio 1:1). The calcium deposition started into the scaffolds belonging to all groups; however, a more homogeneous calcium deposition was always observed in the beads charged with PAMs able to release h-BMP-2 growth factors.

5.4 Conclusion & Perspectives

Bioactive scaffolds charged with GFs can be complementary to mechanical stress, by improving from biochemical point of view an earlier cell differentiation.

Histology results showed dynamic cell culturing significantly impacted osteogenic hMSC differentiation compared to those cultured in static conditions. In addition, those cells supplemented with growth factor-loaded PLGA microspheres had increased expression of osteogenic markers as compared to those cultured with empty microspheres. Specifically, cells exposed to BMP-2 produced greater amounts of ALP, OCN and OPN for all three time points, as evident in the darker and more intense staining, compared to the unloaded microsphere control group. VEGF had the least visible effect on osteogenic marker expression, although still greater than the control. In addition, histology indicated that mixed growth factor supplement had comparable osteogenic effects on the hMSCs as the BMP-2 growth factor alone, further confirming VEGF's limited impact.

Lastly, ELISAs showed sustained growth factors released from microspheres over a 21-day period confirming continuous diffusion to cells; i.e., SEE is a suitable fabrication method of PLGA microspheres to provide sustained release of growth factors. Hence, dynamic flow culturing environment in the TPS bioreactor and sustained-release growth factors from PLGA microspheres show to have a synergistic effect on osteogenic differentiation of hMSCs. Future studies will include optimization of the BMP-2 dose delivered to hMSCs.

Conclusions & Perspectives

Supercritical fluids Emulsion Extraction (SEE) technology offers a new strategy in the biopolymer microsphere production with a better particle size control and excellent encapsulation efficiency. In this PhD work an innovative SEE apparatus, operating in continuous layout (SEE-C), was developed by using a high pressure packed column in counter-current mode. Process parameters such as, pressure, temperature, high pressure phase compositions and flow rate ratios were optimized for the production of PLGA microdevices with a controlled sizes and engineered nanostructure. Taking advantage of the enhanced mass transfer of the supercritical solvent, biopolymer microcarriers were successfully produced with excellent encapsulation efficiency. Moreover, the upgrade of the SEE technology into the continuous process allowed a higher throughput with smaller plant volumes, eliminating all the batch-to batch repeatability problems. This technology was tested for the production of PLGA microdevices to be used in the cell therapy, as a major therapeutic strategy for some specific tissue regeneration. PLGA carriers charged with different bioactive compounds were produced and characterized in terms of bioactive principle encapsulation efficiencies and release profiles. An attempt of diffusion and degradation constants calculation was also performed by using a mathematical model selected from the literature.

PLGA microcarriers charged with bovine serum insulin were tested for the cultivation of embryonic myoblasts (cell line H9c2 from rat) in a FBS serum free medium. Good cell viability and growth were observed on 3 μm PAMs charged with 3 mg/g of insulin. PLGA microcarriers loaded with different growth factors such as h-VEGF and h-BMP-2 were also charged inside an alginate scaffold together with h-Mesenchymal Stem Cells (h-MSCs) that are promising cell source for bone tissue engineering. BMP-2 showed to have a dominant effect on osteogenic marker production compared to VEGF in both static and dynamic conditions, indicating that it is an important growth factor in the differentiation pathway. Hence, dynamic flow culturing environment in the tubular perfusion system bioreactor and sustained-release growth factors from PLGA microspheres shown to have a synergistic effect on osteogenic differentiation of hMSCs. Future studies will include optimization of the BMP-2 dose delivered to h-MSCs.

References

- [1] Van Blitterswijk C.A., Thomsen P., Lindahl A., Hubbell J., Williams D.F., Cancedda R., de Bruijn J., Sohier J., Tissue Engineering Textbook (Eds); Academic Press: London, (2008); 403-454. ISBN: 978-0-12-370869-4.
- [2] Langer R., Vacanti J.P. Tissue engineering. *Science*. 1993. 260 (5110): 920-6.
- [3] Hillsley M., Frangos J. Review: Bone Tissue Engineering: The Role of Interstitial Fluid Flow. *Biotech. Bioeng.* 1994. 43:575-81.
- [4] Martin P. Wound healing--aiming for perfect skin regeneration. *Science*. 1997. 276 (5309):75-81.
- [5] Bello Y.M., Falabella A.F., Eaglstein W.H. Tissue-engineered skin. Current status in wound healing. *Am. J. Clin. Dermatol.* 2001. 2(5):305-13.
- [6] Caplan A.I., Elyaderani M., Mochizuki Y., Wakitani S., Goldberg V.M. Principles of cartilage repair and regeneration. *Clin. Orthop.* 1997. 342:254-69.
- [7] Niklason L.E., Gao J., Abbott W.M., Hirschi K.K., Houser S., Marini R., Langer R. Functional arteries grown in vitro. *Science*. 1999. 284 (5413):489-93.
- [8] Gooch K.J., Blunk T., Courter D.L., Sieminski A.L., Vunjak-Novakovic G., Freed L.E. Bone morphogenetic proteins-2, -12, and -13 modulate in vitro development of engineered cartilage. *Tissue Eng.* 2002. 8(4): 91-601.
- [9] Boublik J., Park H., Radisic M., Tognana E., Chen F., Pei M., Vunjak-Novakovic G., Freed L.E. Mechanical properties and remodeling of hybrid cardiac constructs made from heart cells, fibrin, and biodegradable, elastomeric knitted fabric. *Tissue Eng.* 2005. 11(7-8):1122-32.
- [10] Tranquillo R.T. The tissue-engineered small-diameter artery. *Ann. N. Y. Acad. Sci.* 2002. 961: 51-4.
- [11] Schaner P.J, Martin N.D., Tulenko T.N., Shapiro I.M., Tarola N., Leichter R.F., Carabasi R.A., Dimuzio P.J. Decellularized vein as a potential scaffold for vascular tissue engineering. *J. Vasc. Surg.* 2004. 40(1):146-53.

- [12] Dean D.M., Napolitano A.P., Youssef J., Morgan J.R. Rods, tori, and honeycombs: the directed self-assembly of microtissues with prescribed microscale geometries. *FASEB*. 2007. 21:4005-12.
- [13] Yeh J., Ling Y., Karp J.M., Gantze J., Chandawarkard A., Eng G., Blumling J., Langer R., Khademhosseini A. Micromolding of shape-controlled, harvestable cell-laden hydrogels. *Biomaterials*. 2006. 27:5391-8.
- [14] L'Heureux N., Paquet S., Labbe R., Germain L., Auger F.A. A completely biological tissue-engineered human blood vessel. *FASEB J*. 1998. 12(1):47-56.
- [15] Mironov V., Boland T., Trusk T., Forgacs G., Markwald R.R. Organ printing: computer-aided jet-based 3D tissue engineering. *Trends in Biotechnology*. 2003. 21(4):157-161.
- [16] McGuigan A.P., Sefton M.V. Design and Fabrication of Sub-mm-Sized Modules Containing Encapsulated Cells for Modular Tissue Engineering. *Tissue Engineering*. 2007. 13(5):1069-78.
- [17] McGuigan A.P., Sefton M.V. The thrombogenicity of human umbilical vein endothelial cell seeded collagen modules. *Biomaterials*. 2008. 29:2453-63.
- [18] L'Heureux N., McAllister T.N., de la Fuente L.M. Tissue-engineered blood vessel for adult arterial revascularization. *New England Journal of Medicine*. 2007. 357(14):1451-3.
- [19] Du Y., Lo E., Ali S., Khademhosseini A. Directed assembly of cell-laden microgels for fabrication of 3D tissue constructs. *Proceedings of the National Academy of Sciences*. 2008. 105(28): 9522-7.
- [20] Lim F., Sun A.M. Microencapsulation Islets as Bioartificial Endocrine Pancreas. *Science*. 1980. 210 (21):908-10.
- [21] Nichol J. W., Khademhosseini A. Modular Tissue Engineering: Engineering Biological Tissues from the Bottom Up. *Soft Matter*. 2009. 5(7):1312-1319.
- [22] Mundargi R.C., Babu V.R., Rangaswamy V., Patel P., Aminabhavi T.M. Nano/Micro technologies for delivering macromolecular therapeutics using poly (D,L lactide-co-glycolide) and its derivatives. *J. Control. Release*. 2008. 125:193-209.
- [23] Verrijck R., Smolde I.J., Bosnie N., Begg A.C. Reduction of systemic exposure and toxicity of cisplatin by encapsulation in poly(lactide-co-glycolide). *Cancer Res*. 1992. 52: 6653-6656.

- [24] Meinel L., Illi O.E., Zapf J., Malfanti M., Merkle H.P., Gander B. Stabilizing insulin-like growth factor in poly(lactide-co glycolide) microspheres. *J. Control. Release* 2001. 70:193-202.
- [25] Walter E., Dreher D., Kok M., Thiele L., Kiama S.G., Gehr P., Merkle H.P. Hydrophilic poly(lactide-co- glycolide) microspheres for the delivery of DNA to human derived macrophages and dendritic cells. *J. Control Release* 2001. 76:149-168.
- [26] Luten J., van Nostrum C.F., De Smedt S.C., Hennink W.E. Biodegradable polymers as non-viral carriers for plasmid DNA delivery. *J. Control Release* 2008. 126:97-110.
- [27] Jaklenec A., Wan E., Murray M.E., Mathiowitz E. Novel scaffolds fabricated from protein-loaded microspheres for tissue engineering. *Biomaterials* 2008. 9:185-192.
- [28] Temenoff J.S., Mikos A.G., *Biomaterials. The Intersection of Biology and Materials Science*. Eds. NJ: Pearson Prentice Hall, 2008. ISBN-10-0-13-009710-1.
- [29] Tatard V.M., Venier-Julienne M.C., Benoit J.P., Menei P., Montero-Menei C.N. In vivo evaluation of pharmacologically active microcarriers releasing nerve growth factor and conveying PC12 cells. *Cell Transplant*. 2004. 13(5):573-83.
- [30] Tatard V.M., Venier-Julienne M.C., Saulnier P, Prechter E., Benoit J.P., Menei P, Montero-Menei C.N. Pharmacologically active microcarriers: a tool for cell therapy. *Biomaterials*. 2005. 26(17): 3727-37.
- [31] Mercier N.R., Costantino H.R., Tracy M.A., Bonassar L.J. Poly (lactide-co-glycolide) microspheres as a moldable scaffold for cartilage tissue engineering. *Biomaterials* 2005. 26:1945-1952.
- [32] Kang S.W., Jeon O., Kim B.S. Poly(lactic-co-glycolic acid) microspheres as an injectable scaffold for cartilage tissue engineering. *Tissue Eng.*, 2005. 11: 438-447.
- [33] Hong Y., Gao C.Y., Xie Y., Gong Y.H., Shen J.C. Collagen-coated poly-lactide microspheres as chondrocyte microcarriers. *Biomaterials*, 2005. 26:6305-6313.
- [34] Tan H., Huang D., Lao L., Gao C.; RGD Modified PLGA/Gelatin Microspheres as Microcarriers for Chondrocyte Delivery, *J. Biomed Mater Res Part B: Appl Biomater* 2009. 91:228-238.
- [35] Palmiero C., Imperato G., Urciuolo F., Netti P., Engineered dermal equivalent tissue in vitro by assembly of microtissue precursors, *Acta biomaterialia* 2010. 6(7):2548-53.
- [36] Ma P. X., Scaffolds for tissue fabrication, *Materials today* (2004).

- [37] Zhang J., Zhang H., Wu L., Ding J., Fabrication of three dimensional polymeric scaffolds with spherical pores, *Journal of Material Science* 2006. 41:1725-1730.
- [38] Liu X., Ma P.X., Polymeric scaffold for bone tissue engineering, *Annals of Biomedical Engineering*, 2003. 32:477-482.
- [39] Shin M., Yoshimoto H., Vacanti J.P. In Vivo Bone Tissue Engineering Using Mesenchymal Stem Cells on a Novel Electrospun Nanofibrous Scaffold. *Tissue Engineering*. 2004. 10(1-2):33-41.
- [40] Landers R., Pfister A., Hübner U., John H., Schmelzeisen R. Mülhaupt R. Fabrication of soft tissue engineering scaffolds by means of rapid prototyping techniques . *Journal of Materials Science*. 2002. 37 (15):3107-3116.
- [41] Schugens C., Maquet V., Grandfils C., Jerome R., Teyssie P. Polylactide macroporous biodegradable implants for cell transplantation. II Preparation of polylactide foams by liquid-liquid phase separation, *Journal of Biomedical Material Research* 1996. 30:449-454.
- [42] Harris D.L., Kim B.S., Mooney D. J. Open pore biodegradable matrices formed with gas foaming, *Journal of Biomedical Material Research* 1998. 42:396-401.
- [43] Luciani A., Coccolia V., Orsia S., Ambrosio L., Netti P.A., PCL microspheres based functional scaffolds by bottom-up approach with predefined microstructural properties and release profiles *Biomaterials*, 2008. 29(36):4800-4807.
- [44] Tan W., Desai T.A. Layer-by-layer microfluidics for biomimetic three-dimensional structures. *Biomaterials*. 2004. 25(7-8):1355-64.
- [45] Liu V.A, Bhatia S.N. Three-dimensional photopatterning of hydrogels containing living cells. *Biomed Microdev*. 2002. 4(4):257-266.
- [46] McGuigan A.P., Sefton M.V. Design and Fabrication of Sub-mm-Sized Modules Containing Encapsulated Cells for Modular Tissue Engineering. *Tissue Engineering*. 2007. 13(5):1069-78.
- [47] McGuigan A.P., Sefton M.V. The thrombogenicity of human umbilical vein endothelial cell seeded collagen modules. *Biomaterials*. 2008. 29:2453-63.
- [48] Federovich N.E., Alblas J., DeWijn J.R., Hennink W.E., Verbout A.J., Dhert W.J.A. Hydrogels as Extracellular Matrices for Skeletal Tissue Engineering: State-of-the-Art and Novel Application in Organ Printing. *Tissue Engineering*. 2007. 13(8):1905-1925.

- [49] Roth E.A., Xu T., Das M., Gregory C., Hickman J.J., Boland T. Inkjet printing for high-throughput cell patterning. *Biomaterials*. 2004. 25:3707-3715.
- [50] L'Heureux N., Paquet S., Labbe R., Germain L., Auger F.A. A completely biological tissue-engineered human blood vessel. *FASEB J*. 1998. 12(1):47-56.
- [51] Li W.I., Anderson K.W., Deluca P.P. Kinetic and thermodynamic modelling of the formation of polymeric microspheres using solvent extraction/evaporation method. *J. Contr. Rel*. 1995. 37:187-198.
- [52] Li M., Rouand O., Poncelet D. Microencapsulation by solvent evaporation: State of the art for process engineering approaches. *Int. J. Pharm*. 2008. 363:26-39.
- [53] Mao S., Shi Y., Li L., Xu J., Schaper A., Kissel T. Effects of process and formulation parameters on characteristics and internal morphology of poly(D,L-lactide-co-glycolide) microspheres formed by the solvent evaporation method. *Eur. J. Pharm. Biopharm*. 2008. 68:214-223.
- [54] Yang Y.Y., Chia H.H., Chung T.S. Effect of preparation temperature on the characteristics and release profiles of PLGA microspheres containing protein fabricated by double-emulsion solvent extraction/evaporation method. *J Control Release* 2000. 69:81-96.
- [55] Johansen P, Merkle HP, Gander B. Technological considerations related to the up-scaling of protein microencapsulation by spray-drying. *Eur J Pharm Biopharm* 2000. 50:413-417.
- [56] Brunner G., Gas extraction: an introduction to fundamentals of supercritical fluids and the application to separation processes, Vol. 4 of Topics in physical chemistry, Ed. Techniques Ingénieur, 1994, ISBN 3798509441.
- [57] Singh L., Kumar V., Ratner B.D., Generation of porous microcellular 85/15 poly (lactide-co-glycolide) foams for biomedical applications, *Biomaterials* 2004. 25:2611-2616.
- [58] Mathieu L.M., Montjovent M.O., Bourban P.E., Pioletti D.P., Manson J.A.E., Bioresorbable composites prepared by supercritical fluid foaming, *J. Biomed. Mater. Res. A* 2005. 75:89-94.

- [59] Tsivintzelis, S.I. Marras, I. Zuburtikudis, C. Panayiotou, P.orous poly(lactic acid) nanocomposite scaffolds prepared by phase inversion using supercritical CO₂ as antisolvent, *Polymer*. 2007. 48:6311-13.
- [60] Reverchon E., Cardea S., Rapuano C., A new supercritical fluid-based process to produce scaffolds for tissue replacement, *J. Supercrit. Fluids* 2008. 45:365-370.
- [61] Pisanti P., Yeatts A.B., Cardea S., Fisher J.P., Reverchon E. Tubular perfusion system culture of human mesenchymal stem cells on poly-L-lactic acid scaffolds produced using a supercritical carbon dioxide-assisted process. *J Biomed Mater Res A*. 2012. 100(10): 2563-72.
- [62] Della Porta G., Reverchon E., Supercritical fluid based technologies for particulate drug delivery, Chapter 3, pp. 35-59; In: *Handbook of Particulate Drug Delivery*, Edited by M.N.V. Ravi Kumar, 2008, American Scientific Publishers, ISBN: 978-1-58883-124-8.
- [63] Kongsombut B., Tsutsumi A., Suankaew N., Charinpanitkul T. Encapsulation of SiO₂ and TiO₂ Fine Powders with Poly-lactic-co-glycolic acid by Rapid Expansion of Supercritical CO₂ Incorporated with Ethanol co-solvent. *Ind. Eng. Chem. Res.* 2009. 48:11230-11235.
- [64] Ghaderi R., Artursson P., Carlfors J. A new method for preparing biodegradable microparticles and entrapment of hydrocortisone in DL-PLG microparticles using supercritical fluids. *Eur. J. Pharm. Sci.* 2000. 10(1):1-9.
- [65] Kang Y.Q., Yin G.F., Ping O.Y., Huang X.B., Yao Y.D., Liao X.M., Chen A.Z., Pu X.M. Preparation of PLLA/PLGA microparticles using solution enhanced dispersion by supercritical fluids (SEDS). *J Colloid Interface Sci.* 2008. 322(1):87-94.
- [66] Pini R., Storti G., Mazzotti M., Tai H.Y., Shakesheff K.M., Howdle S.M. Sorption and swelling of poly(DL-lactic acid) and poly(lactic-co-glycolic acid) in supercritical CO₂: An experimental and modelling study. *J Polymer Sci B-Polymer Phys.* 2008. 46(5):483-496.
- [67] Shekunov B.Y., Chattopadhyay P., Seitzinger J., Huff R. Nanoparticles of Poorly Water-Soluble Drugs Prepared by Supercritical Fluid Extraction of Emulsions. *Pharm. Res.* 2006. 23(1):196-204.
- [68] Chattopadhyay P, Shekunov BY, Yim D, Cipolla D, Boyd B, Farr S. Production of solid lipid nanoparticle suspensions using supercritical fluid extraction of emulsions (SFEE) for pulmonary delivery using the AERx system. *Adv Drug Del Rev.* 2007. 59:444-453.

- [69] Kluge J., Fusaro F., Casas N., Mazzotti M., Muhrer G. Production of PLGA micro- and nanocomposites by supercritical fluid extraction of emulsions: I. Encapsulation of lysozyme, *J. Supercrit Fluids*. 2009. 50:327-335.
- [70] Singh M., Sandhu B., Scurto A., Cory Berkland C., Michael S. Detamore M.S., Microsphere-based scaffolds for cartilage tissue engineering: Using subcritical CO₂ as a sintering agent. *Acta Biomaterialia*. 2010. 6 (1): 137-143.
- [71] Jaklenec A., Wan E., Murray M.E., Mathiowitz E. Novel scaffolds fabricated from protein-loaded microspheres for tissue engineering. *Biomaterials*. 2008. 29:185-192.
- [72] Declercq H.A., Gorski T.L., Tielens S.P., Schacht E.H., Cornelissen M.J. Encapsulation of osteoblast seeded microcarriers into injectable, photopolymerizable three-dimensional scaffolds based on D,L-lactide and ε-caprolactone. *Biomacromolecules*. 2005. 6:1608-1614.
- [73] Kang S.W., Jeon O., Kim B.S. Poly-(lactic-co-glycolic acid) microspheres as an injectable scaffold for cartilage tissue engineering. *Tissue Eng*. 2005. 11:438-447.
- [74] Hong Y., Gao C.Y., Xie Y., Gong Y.H., Shen J.C. Collagen-coated poly-lactide microspheres as chondrocyte microcarriers. *Biomaterials*. 2005. 26: 6305-6313.
- [75] Sherwood T.K., Shipley G.H., Holloway F.A. Flooding velocities in packed columns, *Ind. Eng. Chem*. 1938. 30 (7):765-769.
- [76] Brunner G. Counter-current separations. *J. Supercrit. Fluids* 2009. 47 (3):574-582.
- [77] Peters M.S., Timmerhaus K.D. *Plant Design and Economics for Chemical Engineers*, 5th Eds.; McGraw-Hill: New York, 1968.
- [78] Della Porta G., Volpe M.C., Reverchon E. Supercritical cleaning of rollers for printing and packaging industry. *J Supercrit Fluids*. 2006. 37:409-416.
- [79] Smith R.L., Yamaguchi T., Sato T., Suzuki H., Arai K. Volumetric behavior of ethyl acetate, ethyl octanoate, ethyl laurate, ethyl linoleate and fish oil ethyl esters in the presence of supercritical CO₂. *J Supercrit Fluids*. 1998. 13:29-36.
- [80] Sabirzyanov A.N., Il'in A.P., Akhunov A.R., Gumerov F.M. Solubility of Water in Supercritical Carbon Dioxide. *High Temperature*. 2002. 40(2):203-206.
- [81] King M.B., Mubarak A., Kim J.D., Bott T.R. The mutual solubilities of water with supercritical and liquid carbon dioxide. *J Supercrit Fluids*. 1992. 5:296-302.

- [82] Wiebe R., Gaddy V. The solubility of carbon dioxide in water at various temperatures from 12 to 40°C and at pressures to 500 atmospheres. *Critical phenomena*. J Am. Chem. Soc. 1940. 62:815-817.
- [83] De S., Robinson D.H. Particle size and temperature effect on the physical stability of PLGA nano-spheres and micro-spheres containing Bodipy. *AAPS Pharm Sci Tech.* 2004. 5(4): article 53.
- [84] Richardson J.F.; Harker J.H., Backhurst J.R. Liquid-liquid extraction. In: Coulson & Richardson's Chemical Engineering: Particle Technology & Separation Processes, 5th Eds.; Butterworth-Heinemann: Oxford, 2002. pp.721-770.
- [85] Riha V., Brunner G. Separation of fish oil ethyl esters with supercritical carbon dioxide. *J. Supercrit. Fluids.* 2000. 17(1):55-64.
- [86] Lee L.Y., Wang C.H., Smith K.A. Supercritical antisolvent production of biodegradable micro and nanoparticles for controlled delivery of paclitaxel, *J. Control. Release.* 2008. 25:96-106.
- [87] Rosca I.D., Watari F., Uo M. Microparticles formation and its mechanism in single and double emulsion by solvent evaporation. *J Control Release.* 2004. 99:271-280.
- [88] Li W.I., Anderson K.W., Deluca P.P. Kinetic and thermodynamic modeling of the formation of polymeric microspheres using solvent extraction/evaporation method. *J. Contr. Rel.* 1995. 37:187-198.
- [89] Meng F.T., Ma G.H., Liu T.D., Qui W., Su Z.S. Microencapsulation of bovine hemoglobin with high bioactivity and high entrapment efficiency using W/O/W double emulsion technique. *Coll. Surf. B: Biointerf.* 2004. 33:177-183.
- [90] Chattopadhyay P., Gupta R.B. Supercritical CO₂ based formation of silica nanoparticles using water-in-oil microemulsions. *Ind. Eng. Chem. Res.* 2003. 42: 465-472.
- [91] Reverchon E., Della Porta G., Torino E. Production of metal oxide nanoparticles by supercritical emulsion reaction. *J. Supercritical Fluids* 2010. 53:95-101.
- [92] Mattea F., Martin A., Schulz C., Jaeger P., Eggers R., Cocero M.J. Behavior of an Organic Solvent Drop During the Supercritical Extraction of Emulsions. *AIChE J.* 2010. 56 (5):1184-1195.
- [93] Von Burkersroda F., Schedl L., Göpferich A. Why degradable polymers undergo surface erosion or bulk erosion. *Biomaterials.* 2002. 23:4221-4231.

- [94] Okada H., Toguchi H. Biodegradable microspheres in drug delivery. *Crit Rev Ther Drug Carrier Syst.* 1995. 12(1):1-99.
- [95] Della Porta G., Cavalcanti S., Reverchon E., Supercritical Fluid Emulsions Extraction: A Novel Technology for the Production of Poly-lactic-co-glycolic Nanostructured Microdevices. *Proceeding of XX Congresso Nazionale di Bioingegneria*, 8-10 July 2010, Turin, Italy. Eds. Patron Eds. pp. 637-638. ISBN 978-88-555-3082-8.
- [96] Falco N., Reverchon E., Della Porta G., Continuous Supercritical Emulsions Extraction: An Innovative Process Layout For Microcarriers Production, *Proceeding of 9th Conference on Supercritical Fluid and their Application*, Eds. E. Reverchon,. ISBN 88-7897-040-9, pp. 209-214.
- [97] Campardelli R., Reverchon E. Della Porta G. Supercritical extraction of O/W emulsions for the production of biodegradable microcarriers for liposoluble vitamins delivery. *Proceeding of 9th Conference on Supercritical Fluid and their Application*. Eds. E. Reverchon, ISBN 88-7897-040-9, pp. 197-20.
- [98] Errico C., Gazzarri M., Chiellini F. A novel method for the preparation of retinoic acid-loaded nanoparticles. *International Journal Molecular Science.* 2009. 10:2336-2347.
- [99] Loveday S.M., Singh H. Recent advances in technologies for vitamin A protection in foods. *Trends in Food Science and Technology.* 2008. 19: 657-668.
- [100] Jeong Y., Song J., Kang S., Ryu H., Lee Y., Choi C., Shin B., Kim K., Ahn K., Jung S. Preparation of *poly*(dl-lactide-*co*-glycolide) microspheres encapsulating all-trans retinoic acid. *International Journal of Pharmaceutics.* 2003. 259:79-91.
- [101] Yoshida K., Sekine T., Matsuzaki F., Yanaki T., Yamaguchi M. Stability of Vitamin A in Oil-in-Water-in-Oil-Type. *Journal of American Oil Chemists Society.* 1999. 76:1-6.
- [102] Redmond K.A., Nguyen T.S., Ryan R.O. All trans retinoic acid nanodisks. *International Journal Pharmaceutics.* 2007. 333:246-250.
- [103] McClements D.J., Decker E.A., Weiss J. Emulsion-based delivery systems for lipophilic bioactive components. *Journal of Food Science.* 2007.72: 109-124.
- [104] Jeong Y., Kang M., Sun H., Kang S., Kim H., Moon K., Lee K., Kim S., Jung S. All-trans-retinoic acid release from core-shell type nanoparticles of poly(ϵ -caprolactone)/poly (ethylene glycol) diblock copolymer. *International Journal Pharmaceutics.* 2004. 273:95-107.

- [105] Benny O., Menon L.G., Ariel G., Goren E., Kim S., Stewman C., Black P.M., Carroll R.S., Machluf M. Local delivery of polylactic-co-glycolic acid microspheres containing imatinib mesylate inhibits intracranial xenograft glioma growth. *Clinical. Cancer Research*. 2009. 15:1222-1231.
- [106] Burt H.M., Tsallas A., Gilchrist S., Liang L.S. Intra-articular drug delivery systems: Overcoming the shortcomings of joint disease therapy. *Expert Opinion in Drug Delivery*. 2009. 6:17-26.
- [107] Nojehdehian H., Moztarzadeh F., Baharvand H., Nazarian H., Tahriri M. Preparation and surface characterization of poly-L-lysine-coated PLGA microsphere scaffolds containing retinoic acid for nerve tissue engineering: in vitro study. *Colloids and Surfaces B: Biointerfaces*. 2009. 73:23-29.
- [108] Freytag T., Dashevsky A., Tillman L., Hardee G.E., Bodmeier R. Improvement of the encapsulation efficiency of oligonucleotide-containing biodegradable microspheres. *J Control Release* 2000. 69:197-207.
- [109] Newman K.D., McBurney M.W. Poly(lactic-co-glycolic acid) microspheres as biodegradable microcarriers for pluripotent stem cells. *Biomaterials*. 2004. 25:5763-5771.
- [110] Hwang Y.J., Oh C., Oh S.G. Controlled release of retinol from silica particles prepared in O/W/O emulsion: The effects of surfactants and polymers. *Journal of Controlled Release*. 2005. 106:339-349.
- [111] Matsumoto A., Kitazawa T., Murata J., Horikiri Y., Yamahara H. A novel preparation method for PLGA microspheres using non-halogenated solvent. *Journal of Controlled Release*. 2008. 129: 223-27.
- [112] Stievano M., Elvassore N. High-pressure density and vapour-liquid equilibrium for the binary systems carbon dioxide/ethanol, carbon dioxide/acetone and carbon dioxide/dichloromethane. *Supercritical Fluids Journal*. 2005. 33:7-14.
- [113] Sabirzyanov A.N., Il'in AP, Akhunov AR, Gumerov FM. Solubility of water in supercritical carbon dioxide. *High Temperature*. 2002. 40:203-206.
- [114] Sovová H., Jez J., Khachatryan M. Solubility of squalane, dinonyl phthalate and glycerol in supercritical CO₂. *Fluid Phase Equilibria*. 1997. 137(1-2):185-191.

- [115] Freitas S., Merkle H.P., Gander B. Microencapsulation by solvent extraction/evaporation: reviewing the state of the art of microsphere preparation process technology. *Journal of Controlled Release*. 2005.102:313-332.
- [116] Wischke C., Schwendeman S.P. Principles of encapsulating hydrophobic drugs in PLA/PLGA microparticles. *International Journal of Pharmaceutics*. 2008. 364: 298-327.
- [117] Siepmann J., Gopferich A. Mathematical modelling of bioerodible, polymeric drug delivery systems. *Advanced Drug Delivery Review*. 2001. 48:229-247.
- [118] Siepmann J., Siepmann F. Mathematical modelling of drug delivery. *International Journal Pharmaceutics*. 2008. 364: 328-343.
- [119] Lee P.I. Diffusional release of a solute from a polymeric matrix: Approximate analytical solution. *Journal of Membrane Science*. 1980. 7:255-275.
- [120] Chakraborty S., Khanday M., Patra C.N., Patro V.J., Sen K. K. Effects of drug solubility on the release kinetics of water soluble and insoluble drugs from HPMC based matrix formulations. *Acta Pharmaceutica*. 2009. 59:313-323.
- [121] Corrigan O.I., Li X. Quantifying drug release from PLGA nanoparticulates. *European Journal Pharmaceutical Science*. 2009. 37:477-485.
- [122] Faisant N., Siepmann J., Benoit J.P. PLGA-based microparticles: elucidation of mechanisms and a new simple mathematical model quantifying drug release. *European Journal of Pharmaceutical Science*. 2002. 15:355-366.
- [123] Cucchiaroni M., Sohier J., Mitoš K., Kaul G., Zurakowski D., Bezemer J.M., Kohn D., Madry H. Effect of transforming growth factor-beta 1 (TGF- β 1) released from a scaffold on chondrogenesis in an osteochondral defect model in the rabbit. *Cent Eur J Biol*. 2006. 1(1):43-60.
- [124] Gotterbarm T., Richter W., Jung M., Berardi Vilei S., Mainil-Varlet P., Yamashita T., Breusch S.J. An in vivo study of a growth-factor enhanced, cell free, two-layered collagen-tricalcium phosphate in deep osteochondral defects. *Biomaterials*. 2006. 27(18):3387-3395.
- [125] Holland T.A., Bodde E.W., Cuijpers V.M., Baggett L.S., Tabata Y., Mikos A.G., Jansen J.A. Degradable hydrogel scaffolds for in vivo delivery of single and dual growth factors in cartilage repair. *Osteoarthritis Cartilage*. 2007. 15(2):187-197.

- [126] Tatar V.M., Venier-Julienne M.C., Benoit J.P., Menei P., Montero-Menei C.N. In vivo evaluation of pharmacologically active microcarriers releasing nerve growth factor and conveying PC12 cells. *Cell Transplant*. 2004. 13(5):573-583.
- [127] Tatar V.M., Venier-Julienne M.C., Saulnier P., Prechter E., Benoit J.P., Menei P., Montero-Menei C.N. Pharmacologically active microcarriers: a tool for cell therapy. *Biomaterials*. 2005. 26(17):3727-3737.
- [128] Vert M., Doi Y., Hellwich K.H., Hess M., Hodge P., Kubisa P., Rinaudo M., Schué F. Terminology for biorelated polymers and applications (IUPAC Recommendations 2012). *Pure Appl. Chem*. 2012. 84(2):377-410.
- [129] Mundargi R.C., Babu V.R., Rangaswamy V., Patel P., Aminabhavi T.M. Nano/micro technologies for delivering macromolecular therapeutics using poly (D,L-lactide-co-glycolide) and its derivatives. *J Control Release*. 2008. 125(3):193-209.
- [130] Hong Y., Gao C., Xie Y., Gong Y., Shen J. Collagen-coated polylactide microspheres as chondrocyte microcarriers. *Biomaterials*. 2005. 26(32):6305-6313.
- [131] Kang S.W., Jeon O., Kim B.S. Poly(lactic-co-glycolic acid) microspheres as an injectable scaffold for cartilage tissue engineering. *Tissue Eng*. 2005. 11(3-4):438-447.
- [132] Mercier N.R., Costantino H.R., Tracy M.A., Bonassar L.J. Poly (lactide-co-glycolide) microspheres as a moldable scaffold for cartilage tissue engineering. *Biomaterials*. 2005. 26(14):1945-1952.
- [133] Tan H., Huang D., Lao L., Gao C. RGD modified PLGA/gelatin microspheres as microcarriers for chondrocyte delivery. *J Biomed Mater Res B Appl Biomater*. 2009. 91(1):228-238.
- [134] Li M., Rouaud O., Poncelet D. Microencapsulation by solvent evaporation: State of the art for process engineering approaches. *Int.J. Pharm*. 2008. 363: 26-39.
- [135] Oliva A., Fariña J.B., Llabrés M. Influence of temperature and shaking on stability of insulin preparation: Degradation kinetics. *Int. J Pharm*. 1996. 143(2):163-170.
- [136] Shnek D.R., Hostettler D.L., Bell M.A., Olinger J.M., Frank B.H. Physical stress testing of insulin suspensions and solutions. *J Pharm Sci*. 1998. 87(11):1459-1465.
- [137] Bittner B., Morlock M., Koll H., Winter G., Kissel T. Recombinant human erythropoietin (rhEPO) loaded poly(lactide-co-glycolide) microspheres: Influence of the

- encapsulation technique and polymer purity on microsphere characteristics. *Eur J Pharm Biopharm.* 1998. 45(3):295-305.
- [138] Yamaguchi Y., Takenaga M., Kitagawa A., Ogawa Y., Mizushima Y., Igarashi R. Insulin-loaded biodegradable PLGA microcapsules: Initial burst release controlled by hydrophilic additives. *J Control Release.* 2002. 81(3):235-249.
- [139] Govoni M., Bonavita F., Shantz L.M., Guarnieri C., Giordano E. Overexpression of ornithine decarboxylase increases myogenic potential of H9c2 rat myoblasts. *Amino Acids* 2010. 38(2):541-547.
- [140] Bilati U., Allémann E., Doelker E. Nanoprecipitation versus emulsion-based techniques for the encapsulation of proteins into biodegradable nanoparticles and process-related stability issues. *AAPS Pharm. Sci. Tech.* 2005. 6(4):594-604.
- [141] Focarete M.L., Gualandi C., Scandola M., Govoni M., Giordano E., Foroni L., Valente S., Pasquinelli G., Gao C., Gross R.A. Electrospun scaffold of a polyhydroxyalkanoate consisting of ω -hydroxypentenoate repeat units: fabrication and in vitro biocompatibility studies. *J Biomater Sci Polymer Ed.* 2010. 21(10):1283-1296.
- [142] Wang L.Y., Gu Y.H., Su Z.G., Ma G.H. Preparation and improvement of release behavior of chitosan microspheres containing insulin. *Int. J. Pharm.* 2006. 311:187-194.
- [143] De Rosa G., Iommelli R., La Rotonda M.I., Miro A., Quaglia F. Influence of the co-encapsulation of different non-ionic surfactants on the properties of PLGA insulin-loaded microspheres. *J Control Release.* 2000. 69(2):283-295.
- [144] Kawashima Y., Yamamoto H., Takeuchi H., Fujioka S., Hino T. Pulmonary delivery of insulin with nebulized DL-lactide/glycolide copolymer nanospheres to prolong hypoglycemic effect. *J Control Release.* 1999. 62(1-2):279-287.
- [145] Liu R., Huang S.S., Wan Y.H., Ma G.H., Su Z.G. Preparation of insulin-loaded PLA/PLGA microcapsules by a novel membrane emulsification method and its release in vitro. *Colloids Surf B Biointerfaces.* 2006. 51(1):30-38.
- [146] Chakraborty S., Khandai M., Sharma A., Patra ChN., Patro V.J., Sen K.K. Effects of drug solubility on the release kinetics of water soluble and insoluble drugs from HPMC based matrix formulations. *Acta Pharm.* 2009. 59(3):313-323.
- [147] Gallagher K.M., Corrigan O.I. Mechanistic aspects of the release of levamisole hydrochloride from biodegradable polymers. *J Control Release.* 2000. 69(2):261-272.

- [148] Malafaya P.B., Oliveira J.T., Reis R.L. The effect of insulin-loaded chitosan particle-aggregated scaffolds in chondrogenic differentiation. *Tissue Eng Part A*. 2010. 16(2):735-747.
- [149] Langer, R., *Tissue engineering*. *Mol Ther.*, 2000. 1(1): 12-5.
- [150] Volkmer E., Drosse I., Otto S., Stangelmayer A., Stengele M., Kallukalam B.C., Hypoxia in static and dynamic 3D culture systems for tissue engineering of bone. *Tissue Eng A* 2008. 14:1331-1340.
- [151] Meinel L., Karageorgiou V., Fajardo R., Snyder B., Shinde-Patil V., Zichner L. Bone tissue engineering using human mesenchymal stem cells: Effects of scaffold material and medium flow. *Annals of Biomedical Engineering*, 2004. 32(1):112-122.
- [152] Stiehler M., Bunker C., Bastrup A., Lind M., Kassem M., Mygind T. Effect of dynamic 3-D culture on proliferation, distribution, and osteogenic differentiation of human mesenchymal stem cells. *Journal of Biomedical Materials Research Part A*. 2009. 89(1):96-107.
- [153] Wang T.W., Wu H.C., Wang H.Y., Lin F.H., Sun J.S. Regulation of adult human mesenchymal stem cells into osteogenic and chondrogenic lineages by different bioreactor systems. *Journal of Biomedical Materials Research Part A*. 2009. 88(4):935-946.
- [154] Zhang Z.Y., Teoh S.H., Chong W.S., Foo T.T., Chng Y.C., Choolani M., A biaxial rotating bioreactor for the culture of fetal mesenchymal stem cells for bone tissue engineering. *Biomaterials*. 2009. 30(14):2694-2704.
- [155] Bancroft G.N., V.I. Sikavitsas, and A.G. Mikos, Design of a flow perfusion bioreactor system for bone tissue-engineering applications. *Tissue Engineering*. 2003. 9(3): 549-554.
- [156] Gomes M.E., Sikavitsas V.I. Behraves E., Reis R.L., Mikos A.G. Effect of flow perfusion on the osteogenic differentiation of bone marrow stromal cells cultured on starch-based three-dimensional scaffolds. *Journal of Biomedical Materials Research Part A*. 2003. 67 (1): 87-95.
- [157] Holtorf H.L., Jansen J.A., Mikos A.G., Flow perfusion culture induces the osteoblastic differentiation of marrow stromal cell-scaffold constructs in the absence of dexamethasone. *Journal of Biomedical Materials Research Part A*. 2005. 72A(3): 326-334.

- [158] Janssen F.W., Oostra J., Van Oorschot A., Van Blitterswijk C.A. A perfusion bioreactor system capable of producing clinically relevant volumes of tissue-engineered bone: In vivo bone formation showing proof of concept. *Biomaterials*. 2006. 27(3): 315-323.
- [159] Bancroft G.N., Sikavitsas V.I., Mikos A.G., Design of a flow perfusion bioreactor system for bone tissue-engineering applications. *Tissue Engineering*. 2003. 9(3):549-554.
- [160] Bilodeau K., Mantovani D., Bioreactors for tissue engineering: Focus on mechanical constraints. A comparative review. *Tissue Engineering*. 2006. 12(8):2367-2383.
- [161] Sikavitsas V.I., Temenoff J.S. Mikos A.G., Biomaterials and bone mechanotransduction. *Biomaterials*. 2001. 22(19): 2581-2593.
- [162] Rubin J., Rubin C., Jacobs C.R., Molecular pathways mediating mechanical signaling in bone. *Gene*. 2006. 367:1-16.
- [163] Weinbaum S., Cowin S.C., Zeng Y., A Model for the Excitation of Osteocytes by Mechanical Loading-Induced Bone Fluid Shear Stresses. *Journal of Biomechanics*, 1994. 27(3):339-360.
- [164] Mauney J.R., Volloch V., Kaplan D.L. Role of adult mesenchymal stem cells in bone tissue-engineering applications: current status and future prospects. *Tissue Eng*. 2005. 11:787-798.
- [165] Caplan A.I., Adult mesenchymal stem cells for tissue engineering versus regenerative medicine. *Journal of Cellular Physiology*. 2007. 213(2):341-347.
- [166] Porada C.D., Zanjani E.D., Almeida-Porad G., Adult mesenchymal stem cells: a pluripotent population with multiple applications. *Curr Stem Cell Res Ther*. 2006. 1(3):365-369.
- [167] Szpalski, C., Wetterau M., Barr J., Warren S.M. Bone Tissue Engineering: Current Strategies and Techniques. Part I: Scaffolds. *Tissue Eng Part B Rev*. 2012. 18(4):246-257.
- [168] Szpalski C., Barbaro M., Sagebin F., Warren S.M. Bone Tissue Engineering: Current Strategies and Techniques. Part II: Cell Types. *Tissue Engineering Part B: Rev*. 2012. 18(4):258-269.
- [169] Yeatts A.B., Fisher J.P Tubular Perfusion System for the Long-Term Dynamic Culture of Human Mesenchymal Stem Cells, *Tissue Engineering: Part C*. 2011. 17 (3):337-348.

- [170] Gomes M.E., Bossano C.M. Johnston C.M. Reis R.L. Mikos A.G. *In vitro* localization of bone growth factors in constructs of biodegradable scaffolds seeded with marrow stromal cells and cultured in a flow perfusion bioreactor. *Tissue Engineering*. 2006. 12(1):177-188.
- [171] Kannan R.Y., Salacinski H.J., Sales K., Butler P., Seifalian A.M. The roles of tissue engineering and vascularisation in the development of micro-vascular networks: a review. *Biomaterials* 2005. 26:1857-1875.
- [172] Hoeben A., Landuyt B., Highley M.S., Wildiers H., Van Oosterom A.T., De Bruijn E.A. Vascular endothelial growth factor and angiogenesis. *Pharmacol Rev.*2004 . 56:549-80.
- [173] Bessa P.C., Casal M., Reis R.L., Bone morphogenetic proteins in tissue engineering: the road from the laboratory to the clinic, part I (basic concepts). *J Tissue Eng. Regen. Med.* 2008. 2(1): 1-13.
- [174] Bessa P.C., Casal M., Reis R.L., Bone morphogenetic proteins in tissue engineering: the road from laboratory to clinic, part II (BMP delivery). *J. Tissue Eng. Regen. Med.* 2008. 2(2-3):81-96.
- [175] Betz M.W., Caccamese J.F., Coletti D.P., Sauk J.J., Fisher J.P. Tissue response and orbital floor regeneration using cyclic acetal hydrogels. *J Biomed Mater Res A*. 2008. 90A:819-29.
- [176] Betz M.W., Yeatts A.B., Richbourg W.J., Caccamese J.F., Coletti D.P., Falco E.E., Fisher J.P. Macroporous hydrogels upregulate osteogenic signal expression and promote bone regeneration. *Biomacromolecules* 2010. 11:1160-1168.
- [177] Frohlich M., Grayson W.L., Marolt D., Gimble J.M., Kregar-Velikonja N., Vunjak-Novakovic G. Bone grafts engineered from human adipose-derived stem cells in perfusion bioreactor culture. *Tissue Eng Part A*. 2010. 16:179-89.
- [178] Yeatts A.B., Gordon C.N., Fisher J.P. Formation of an Aggregated Alginate Construct in a Tubular Perfusion System. *Tissue Engineering: Part C*. 2011. 17(12):1171-1178.
- [179] Truskey G.A., Yuan F., Katz, DF. *Transport Phenomena in Biological Systems*. Upper Saddle River: Eds Pearson Prentice Hall 2004.
- [180] Li D., Tang T., Lu J., Dai K. Effects of flow shear stress and mass transport on the construction of a large-scale tissue engineered bone in a perfusion bioreactor. *Tissue Eng Part A*. 2009. 15: 2773-2778.

List of publications

Della Porta G., Nyuen B., Campardelli R., Reverchon E., Fisher J., Synergistic effect of sustained release growth factors from PLGA microspheres and dynamic bioreactor flow on hMSC osteogenic differentiation in alginate scaffolds, in preparation 2013.

Della Porta G., Falco N., Giordano E., Reverchon E., PLGA Microcarriers By Supercritical Emulsion Extraction: a Study on Bioactive Signal Release in Myoblast Culture, submitted to *Journal of Biomaterial Science*, 2012.

Campardelli R., Reverchon E., **Della Porta G.** Biopolymer particles for protein and peptides sustained release produced by supercritical emulsion extraction, 20th International Congress of Chemical and Process Engineering, August 25-29, 2012, Prague, Czech Republic, then published on: *Procedia Engineering*, 2012, Vol. 4, pp. 268-275.

Della Porta G., Giordano E., Reverchon E., SEE-C technology for the production of PLGA microdevices to be used as bioactive scaffold for cell growth in tissue engineering, *10th International Symposium on Supercritical Fluids*, May 13-16, 2012 San Francisco, CA, USA.

Della Porta G., Castaldo F., Scognamiglio M., Paciello L., Parascandola P., Reverchon E. Bacteria microencapsulation in PLGA microdevices by supercritical emulsion extraction, *Journal of Supercritical Fluids*, 2012, Vol. 63, pp. 1-7.

Della Porta G., Falco N., Reverchon E., Continuous Supercritical Fluid Emulsions Extraction: Capabilities and Performances of an Innovative Process Layout for Biopolymer Microspheres Production. *Proceedings of 13th European meeting on Supercritical Fluids*, October 9-13, 2011, De Hague, (Netherland).

Campardelli R., **Della Porta G.**, Reverchon E., Supercritical fluid extraction of emulsions to produce biopolymers microparticle and nanoparticle. *Proceedings of 13th European meeting on Supercritical Fluids*, 2011, October 9-13, De Hague, (Netherland).

Della Porta G., Campardelli R., Falco N., Reverchon E., PLGA Microdevices for Retinoids Sustained Release Produced by Supercritical Emulsion Extraction: Continuous Versus

Batch Operation Layouts. *Journal of Pharmaceutical Science*, 2011, Vol. 100(10), pp.4357-4367.

Falco N., Reverchon E., **Della Porta G.**, Continuous supercritical fluid emulsion extraction: a low impact route for biopolymer microspheres production. *AIChE Spring Meeting & 7th Global Congress on Process Safety*, 2011, 11-13 March, Chicago USA.

Della Porta G., Falco N., Reverchon E. Continuous Supercritical Emulsions Extraction: A New Technology For Biopolymer Microparticles Production. *Biotechnology & Bioengineering Journal.*, 2011, Vol. 108 (3), pp. 676-686.

Campardelli R., Reverchon E. **Della Porta G.** Supercritical extraction of O/W emulsions for the production of biodegradable microcarriers for liposoluble vitamins delivery. *Proceeding of 9th Conference on Supercritical Fluid and their Application*, Sept. 6-8, 2010, Sorrento, Italy. Eds. E. Reverchon, ISBN 88-7897-040-9, pp. 197-202.

Falco N., Reverchon E., **Della Porta G.**, Continuous Supercritical Emulsions Extraction: An Innovative Process Layout For Microcarriers Production, *Proceeding of 9th Conference on Supercritical Fluid and their Application*, Sept. 6-8, 2010, Sorrento, Italy Eds. E. Reverchon,. ISBN 88-7897-040-9, pp. 209-214.

Della Porta G., Cavalcanti S., Reverchon E., Supercritical Fluid Emulsions Extraction: A Novel Technology for the Production of Poly-lactic-co-glycolic Nanostructured Microdevices. *Proceeding of II Congresso Nazionale di Bioingegneria*, 8-10 July 2010, Turin, Italy. Eds. Patron Eds. pp. 637-638. ISBN 978-88-555-3082-8.